國 立 交 通 大 學

機 械 工 程 學 系
碩 士 論 文

改善毛細泵吸迴路熱傳性能應用在電子冷卻

之實驗研究

**An Experimental Study of Improving Heat Transfer Performance of
a Capillary Pumped Looped for Electronics Cooling**

研 究 生：廖 峻 樟

指 導 教 授：林 清 發 博士

中 華 民 國 九 十 六 年 六 月

改善毛細泵吸迴路系統在電子冷卻上之實驗研究

Experimental Study of an Improved Capillary Pumped Looped System
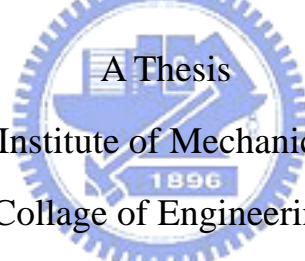for Electronics Cooling

研 究 生：廖 峻 樟　　　　　　　Student：Chun-Chang Liao

指導教授：林 清 發　　　　　　　Advisor：Tsing-Fa Lin

國立交通大學

機械工程學系

碩士論文初稿

A Thesis

Submitted to Institute of Mechanical Engineering

Collage of Engineering

National Chiao Tung University

In Partial Fulfillment of the Requirements

For the degree of

Master of Science

In

Mechanical Engineering

June 2007

Hsinchu, Taiwan, Republic of China

中 華 民 國 九 十 六 年 六 月

國 立 交 通 大 學

論 文 口 試 委 員 會 審 定 書

本校＿＿機 械 工 程＿＿學系碩士班＿＿＿廖峻樟＿＿＿君

所提論文（中文）改善毛細泵吸迴路熱傳性能應用在電子冷卻之＿＿

實驗研究＿＿＿＿＿＿＿＿＿＿＿＿＿＿＿＿＿＿＿＿＿＿

（英文）An Experimental Study of Improving Heat Transfer＿

Performance of a Capillary Pumped Looped for Electronics

Cooling＿＿＿＿＿＿＿＿＿＿＿＿＿＿＿＿＿＿＿＿＿

合於碩士資格水準、業經本委員會評審認可。

口試委員：＿＿＿＿＿＿＿＿＿＿　＿＿＿＿＿＿＿＿＿＿

＿＿＿＿＿＿＿＿＿＿　＿＿＿＿＿＿＿＿＿＿

＿＿＿＿＿＿＿＿＿＿　＿＿＿＿＿＿＿＿＿＿

指導教授：＿＿＿＿＿＿＿＿＿＿　＿＿＿＿＿＿＿＿＿＿

系 主 任：＿＿＿＿＿＿＿＿＿＿　教授

中 華 民 國　　96　　年　　6　　月　　8　　日

誌 謝

　　時光飛逝，想當初才剛進交大，對於一切總是那麼地陌生。由於學長與學弟的關心與幫助，讓我在這兩年的研究所生活過得非常充實與開心。在這兩年的研究過程中，林清發老師的教學態度與研究精神都是值得我學習的對象，相信對於往後不管是工作或是學習上都是很有幫助的。然而，從一開始對於電子冷卻方面的知識一竅不通，直到現在本論文的完成，要感謝的人很多，若不是有洪義祥學長的細心教導，以及工研院劉家宏博士和張文瑞學長的從旁協助，可能我要花兩倍甚至更多的時間才能完成。在此，我由衷的感謝老師、學長與學弟。

　　當然在研究室的兩年中，實驗室的好夥伴是不可少的，奎銘、凱文與政陞不管在修課或做實驗的過程都是亦師亦友。其次對研究室成員尚緯學長、汎鈞學長、建安學長、浚圩、永龍、壹龍、長志等人感謝他們分享在實驗室的低潮與喜悅。

　　還要感謝清華大學工科系潘欽教授、清華大學動機系洪英輝教授與成功大學機械系何清政教授在口試中提出各項建設性的建議，使得本論文更趨於完備。

　　最後要感謝家人與所有好朋友在背後的的默默關心與支持，對於每一個人的好，我一直心存感謝著。

<div align="right">廖峻樟　　2007, 6 於新竹交大</div>

改善毛細泵吸迴路熱傳性能應用在電子冷卻之實驗研究

研究生：廖峻樟　　　　　　指導教授：林清發 博士

國立交通大學機械工程學系

摘要

本實驗主要是研究並建立一套應用於電子冷卻的改良式毛細泵吸迴路系統，數種改良蒸發器設計以增進熱傳性能的方法在本實驗中被研究。這些方法包括在蒸氣溝槽的側面及底面製造粗糙面，使多孔材料中的液體能潤濕溝槽表面以增加蒸發面積。其次，在蒸發器內部加入一均熱片的影響也被探討。由針狀及平板鰭片構成的蒸氣通道對毛細泵吸迴路性能的影響也進一步在本研究中探討。

本研究中使用一加熱面積為 $30{\times}30\mathrm{mm}^2$ 的加熱銅塊來模擬發熱中的晶片，均熱片的加熱面積為 $57{\times}57\mathrm{mm}^2$ 並直接連接在加熱銅塊的上方。均熱片上方刻有 10 個溝槽供蒸氣流進蒸氣管路，每個溝槽的深度為 3mm，寬度為 2.4mm，溝槽的尺寸和文獻[34]中未使用均熱片的系統相同以便於比較。

實驗的結果指出工作流體的填充量會影響到整個系統的熱傳能力，且在最高的散熱功率以及最低的熱阻值會發生在一最佳的充填量，在大於最佳填充量時，增加填充量反而會使系統的最高散熱功率

下降、最低熱阻值升高，增加蒸發器及冷凝器間的相對高度也會提高整個系統的熱傳能力。另外，使用針狀鰭片來構成溝槽的設計並無法增進整個系統的熱傳能力，使用均熱片則能有效的提升熱傳能力，在溝槽的側面及底面使用粗糙面的設計亦能有效的增進整個系統的熱傳能力。

An Experimental Study of Improving Heat Transfer Performance of a Capillary Pumped Looped for Electronics Cooling

Student：Chun-Chang Liao   Advisor：Prof. Tsing-Fa Lin

Institute of Mechanical Engineering

National Chiao Tung University

ABSTRACT

In the present study, an experimental capillary pumped loop for electronics cooling based on an improved system design is established. Several methods to improve the thermal performance of the loop by improving the evaporator design are investigated. These include roughing the vertical and bottom surfaces of the grooved channels to allow the liquid in the wick to wet the surfaces, which in turn greatly increases the surface area for the liquid vaporization. Besides, the possible heat transfer augmentation in the evaporator section through the use of a heat spreader on the heat dissipating chip is explored. Furthermore, the CPL performance difference between the vapor channels formed by plane fins and pin fins is also examined.

The heat dissipating chip with a surface area of 30×30mm^2 is modeled by a heated copper plate of the same surface area in this study. The heat spreader, also a copper plate, is chosen to have a much larger surface area of 57×57 mm^2, which is mounted directly on the heated copper plate. Ten grooved channels are machined on the surface of the heat spreader. Each grooved channel is 3mm in height and 2.4mm in width. The height and width of the channel are the same as that in the previous study [34] without using heat spreader.

The measured data indicate that an optimal liquid inventory exists at which $Q_{e,max}$ is the highest and R_{th} is the lowest for a given relative condenser-evaporator

height for the CPL with a given evaporator design. Besides, increasing or decreasing the liquid inventory from this optimal value causes a reduction in $Q_{e,max}$ and a raise in R_{th}. Moreover, an increase in the relative height between the condenser and evaporator results in a significant improvement in the CPL performance with a much higher $Q_{e,max}$ and a much lower R_{th}. Furthermore, there is no noticeable enhancement in the heat transfer performance of CPL by using a pin fin block to form the grooved channels. However, the use of a large heat spreader in the evaporator can enhance the heat transfer performance greatly. Finally, roughing the vertical and bottom surfaces of the grooved channels can also significantly enhance the heat transfer performance of the CPL.

CONTENTS

LIST OF FIGURES

LIST OF TABLES

NOMENCLATURE

A   cross sectional area, m^2

c_p specific heat, J/kg℃

D   diameter of tube, m

f   friction factor

F   dimensionless factor

g   gravitational acceleration, m/s^2

H$_g$ relative height between evaporator and condenser, m

h   relative height, m, or heat transfer coefficient, W/m^2℃

h$_{n,t}$ heat transfer coefficient from the top of evaporator section to ambient, W/m^2℃

h$_{n,r}$ heat transfer coefficient from the radial surface of evaporator section to ambient, W/m^2℃

h$_{n,b}$ heat transfer coefficient from the bottom of evaporator section to ambient, W/m^2℃

K   permeability, m^2

k   thermal conductivity, W/m K

I   measured current from DC power supply, A

L   length, m, or liquid inventory

$\dot{m}$ mass flow rate, kg/s

N   number of grooved channel

P   pressure, kPa

Q   heat load, W

R   thermal resistance, ℃/W

Re   Reynolds number

T   temperature,℃

V   measured voltage from DC power supply; velocity, m/s

z   thickness of wick, m

Greek Symbols

ΔP	pressure drop, kPa
ΔT	temperature difference, ℃
ρ	density, kg/m^3
σ	surface tension, N/m
δ	cotton gauze layer thickness, m
μ	viscosity, N-S/m^2
ε	porosity, %
ℓ	thickness of wick
θ	contact angle

Subscripts

cap	capillary term
cold	cooling water temperature
cond	condenser
e	effective power input
evap	evaporator
env	environment
g	gravitational or grooved channel
i	inner wall
l	liquid phase
loss	loss term
n	natural convection
o	outer wall
s	surface area
T	teflon
t	total power input
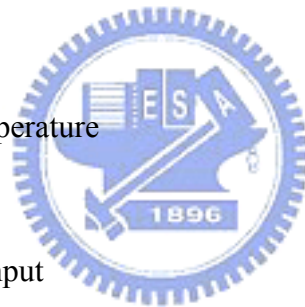
th   thermal resistance

v   vapor phase

vg   vapor in grooved channel

w   wick structure

z   z direction

CHAPTER 1

INTRODUCTION

1.1 Motive

Over the past few years, thermal management has become a major challenge in electronics cooling because of the quick increase in the computational frequencies of microprocessors. It is well known that the surface temperature of the CPU chips should not exceed 85℃ to avoid the system shutdown. In just a recent past, the heat dissipation in CPUs was about 10W for the 80486 series. Now for Pentium D series, the heat dissipation is over 130W and the heat dissipation area is about 9 cm^2. In addition, spacing is relatively limited for thermal modules especially when applied to portable electronic devices, like notebook computer or PDA. The conventional thermal solutions based on air-cooling could not remove the heat generated in the today's chips. Recently, some solutions based on liquid cooling are utilized to take the high heat dissipation away. The liquid cooling can be used with or without boiling. Moreover, the two-phase heat transfer associated with boiling or condensation has high latent heat involved in the process, hence it is known to be the most effective and popular.

Several cooling approaches based on two-phase liquid cooling, such as liquid jet impingement, spray, heat pipe and capillary pumped loop, have been developed. Among these approaches, the jet impingement or spray cooling needs extra power to drive the flow. Thus they are not practical in a self-regulated loop system preferred in electronics cooling. The heat removal capability of heat pipes is limited by several physical limits, such as sonic limit, capillary limit, viscous limit, boiling limit, and entrainment limit, hence the use of heat pipes is often not sufficient to cool high heat

flux surface. For these reasons, the applications of capillary pumped loops to the electronics cooling have received increasing attention in recent years.

Capillary pumped loop (CPL) is a two-phase thermal management system which circulates the working fluid by the surface tension forces developed in a fine-pore wick. A functional schematic of a CPL is illustrated in Fig. 1.1. It consists of an evaporator, a condenser, a liquid reservoir, and liquid and vapor transport lines. The wick structure is contained in the evaporator. As the heat load is imposed on the evaporator, the liquid in the evaporator vaporizes and moves to the condenser through the vapor line. The condenser condenses the vapor and rejects the heat to the ambient. Then the liquid which is pumped by the capillary force generated by the wick returns to the evaporator. A typical evaporator design is schematically shown in Fig. 1.2. More specifically, the evaporator consists of a grooved copper plate attached on the wick surface, acting as the heating zone, and the vapor can flow in the grooves.

Compared with the conventional heat pipes, CPL has several advantages. In the CPL, the liquid and vapor have different transport lines to avoid the two-phase interaction. Thus the liquid-vapor counter-current flow is avoided and entrainment limit will not occur. Besides, there is no wick structure in the loop except the evaporator. This reduces the pressure drop in the system. According to these reasons, CPL has a higher heat transfer capability and a longer transport distance along with a smaller temperature difference.

1.2 Literature Review

It is well known that CPL was first developed for thermal management in space mission. The initial concept of CPL was proposed at NASA Lewis Research Center by Stenger [1]. But not until the late-1970s serious CPL development for spacecraft applications began. In the 1980s, extensive ground tests and flight and commercial

experiments for CPL systems have been performed. In 1993, Ku [2] surveyed capillary pumped loop technology development since the late-1970s. Characterization of CPL and verification of CPL performance were addressed. He also presented some performance anomalies like sudden deprime of evaporators, evaporator deprime during rapid power step down and pressure oscillations during steady operation. Deprime is a CPL failure mode that the vapor or gas appear in the liquid core of the evaporator. The gas interrupts the contact between the liquid and wick. Hence the capillary force does not work.

A CPL would perform its designed functions after it is successfully started. Maidanik et al. [3] investigated the startup period of CPL through experimental and analytical methods. They indicated that the startup can be divided into three stages. In the first stage, the input power is applied to increase the sensible heat of working fluid. As the liquid temperature rises and reaches the required superheat at the onset of nucleate boiling, boiling occurs and the evaporator temperature lowers quickly. This is the second stage. In the third stage the evaporator temperature becomes constant and then the CPL is successfully started. They also found that there is a minimum heat load to ensure a reliable startup. Ku [2], Meyer et al. [4], Hoang and Ku [5], and LaClair and Mudawar [6] also agreed with these findings. Hoang and Ku [5] also discussed the pressure spikes caused by the formation of the bubbles. Sometimes the pressure spike can exceed the capillary limit of the wick. Thus the vapor penetrates the wick into the liquid core. LaClair and Mudawar [6] developed an analytical model to explain the minimum heat load. They indicated that the minimum heat load is required to produce a suitable subcooling in the liquid core so that nucleation can not occur in the liquid core and any bubbles which penetrate the wick can be condensed.

When a CPL operates in steady state, the pressure and temperature oscillations in the loop can still be observed. Large amplitude oscillations will result in negative

effects on the CPL performance. The causes of pressure and temperature oscillations have been studied theoretically by Hoang and Ku [5, 7]. They believed that the hydrodynamic instability of CPL fluid flow, which was caused by the interaction among the components, led to the oscillation. They also developed a model to predict the oscillation amplitudes. Ku and Hoang [8] showed that the test data were in an excellent agreement with the theoretical model. They also found that the growth and collapse of bubbles was the major reason for the oscillations. Kolos and Herold [9] reached the same conclusion. The experimental results presented by Ku and Hoang [8], O'Connell and Hoang [10] and O'Connell et al. [11] demonstrated that the amplitudes of oscillations could be affected by the properties of components and the operating conditions, such as wick porosity, transport line diameter, input power, and so on.

The operation characteristics of CPL systems subject to various heat loads have been examined in the literature. Ku [2, 12] indicated that the evaporator deprime occurred when the input power was reduced suddenly. Pouzet et al. [13] applied a stepwise heat load to a CPL to study the fundamental response mechanisms. They observed that the system operation would reach a new steady state after certain response time following the change in heat load. Bazzo and Riehl [14] obtained similar test results in a small-scale CPL. The long term heat load profile tests were carried out. They also discussed the effects of different working fluid and noted that a working fluid with a higher latent heat can reduce the startup time and the response time. Besides, a lower superheat in evaporator was also observed.

Since there are no mechanical pumps in CPL systems, the heat transfer performance can be affected by the gravity. Meyer et al. [4] demonstrated the successful CPL operation whether the evaporator was higher or lower than the condenser. The temperature difference between the evaporator and condenser is

known to vary with their height difference. For the evaporator at a higher elevation, Dickey and Peterson [15] and Liao and Zhao [16] showed that the CPL thermal resistance decreased at decreasing height difference. Similarly, Chen and Lin [17] indicated that the CPL thermal resistance decreased at increasing height difference when the condenser is at a higher elevation. They also observed that there is an optimum liquid inventory which led to the minimum thermal resistance.

The heat and mass transfer characteristics in a flat-plate type wick have been examined by several groups. Liao and Zhao [16] studied the effects of wick thickness, particle size and inlet temperature of liquid experimentally. They draw the following conclusions:

1) The heat transfer coefficient increases to a maximum value and then decreases afterward while the imposed heat flux increases.

2) There exists an optimum particle size for maximum heat transfer coefficient. However, the critical heat flux is shown to increase with the decrease of particle size.

3) The critical heat flux increases with a decrease in the thickness, but the thickness does not show noticeable effects on the heat transfer coefficient.

4) Both the heat transfer coefficient and critical heat flux increase with the inlet temperature increase.

They also explored the phase change behavior in the wick experimentally [16, 18, 19]. The process of the two-phase zone growth in the wick has been investigated. When the imposed heat flux was sufficiently high, the vapor film was observed beneath the heated fin.

Some numerical simulations were also conducted to study the flow and heat transfer within the porous structure in the evaporator. Cao and Faghri [20, 21] investigated the flat-plate type evaporator numerically. The results showed that as the bubble grew to a size to cover the heater surface, the liquid was blocked and could not

contact the heater surface. Thus the wall superheat increases rapidly. A huge amount of vapor generates due to the high wall superheat, causing the pressure increase and finally destroying the liquid-vapor interface. Huang et al. [22] developed a mathematical model to predict the phase change in a porous wick. They showed that instead of an evaporative interface, the phase change occurred in a two phase zone between the vapor zone and the liquid zone in the wick. Hanlon and Ma [23] developed a mathematical model to study the heat transfer capability for a sintered wick structure. Their results showed that the evaporation heat transfer coefficient could be enhanced by reducing the average particle size. They also proposed that thin film evaporation played an important role in the enhancement of evaporating heat transfer. The wick structures discussed above are all considered to be formed from particles of a single pore size. When there existed a pore size distribution, Figus et al. [24] showed that the pore size distribution could restrict the performance.

Several methods have been developed to improve the CPL performance previously. Mo et al. [25, 26] combined the CPL with the electrohydrodynamic technique. They successfully reduce the startup time and show a good enhancement of thermal performance by applying an electric field to the evaporator wick. Besides, the depriming phenomenon can also be prevented. Muraoka et al. [27] used a porous structure inside the condenser to stabilize the interface between the liquid and vapor phases. In order to prevent the gas accumulation in the liquid core, Hoang [28, 29] proposed a new design concept. A minor loop is used to remove the gas in the liquid core. The test results show that the deprime can be successfully prevented.

As the CPL technology was first developed for spacecraft applications, the dimensions of the systems are in the order of meters. The large scale CPL systems have been extensively studied before. In order to apply the CPL technology to electronics cooling, we need to reduce the dimensions of the components. Delil et al.

[30] reported that small evaporators tend to deprime more easily probably due to an insufficient subcooled liquid supply to the porous wick. Bazzo and Riehl [14] examined the operation characteristics of a small-scale CPL system. The similarity between the large and small scale systems was verified. Most of the CPL evaporators discussed above are designed with a cylindrical evaporator. For the practical utility in electronics cooling, a flat shape evaporator is proposed [17, 31]. Some important characteristics and results of the previous works for CPL reviewed above are listed in Table 1.1.

Heat spreader is often used as a heat sink in electronics cooling to reduce the thermal resistance of the heat sink by increasing the heat exchange area with the coolant. Feng and Xu[32] showed that the spreading resistance was affected by the thickness of the spreader, the ratio of heating area and spreading area, and the location of the heater. Maranzana et al. [33] proposed a method to determine the optimal thickness for the minimum spreading resistance.
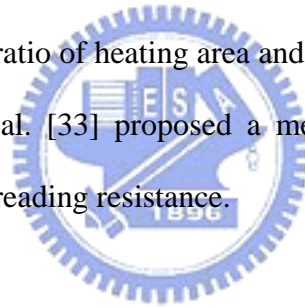
1.3 Objective

Over the past, the large scale CPL systems have been successfully used for spacecraft applications. But the characteristics of the small scale CPL systems for electronics cooling are less explored. In the present study, an experimental capillary pumped loop system for electronics cooling will be established to test its performance. Methods to improve the thermal performance of the loop will be investigated in this study. The performance difference between using the plane fins and pin fins to form the grooved channels will be examined at first. Besides, the possible heat transfer augmentation in the evaporator section through the use of heat spreader attached to the heat dissipating chip will be examined. Finally, roughing the vertical and bottom surfaces of the parallel grooved channels to allow the liquid in the wick to wet the

surfaces, which in turn greatly increases the surface area for the liquid vaporization,

will be tested.

Table 1.1 Summary of results in previous CPL studies

Authors	$Q_{e,max}$ (W)	$q"_{e,max}$ (W/cm^2)	$T_{evap,max}$ (℃)	$R_{th,min}$ (K/W)	H_g (cm)	wick properties	working fluid	Applications	notation
Maidanik et al. (1993)	775	3.5	32		0	pore radius 1.3 μm, polyethylene	ammonia	Spacecraft	
Meyer et al. (1993)	1129	7.9	90	0.0125	-200	pore size 1.5 μm, porosity 70% , sintered nickel	ammonia	spacecraft	
Ku and Hoang (1995)	700	1.8	40	0.077	0	permeability , 4.43*10^-13 m^2	ammonia	spacecraft	
O'Connell and Hoang (1996)	500	1.27	30		0	pore radius 19.08 , 16.12 , 13.02 , 8.3 μm	ammonia	spacecraft	
O'Connell and Ku (1996)	500	1.27	30		0	pore radius 16.12 , 13.02 μm	ammonia	spacecraft	
Pouzet et al. (2004)	600	5	33	0.058	0	pore radius 20 μm, polyethylene	R-134A	spacecraft	
Mo et al. (1999)	50	0.25	26.5	0.04	0	pore radius 1.5 μm, polyethylene	R-134A	spacecraft	

Table 1.1 Continued (1)

Authors	$Q_{e,max}$ (W)	$q"_{e,max}$ (W/cm^2)	$T_{evap,max}$(°C)	$R_{th,min}$(K/W)	H_g (cm)	wick properties	working fluid	Applications	notation
Mo et al. (2000)	650	3.21	26	0.004	0	pore radius 1.5 μm, polyethylene	R-134A	spacecraft	
Bazzo and Riehl (2003)	50	2.09	40	0.6	0	pore radius 20 μm , porosity 60% , permeability 10^-12 m^2 , polyethylene	acetone	electronics cooling	
Bazzo and Riehl (2003)	50	2.09	30	0.34	0	pore radius 20 μm , porosity 60% , permeability 10^-12 m^2 , polyethylene	ammonia	electronics cooling	
Dickey and Peterson (1994)	130	2.87	58	0.15	0	sintered nickel, pore radius 1~1.5 μm, porosity 70%	ammonia	electronics cooling	
Chen and Lin (2001)	40	2.5	83	1.28	12	pore radius 10.5 μm , permeability 6*10^-13 m^2 , polyethylene	FC-72	electronics cooling	

Table 1.1 Continued (2)

Authors	$Q_{e,max}$ (W)	$q"_{e,max}$ (W/cm^2)	$T_{evap,max}$(°C)	$R_{th,min}$ (K/W)	H_g (cm)	wick properties	working fluid	Applications	notation
Liao and Zhao (1999)	887	32	168	0.048	-0.5	partical diameters 0.55, 1.09, 1.99, 2.56 mm, packed glass beads	water	electronics cooling	only evaporator
Liao and Zhao (2000)	256	32	144.6	0.104	1	partical diameters 1.99 mm, packed glass beads	water	electronics cooling	only evaporator
Zhao and Liao (2000)	740	25.9	135	0.032	-3.5	partical diameters 1.09 mm, packed glass beads	water	electronics cooling	only evaporator
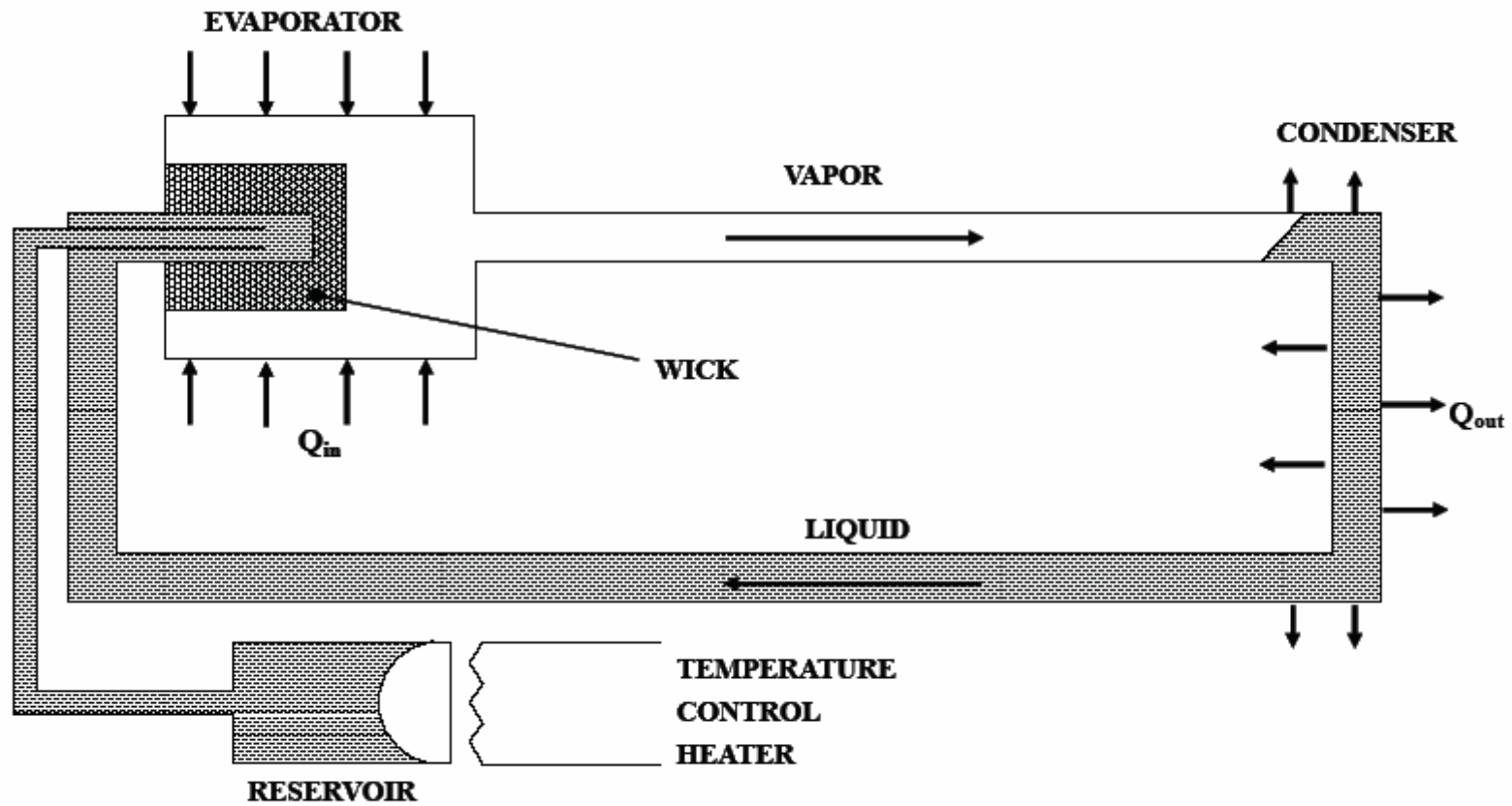
Fig. 1.1 Schematic of a typical capillary pumped loop

Wick

Liquid

Liquid

vapor

fin

vapor

vapor

Grooved
channel

fin

vapor

Heat

Heat

Grooved copper block
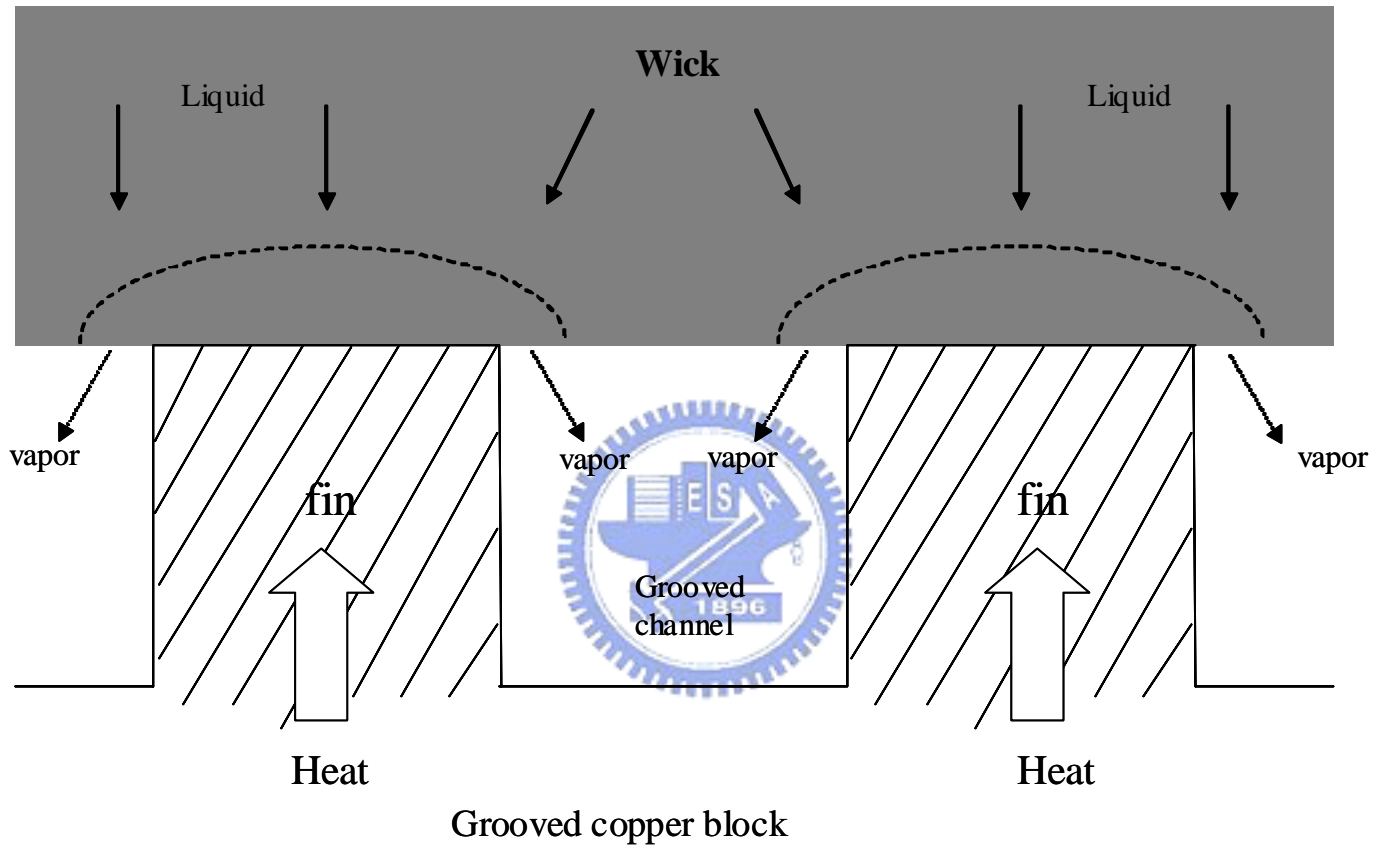
Fig. 1.2 Schematic of a typical evaporator design

CHAPTER 2

EXPERIMENTAL APPARATUS AND PROCEDURES

In the present study, the experimental system established to test an improved design of a CPL is schematically shown in Figure 2.1. The experimental system consists of four major parts, namely, a test CPL loop, a fluid inventory unit, a cold-water loop and a measurement unit. These parts are described in the following.

2.1 CPL Test Loop

The present test CPL loop includes an evaporator, a condenser, and vapor and liquid transport lines and it is shown in Figure 2.2 by a three-dimensional plot. The details of the dimensions and materials used for various components in the loop are given in Table 2.1. Note that here the evaporator and condenser are plotted at the same height and the gravity effects do not exist. But in the actual test we can vary the relative height of the evaporator and condenser.

Plots showing the detailed structure of the evaporator are given in Figure 2.3. Typically, the evaporator consists of a wick structure, a heater and a grooved block. Instead of the grooved channels formed by the parallel plane fins adopted in the previous study [34], the vapor channels formed by the parallel square pin fins are tested here. Two types of pin fins of different sizes are chosen, as schematically shown in Figures 2.4 and 2.5. The type-1 pin fins are much smaller and more space is available for the liquid vaporization to take place. The dimensions of the pin fins are given in Figures 2.4 and 2.5. Besides, a heat spreader with grooved channels made from a copper plate of 10-mm thick will be tested in this investigation. The grooved vapor channels formed by parallel plane fins on a copper plate with a much larger

surface area than the directly heated copper block, the so called heat spreader, are schematically shown in Figure 2.6. Moreover, the grooved channels with rough vertical and bottom surfaces are also tested. The surface roughness is produced from the sand blasting process, which uses tiny particles to directly hit the surfaces. Specifically, the Al_2O_3 particles of $120\,\mu$m in mean diameter are used here. The photo of the rough surface is shown in Figure 2.7. Two resistance heaters are inserted into the 30mm×30mm heated copper block to simulate a heat dissipating CPU and the heaters are covered with thermal grease to reduce the thermal contact resistance. The wick used in present study is made from open-cell blowing foam of polyvinyl alcohol (PVA), and the structure of this PVA is illustrated by the photos given in Figure 2.8 (its mean pore radius is $21\,\mu$m, porosity 65%, and permeability $3.0\times10^{-11}m^2$) and the wick layer is $30mm\times30mm\times3mm$ and $57mm\times57mm\times6mm$ in size. The outside surfaces of the heated copper block, grooved copper block and wick are all thermally insulated by teflon wraps. They are then installed in a cylindrical teflon base. In order to further reduce heat loss, the outside surface of the whole evaporator is covered with a superlon insulation layer of 8-mm in thickness. An observational window is also opened in the teflon cover to facilitate the visualization of the flow in the grooved vapor channels. The evaporator is connected with the condenser through the liquid and vapor transport lines.

In designing the condenser, the heat transfer area and the cooling mechanisms to cool down the working fluid need to be considered. Specifically, the condenser must have the following characteristics:

1) Small temperature difference between the condenser and heat sink.

2) Small flow resistance inside the condenser.

3) Small gravity force effect under 1G environment.

4) High reliability and light weight.

5) Easy fabrication and low cost.

Herein, we chose a double-tube heat exchanger as the condenser. Cold water is used to condense the vapor and to control the temperature of the condenser.

The transport lines include the vapor line and liquid line. In normal operation the vapor from the evaporator flows through the vapor line and enters the condenser and the liquid from the condenser flows to the evaporator through the liquid line. In order to reduce the friction loss, smooth teflon tubes with inner diameter of 4.5 mm are chosen for the vapor line and liquid line.

2.2 Fluid Inventory Unit

Before the working fluid is input to the CPL, it is important to insure that the system is in a vacuum condition and no noncondensible gas exists in the CPL. The working fluid inventory unit includes a working fluid tank, a dispensing burette, and a vacuum pump, which connects with the CPL loop through tubes and valves.

To maximize the capillary limit and heat transport of the CPL, the working fluid should have the following properties:

1) large surface tension

2) high density

3) large latent heat

4) low viscosity

In this study deionized water is chosen as the working fluid.

2.3 Cold-Water Loop

The cold-water loop is designed for condensing the water vapor from the evaporator. Using a cold-water thermostat and a spherical valve, we can adjust the temperature and flow rate of cold water in the cold-water loop. This arrangement

allows us to control the temperature of the condenser.

2.4 Measurement Unit

T-type (copper-constantan) thermocouples are used to measure the temperatures at selected locations in the test CPL loop. Specifically, six calibrated thermocouples are employed to measure the temperature of the copper blocks with pin fins and plane fins on it. The locations of the thermocouples in the block are schematically shown in Figures 2.4 and 2.5. To estimate the heat loss from the evaporator, the temperature of the outer surface of the adiabatic cotton is also measured, as schematically shown in Figure 2.9. Besides, the temperature of the working fluid at the inlets and exits of the evaporator and condenser shown in Figure 2.2 are measured.

Four pressure sensors (YOKOGAWA FP101A) are used to measure the pressure at the inlets and exits of the evaporator and condenser. The accuracy of the pressure measurement is $\pm0.25\%$ for the measured range of 0~200 kPa

2.5 Equipments

1) DC Power Supply:

A DC power supply of 60V and 3A is selected to supply the required electric current to the heaters in the evaporator section. The DC current through the heaters is measured by a Yokogawa DC meter with an accuracy of $\pm0.2\%$. Then the voltage drop across the heater is measured by a Yokogawa multimeter. Thus the power input to the heater can be calculated.

2) Data Acquisition:

The data acquisition unit employed to record the signals from various transducers is a 30-channel data logger (YOKOGAWA MW-100), which is

connected to a personal computer. The voltage signals from the thermocouples are converted into the temperature by the internal calibration equations in the computer and are displayed on the screen simultaneously.

3) Thermostat:

The maximum cooling capacity of the thermostat is 1,200 W with a maximum water volume flow rate of 5 L /min

4) Vacuum Pump:

An oil rotary vacuum pump (VLVAC G-100D) with an ultimate pressure of 5×10^{-4} torr and a pumping speed of 120 L/min is used here

2.6 Experimental Procedures

Before each experiment, the vacuum pump is connected with the CPL to get rid of the non-condensable gas possibly existing in the CPL loop. Then the working fluid is injected into the CPL from the fluid inventory unit. Besides, the thermostat of the cold-water loop is set at a predetermined level and the DC power supply is turned on to input the preset amount of heat to the evaporator. After the system reaches a statistically stable state, the temperature and pressure data from various transducers are recorded and processed by the data acquisition unit.

2.7 Experimental Parameters

In the present study the experimental parameters include the input power to the evaporator, the liquid inventory in the loop, and the elevation difference between the condenser and evaporator. The ranges of the experimental parameters to be investigated are listed in Table 2.2.

Table 2.1 Geometric and material characteristics of the present CPL system.

Evaporator		
Wick structure	Size (mm³)	$30 \times 30 \times 3$
		$57 \times 57 \times 6$
	Mean pore radius (μm)	21
	Porosity (%)	65
	Permeability (m²)	$3.0 \times 10^{-11} m^2$
	Material	polyvinyl alcohol
Rectangular pin fin block	Size (mm³)	$30 \times 30 \times 7$
	Material	copper
Spreader grooved block	Size (mm³)	$57 \times 57 \times 10$
	Material	copper
Condenser		
Outer tube	Inner diameter (mm)	20
	Length(mm)	350
	Material	copper
Inner tube	Outer diameter (mm)	6.35
	Inner diameter (mm)	4.5
	Length(mm)	350
	Material	copper
Transport Line		
Liquid line	Outer diameter (mm)	6.35
	Inner diameter (mm)	4.5
	Length(mm)	790
	Material	teflon
Vapor line	Outer diameter (mm)	6.35
	Inner diameter (mm)	4.5
	Length(mm)	790
	Material	teflon

Table 2.2 Experimental parameters

Parameter	Range	Unit
Input power	15 ~ 400	W
Liquid inventory	40 ~ 75	%
Cooling water temperature in condenser	25	^{o}C
Relative height between the evaporator and condenser	0 ~ 10	cm
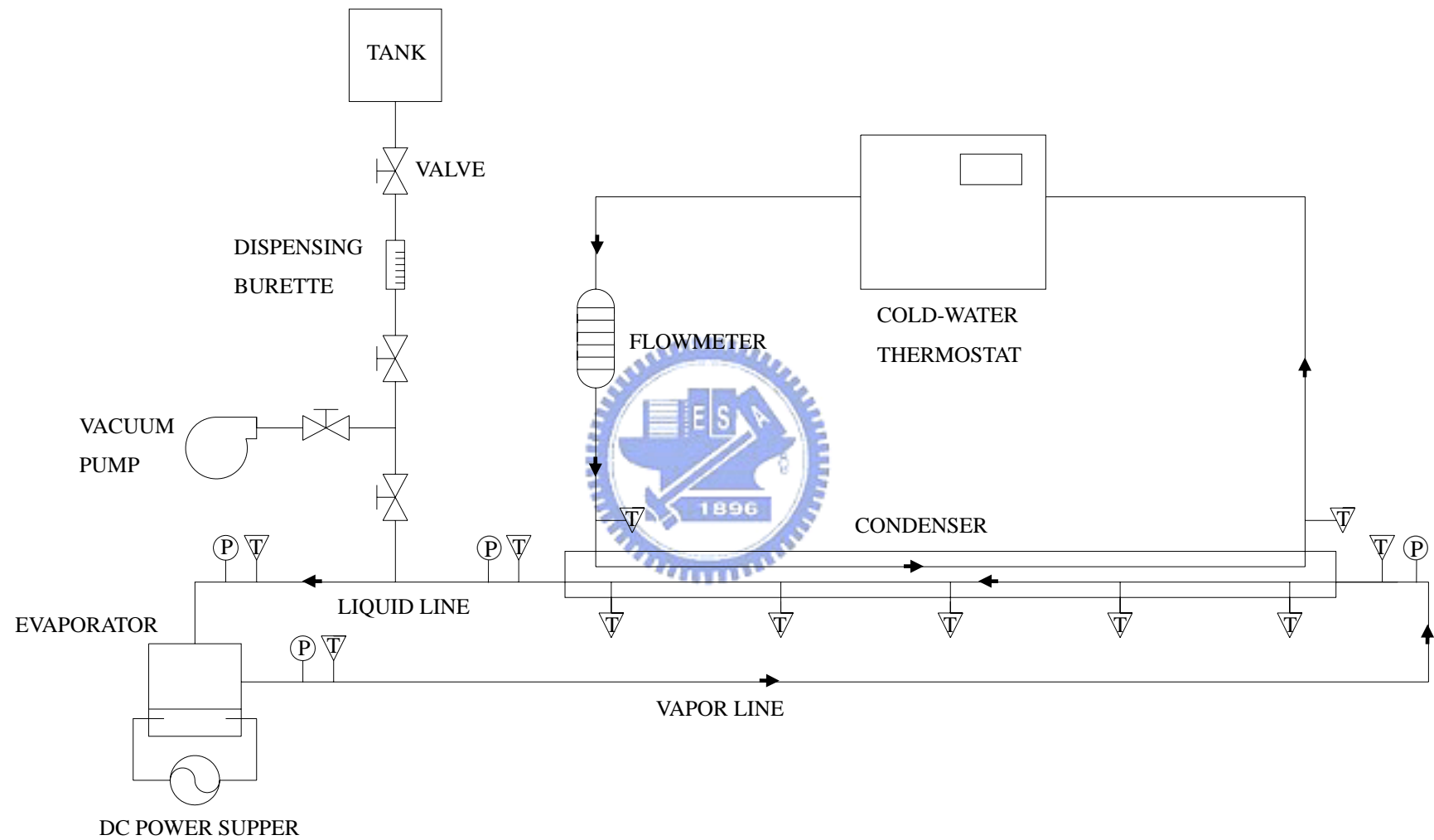
Fig. 2.1 Schematic diagram of experimental apparatus.
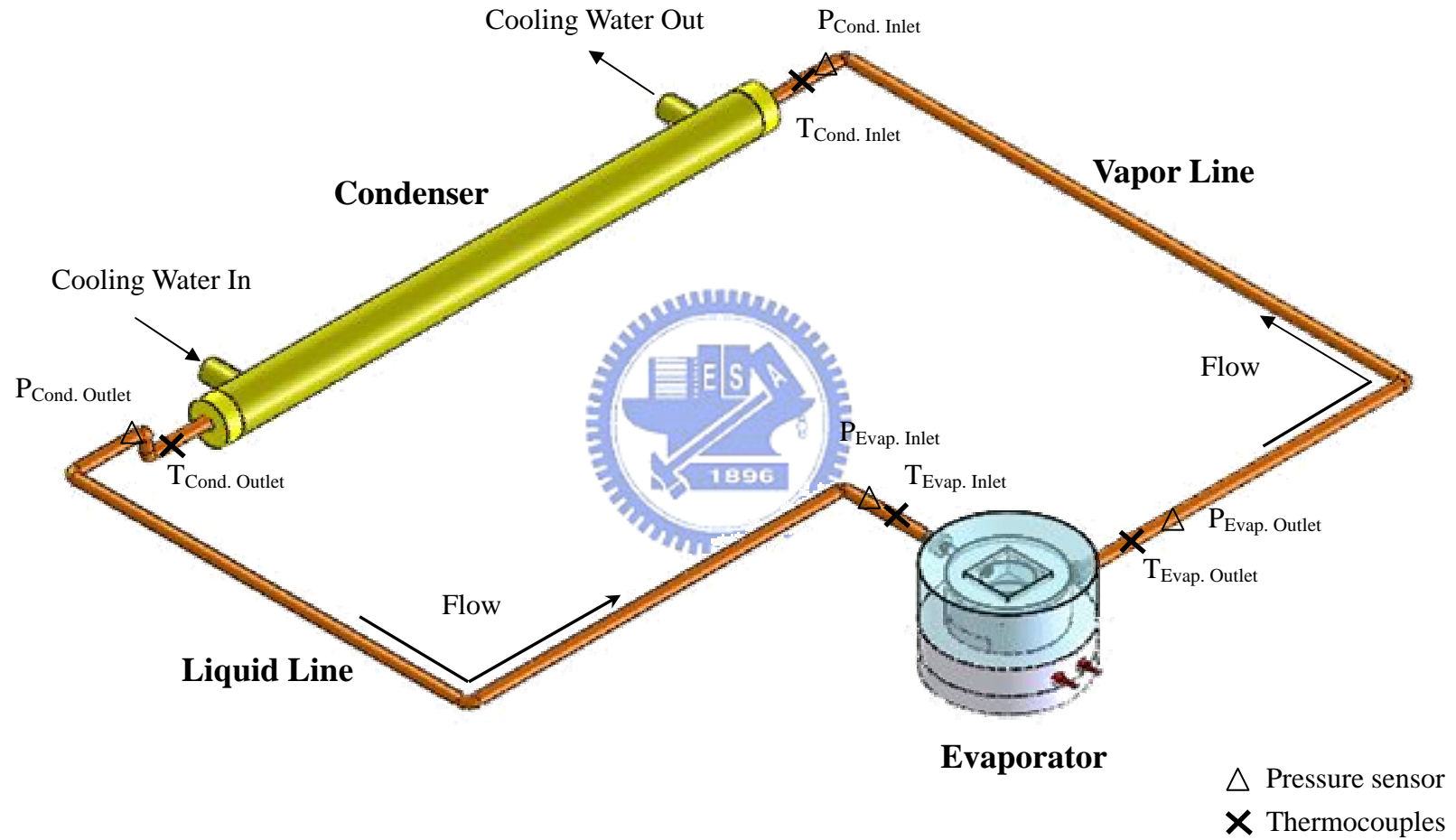
Fig. 2.2 Three-dimensional plots illustrating the CPL test loop.

Liquid

Vapor

Acrylic

Teflon cover

Window

Wick structure

Rectangular pin
fin block

Resistance
heaters

Heated copper
block

Teflon base
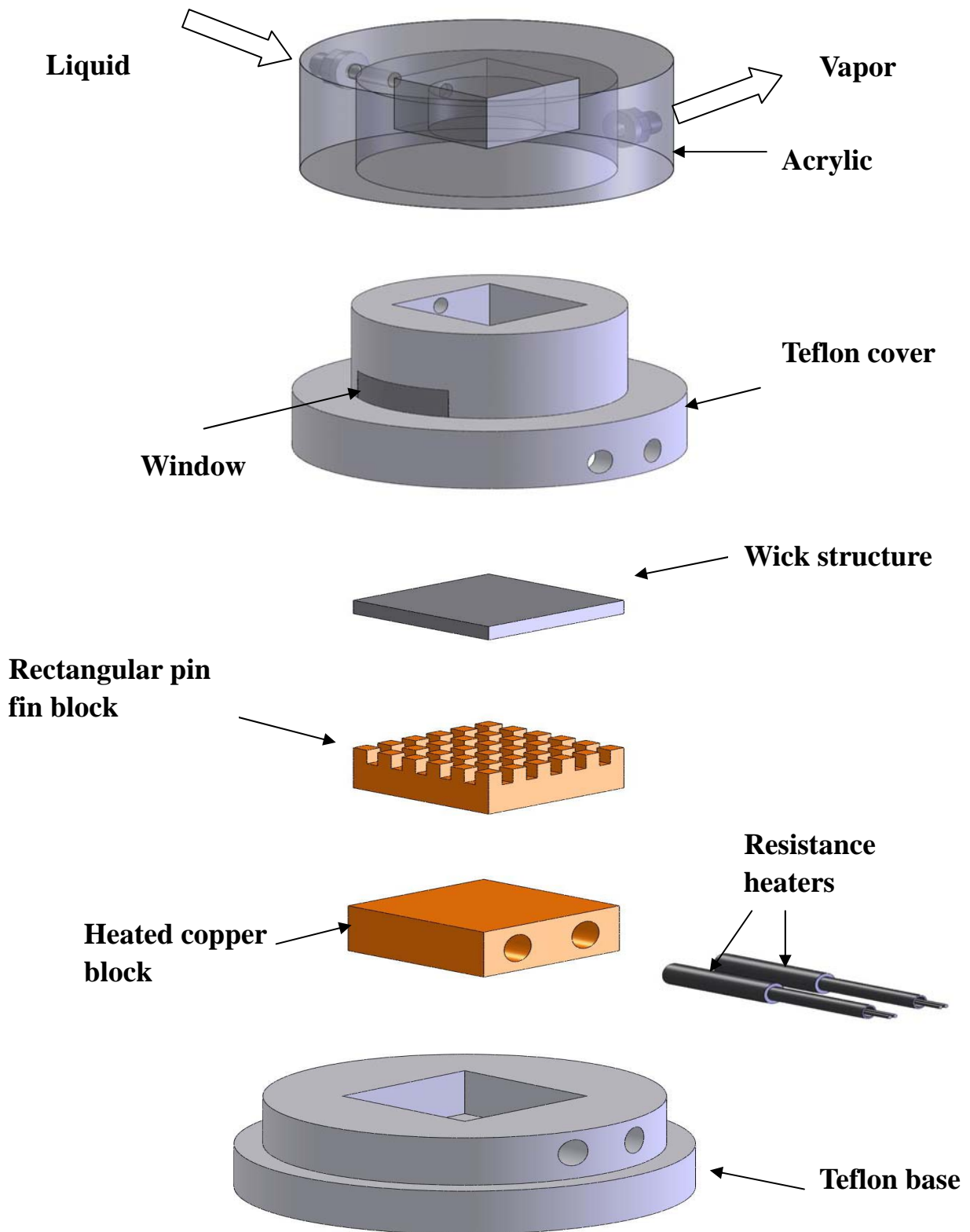
Fig. 2.3 The detailed structure of evaporator.
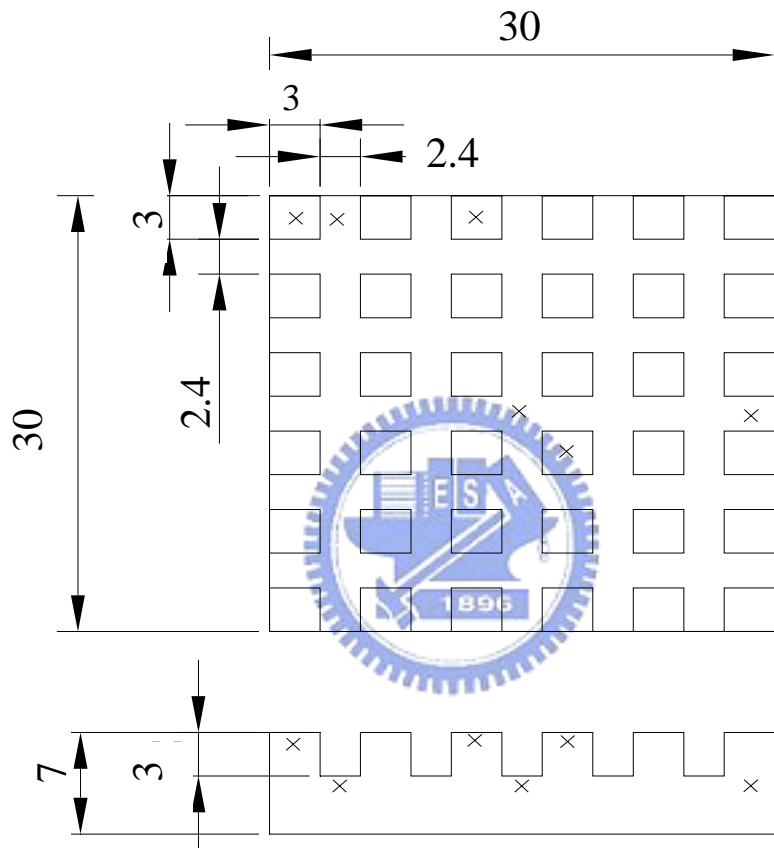
✕ Locations of
thermocouples

Unit : mm

Fig 2.4 The details of the dimensions of the type-1 pin fin block.

× Locations of
thermocouples

Unit : mm

Fig 2.5 The details of the dimensions of the type-2 pin fin block.

57

57

3

2.4

10
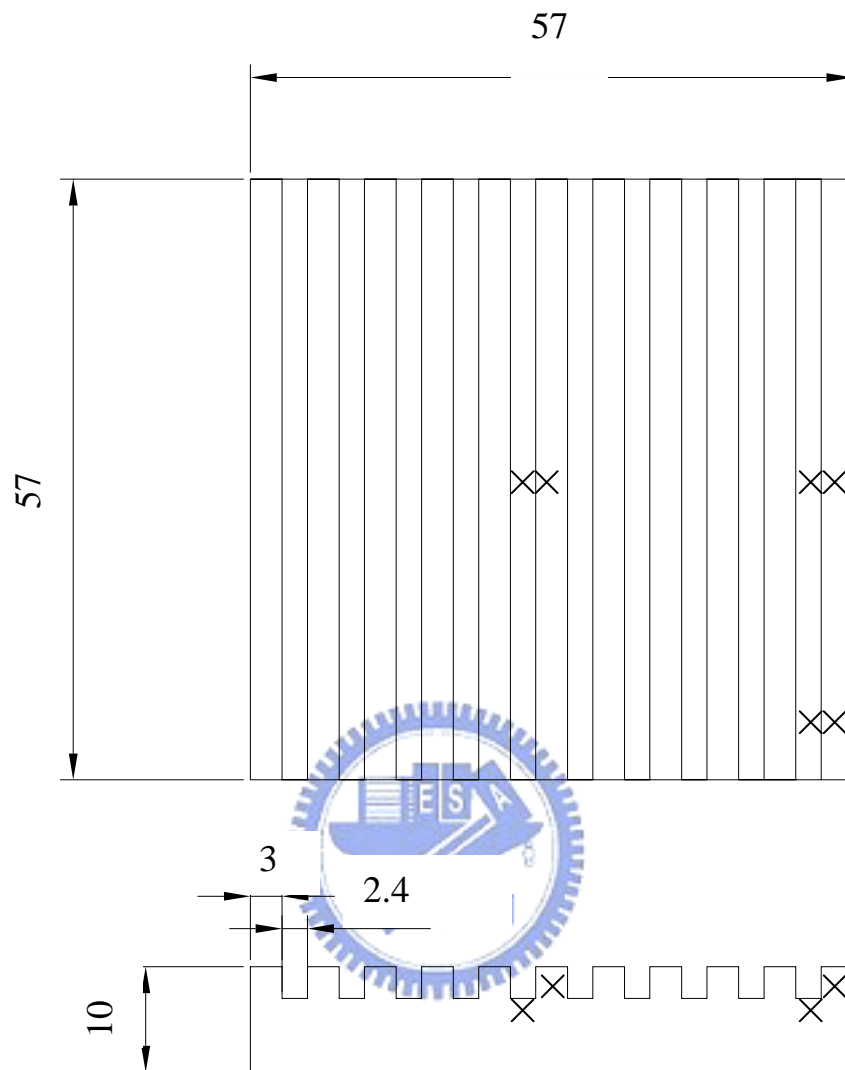
✕ Locations of
   thermocouples
Unit : mm

Fig 2.6 The details of the dimensions of the spreader grooved block.

26

1mm
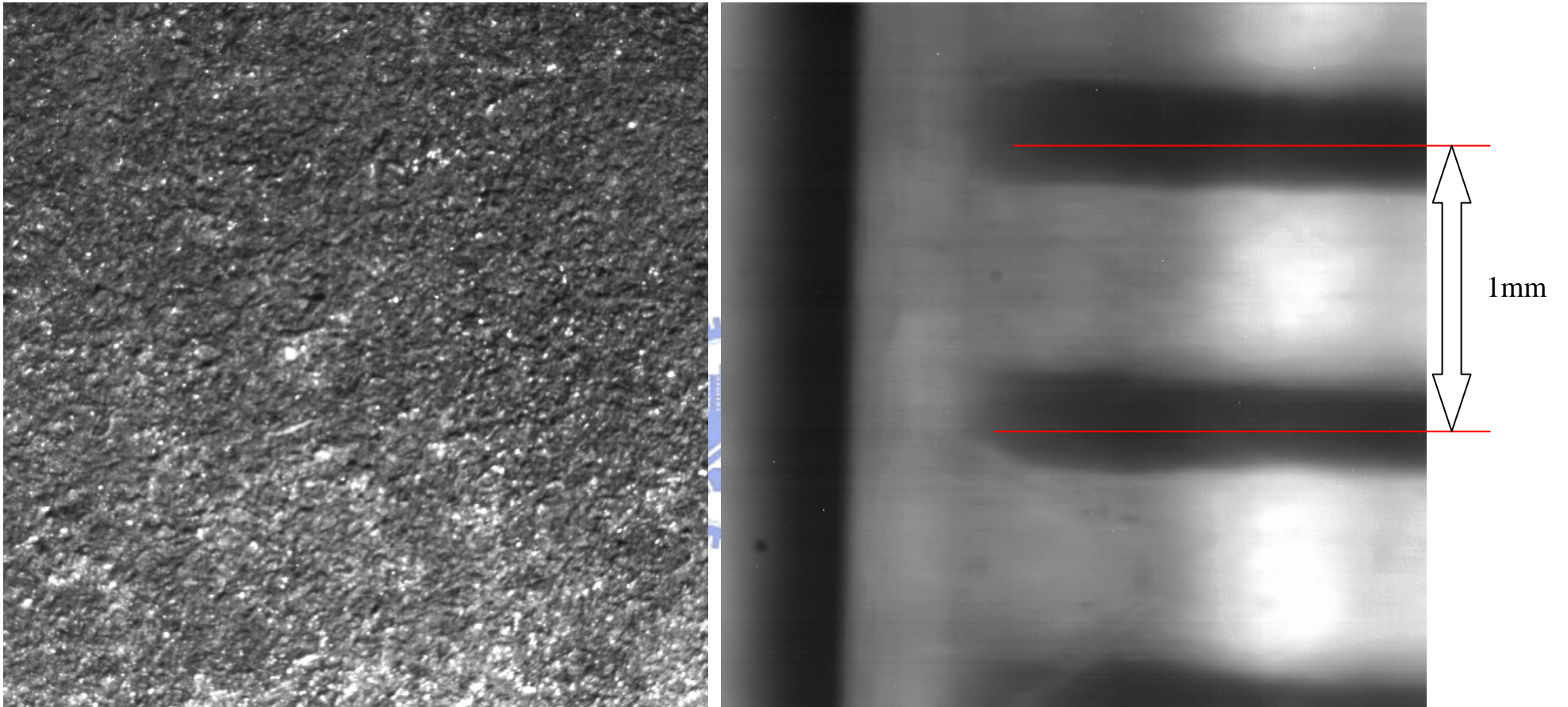
Fig. 2.7 Photographs of the roughing surface.
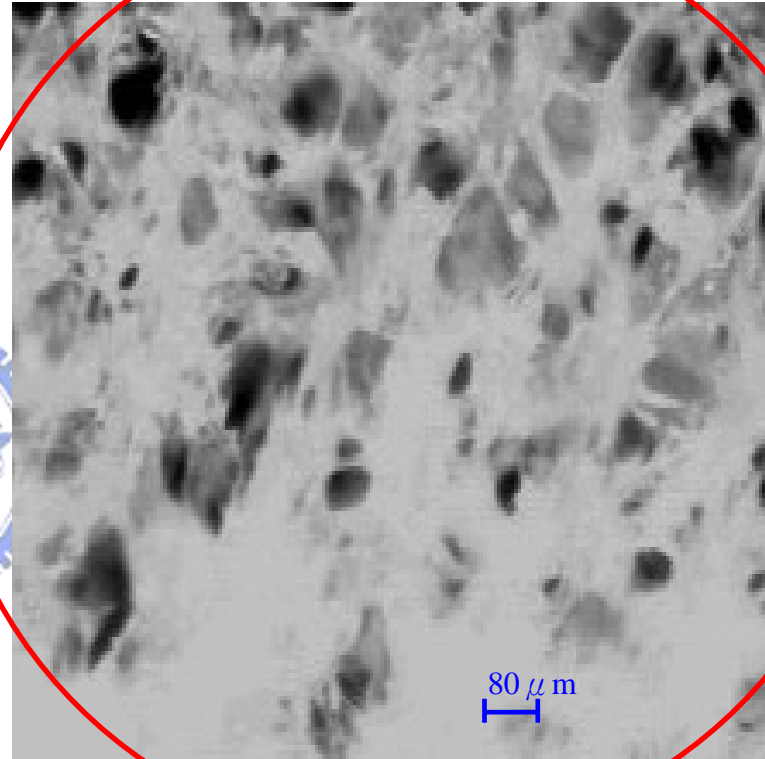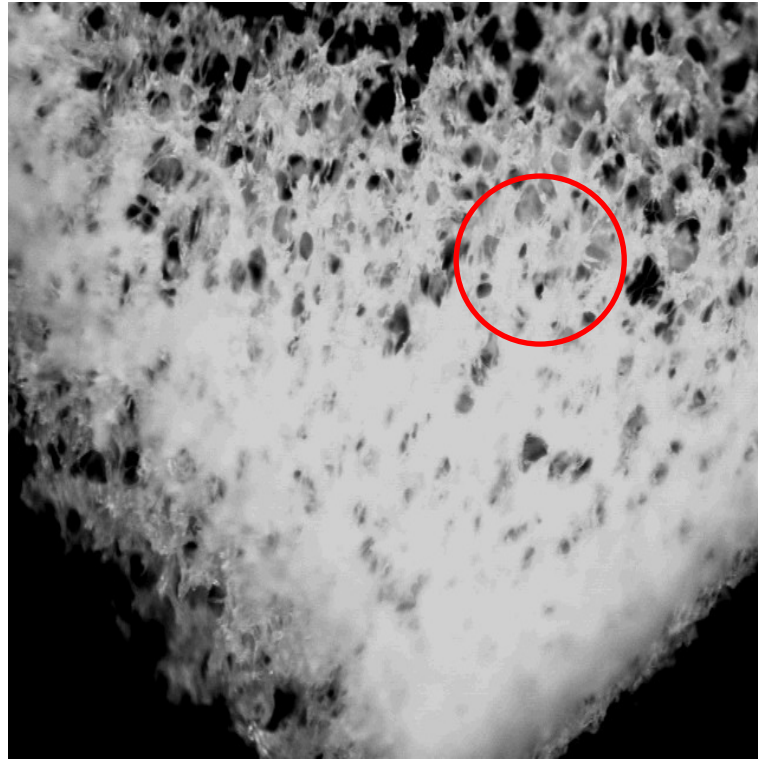
Fig. 2.8 Photographs of the polyvinyl alcohol.
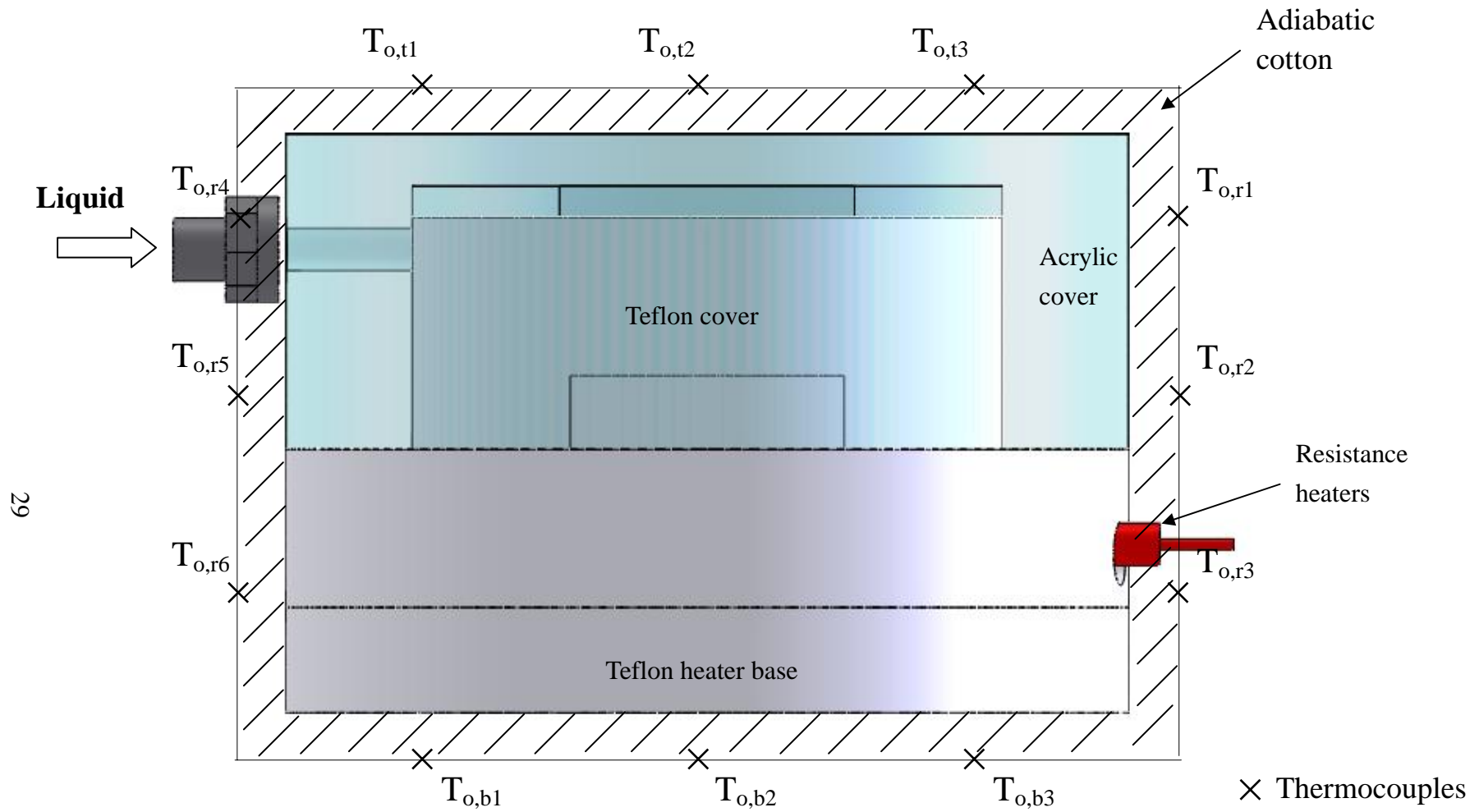
Fig. 2.9 Locations of the thermocouples at the outer surface of the adiabatic cotton

CHAPTER 3

DATA REDUCTION AND SIMPLE ANALYSIS

In the present test of an improved CPL system design, a data reduction analysis is needed to calculate the system thermal resistance from the measured raw data. On the other hand, the thermodynamic states, heat transfer limitation and pressure drop in the CPL loop are discussed in the following.

3.1 Data Reduction

Conventionally, the concept of the thermal resistance is adopted to represent the CPL performance. It shows the heat removal capacity of a CPL. The thermal resistance is usually defined as

$$R_{th} = \frac{T_{evap} - T_{cond}}{Q_e}$$

(3.1)

where T_{evap} is the mean measured temperature at the selected locations of the grooved block in the evaporator, T_{cond} is the mean temperature of the working fluid in the condenser, and Q_e is the effective power input to the CPL. The total power input Q_t and the effective power input Q_e are respectively evaluated from the equations:

$$Q_t = V \cdot I \qquad (3.2)$$

where V and I are individually the voltage drop across and electric current through the resistance heaters, and

$$Q_e = Q_t - Q_{loss} \qquad (3.3)$$

Here the heat loss from the evaporator Q_{loss} is approximately estimated from

the relation

$$Q_{loss} = h_{n,t} A_t (\overline{T_{o,t}} - T_{amb}) + h_{n,r} A_r (\overline{T_{o,r}} - T_{amb}) + h_{n,b} A_b (\overline{T_{o,b}} - T_{amb}) \tag{3.4}$$

indicating that the natural convection heat transfer from the outside surfaces of the evaporator to the ambient includes three major parts, namely, from the top, circumferential and bottom surfaces of the evaporator to the ambient. The associated natural convection heat transfer coefficients can be approximately evaluated from the empirical correlations [35] as

$$h_{n,t} = 1.32 \left[\frac{(\overline{T_{o,t}} - T_{amb})}{d} \right]^{0.25} \tag{3.5}$$

$$h_{n,r} = 1.42 \left[\frac{(\overline{T_{o,r}} - T_{amb})}{d} \right]^{0.25} \tag{3.6}$$

$$h_{n,b} = 0.59 \left[\frac{(\overline{T_{o,b}} - T_{amb})}{d} \right]^{0.25} \tag{3.7}$$

where h_n is the natural convection heat transfer coefficient from the outside surface of the superlon insulation layer to the ambient, A is the outside surface area of the superlon insulation layer, $\overline{T_o}$ is the average temperature of the outer surface of the superlon insulation layer, T_{amb} is the ambient temperature, and d is the diameter of the evaporator. The relative heat loss from the evaporator is defined as

$$\varepsilon = \frac{(Q_t - Q_e)}{Q_t} \times 100 \% \tag{3.6}$$

From the thermocouple data measured at the outside surface of the adiabatic cotton covering the evaporator, the heat loss from the evaporator to the ambient is estimated. The results from this estimation show that the heat losses for all cases investigated here are all less than 3.0 %.

3.2 Thermodynamic States and Heat Transfer Limitation

As discussed in chapter 1, CPL is a two-phase liquid-vapor heat transport device consisting of an evaporator containing a wick structure, a condenser, a reservoir, and distinct liquid and vapor lines. There is no reservoir element in the present study. Figure 3.1(a) schematically shows a typical CPL system without reservoir. The corresponding thermodynamic states of the working fluid at various locations of the CPL are indicated in Fig. 3.1(b). At location 1 (the wick-copper block contacted heating zone), liquid vaporizes at the saturation state and the vapor moves through the grooves, resulting in some pressure loss and the vapor becomes superheated at location 2. The vapor finally flows into the vapor line. Some pressure loss also results in the vapor line as the vapor moves through it and the vapor is still superheated at location 3. After entering the condenser, the vapor condensation occurs. Thus we have two-phase liquid-vapor mixture at locations 4 and 5. Beyond location 5, all vapor is condensed and the working fluid is in liquid state. The working fluid continues to cool down in the condenser and reaches a subcooled temperature at the condenser exit at location 7. The liquid flows back to the evaporator through the liquid line, accompanying with some pressure loss. At the inlet of the evaporator (location 8) the liquid is subcooled. As the liquid moves into the wick, it gets heated. Boiling and evaporation take place near the wick- copper block contacted region at location 9. This completes the thermodynamic cycle for the CPL.

The heat transfer limits of a CPL are similar to that of heat pipe. The major heat transport limits for a CPL are:

1) Capillary limit:

In a normal CPL operation, the wick structure should produce sufficient capillary force to drive the vapor and liquid flows. For a raise in the heat input to the evaporator, the liquid and vapor flows speed up, leading to an increase in the flow

resistance as the menisci form at the liquid/vapor interface. This means that the capillary force should be high enough to circulate the flow of the working fluid along the loop. When the radii of curvature for the menisci get larger at a higher heat input so that they are equal to the capillary radius, the capillary pressure reaches a maximum level, resulting the so called "capillary limit".

2) Boiling limit:

As the heat input to the evaporator exceeds certain value, boiling of liquid begins and vapor bubbles start to appear inside the wick structure. At a relatively high heat input bubbles are generated at a large size and at a vary high rate. The bubbles would block the wick structure and form a layer of vapor film in the contact zone. Therefore, the resulting thermal resistance becomes very large and heat transfer capability of the CPL deteriorates. This is designated as the "boiling limit".

3) Sonic limit:

The vapor mass flux is known to increase with the magnitude of the heat input. As the vapor speed arrives at the sonic point, the flow in the CPL will be choked, resulting the "sonic limit".
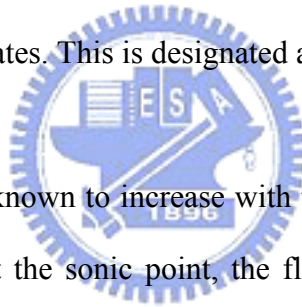
3.3 System Pressure Drop Analysis

In view of the presence of the capillary limit, the maximum capillary pressure generated in the wick should be greater than or equal to the overall loop pressure drop for a CPL to function well. Hence,

$$\Delta P_{cap,\max} \geq \Delta P_v + \Delta P_l + \Delta P_{vg} + \Delta P_w + \Delta P_g \tag{3.7}$$

here $\Delta P_{cap,\max}$ is the maximum capillary pressure, ΔP_v the total pressure drop in the vapor line, ΔP_l the total pressure drop in the liquid line, ΔP_{vg} the total pressure drop in the grooved channels, ΔP_w the total pressure drop of fluid passing through

the wick structure, and ΔP_g the pressure drop due to the gravity. These terms are described in the following.

3.3.1 Maximum capillary pressure

In a steady CPL operation, the capillary pressure can be calculated from the contacted angle of vapor-liquid interface θ, working fluid surface tension σ and effective capillary radius r_c. When the contact angle is equal to zero, we obtain a maximum capillary pressure. In that case, the curvature radius of the vapor-liquid interface is equal to the effective capillary radius. Specifically,

$$\Delta P_{cap} = \frac{2\sigma \cos\theta}{r_c} \tag{3.8}$$

When $\theta = 0$,

$$\Delta P_{cap,\max} = \frac{2\sigma}{r_c} \tag{3.9}$$

3.3.2 Pressure drops in transport lines

The transport lines include the vapor line and liquid line. Note that in the transport lines the fluid flow in the tubes is assumed to be fully-developed. The total pressure drop in the tube due to the friction, the so called "major losses", can be evaluated from the relation

$$\Delta P_{major} = f \frac{L}{D} \frac{\rho V^2}{2} \tag{3.10}$$

where f is the friction factor, L is the flow length, D is the tube diameter, ρ is the density of working fluid, V is the average speed of the working fluid.

If the flow is laminar and fully–developed for the Reynolds number ≤ 2300, the friction factor can be expressed in a simple relation as

$$f = \frac{64}{Re} \tag{3.11}$$

For 2300 < Re <10,000 the friction factor can be approximately evaluated from the Gnielinski correlation [36] as

$$f = \left(1.82 \log_{10} \mathrm{Re} - 1.64\right)^{-2} \qquad \qquad . (3.12)$$

For Re > 10,000 the flow can be considered as turbulent. When the tube is smooth and the flow is turbulent, the friction factor can be approximately evaluated from the Blasius correlation [37] as

$$f = \frac{0.316}{\mathrm{Re}^{1/4}} \qquad \qquad (3.13)$$

3.3.3 Pressure drop in grooved channels

The pressure drop resulting from the vapor passing through grooved channels of the evaporator can be estimated as

$$\Delta P_{vg} = f \frac{L}{D_h} \frac{\rho V^2}{2} \qquad \qquad (3.14)$$

where L is the grooved channel length and D_h is the hydraulic diameter of each grooved channel.

3.3.4 Pressure drop in wick structure

According to the Darcy's law for a low speed single-phase liquid flow moving in a porous medium and assuming the flow being one-dimensional in z-direction and laminar, the flow speed can be approximated as

$$V_z = -\frac{K_w}{\mu_l} \left(\frac{\partial p}{\partial z} \right) \qquad \qquad (3.15)$$

From the Conservation of Mass, we also have

$$V_z = \frac{\dot{m}}{\rho_l A_c} \qquad \qquad . \quad ..(3.16)$$

Combining the above two equations gives

$$\Delta P_w = \frac{\mu_l \dot{m} \ell}{\rho_l A_c K_w}$$

(3.17)

here K_w is the permeability of wick structure, μ_l is the liquid viscosity of the working fluid, ℓ is the thickness of the wick structure, A_c is the cross-sectional area of the wick structure, $\dot{m}$ is the mass flow rate, and V_z is the vertical flow velocity.

3.3.5 Pressure drop due to gravity

If there is a relative height between the evaporator and condenser, the gravitational head should be considered. It can be calculated from the relation

$$\Delta P_g = \rho_l g h \tag{3.18}$$

where g is the gravitational acceleration, h is the difference in the heights of the evaporator and condenser.

3.4 Estimate of Mass Flow Rate

In a steady CPL operation, the energy balance for the evaporator can be expressed as

$$Q_e = Q_{h_{fg}} + Q_{C_P \Delta T} \tag{3.19}$$

Assuming the sensible energy transfer is small compared with the latent energy transfer, the above equation can be written as

$$Q_e \approx Q_{h_{fg}} = \dot{m} \, h_{fg} \tag{3.20}$$

thus the mass flow rate of the working flow in the CPL can be calculated from the relation

$$\dot{m} = \frac{Q_e}{h_{fg}} \tag{3.21}$$

here Q_e is the effective power input to the CPL, $\dot{m}$ is the mass flow rate, and h_{fg} is the latent heat of evaporation. Using this estimated mass flow rate in the above equations for the pressure drop analysis we can evaluate the pressure drops in each section of the CPL.

3.5 Uncertainty Analysis

Uncertainties of the thermal resistance are estimated according to the procedures

proposed by Kline and McClintock [38]. The detailed results from this uncertainty

analysis are summarized in Table 3.1.

Table 3.1   Summary of the uncertainty analysis

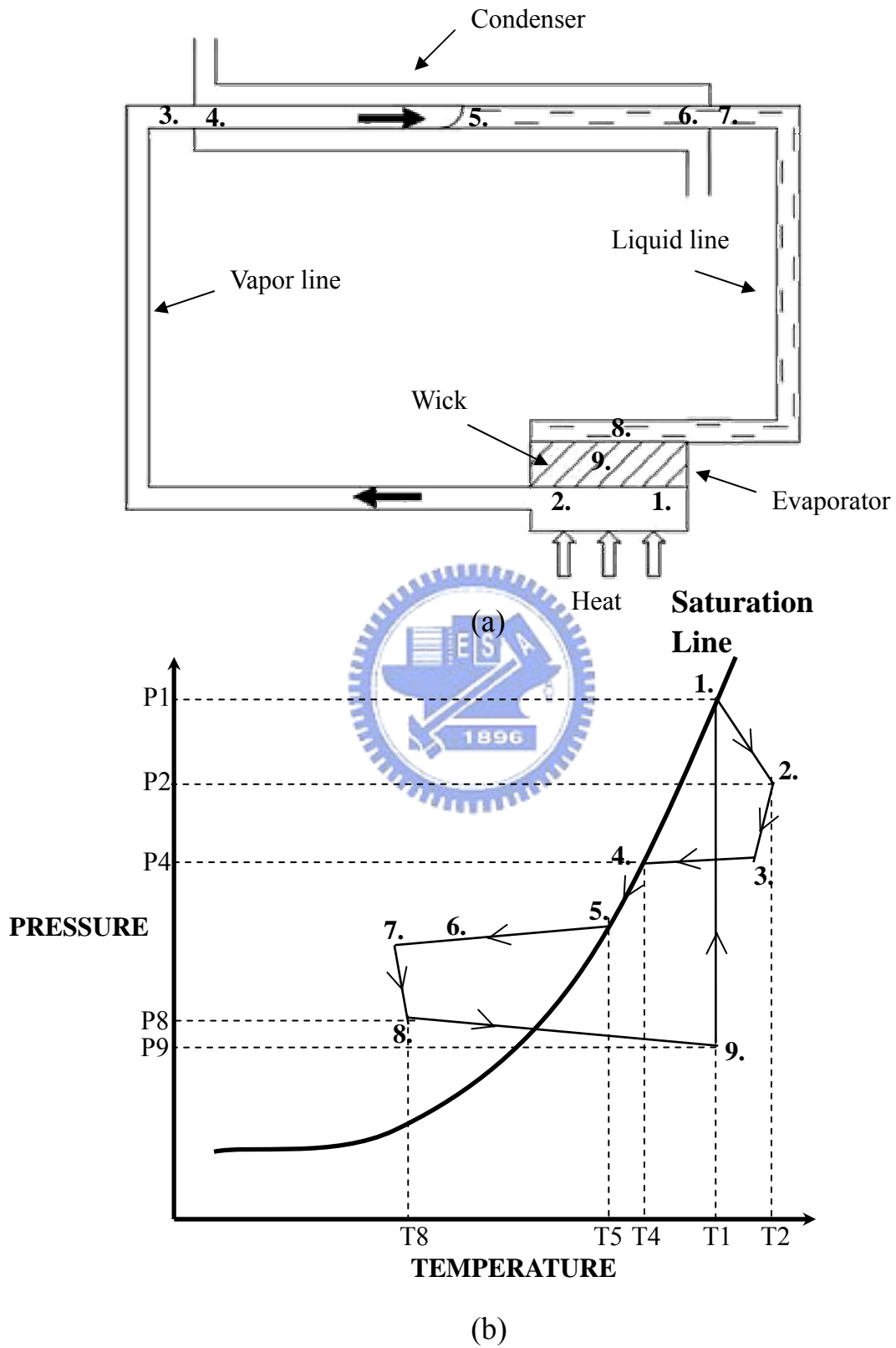| Parameter	Uncertainty
Length of grooved copper block (m)	±0.0005
Width of grooved copper block (m)	±0.0005
Thickness of grooved copper block (m)	±0.0005
Dimensions of grooved channel (m)	±0.00005
Temperature, T (℃)	±0.2
Temperature difference, ΔT (℃)	±0.28
Current, I (%)	±0.206
Voltage, V (%)	±0.05
Total heat load, Q_t (%)	±0.212
Heat loss, Q_{loss} (%)	±10.2
Thermal resistance, R (%)	±11.1

Fig. 3.1 Schematic of CPL system (a) and the corresponding P-T diagram at various locations (b).

CHAPTER 4

RESULTS AND DISCUSSION

This chapter presents the experimental data obtained in the present investigation of an improved CPL system. The effects of the liquid inventory and the relative height between the evaporator and condenser on the heat transfer performances of the CPL with three different improved designs are examined. The liquid inventory is defined as the ratio of the total volume of working fluid in the loop to the total loop volume available for the working fluid. Table 4.1 gives the volume of each component in the CPL system available for the working fluid to pass through. The results obtained here for the grooved channels formed by the square pin fins are compared with those for the grooved channels formed by the plane fins measured in the previous study [34]. Besides, the effects of using the heat spreader and roughing the vertical and bottom surfaces of the grooved channels on the CPL performance will be examined.

In the experiment, the mean evaporator temperature ($\overline{T}_{evap}$) and condenser temperature ($\overline{T}_{cond}$), which are the average temperatures measured at selected locations in the block containing the grooved channels and the condenser (double-tube heat exchanger), and the temperatures of the working fluid measured at the inlets and exits of the evaporator and condenser shown in Figures 2.2, 2.4 and 2.5 will be inspected. It should be mentioned that the experimental test of the present CPL system will be terminated as the mean evaporator temperature exceeds 80℃.

4.1 Performance Comparison between Vapor Channels Formed by Pin Fins and Plane Fins

In testing the CPL performance with the vapor channels formed by the pin fins

and plane fins, the relative height between the evaporator and condenser is first fixed

at 0 cm, and the liquid inventory is at 62%. Figure 4.1 shows the results from this test.

It is first noted that the maximum heat transfer performance of the type-2 pin fin

block is about 120W before $\overline{T}_{evap}$ exceeds 80℃ and it is lower than that for the

type-1 pin fin block and grooved block. This clearly indicates that using the pin fins to

form the vapor channels in the copper block is less effective in vapor transport than

the grooved channels. This result, in turn, is the consequence of the vapor flows in

various parts of channels formed by the pin fins being normal to each other, causing a

mutual retarding of the vapor to move slower into the vapor transport line. It was

further noted in the test that the amplitude of the temperature oscillation in the

evaporator for the pin fin blocks is about 1℃.

Then, comparison is made for different liquid inventories with the relative

height between the evaporator and condenser fixed at 0 cm. The liquid inventory is

varied from 50% to 75%. The test is conducted for the type-1 pin fin block and the

results are shown in Figure 4.2. These results are compared with that for the grooved

block in Figures 4.3 - 4.5. Note from the results in Figure 4.2 for the type-1 pin fin

block that at the liquid inventory of 62% the CPL has the highest heat transfer

capability $Q_{e,max}$ of 141W. For the other two liquid inventories $Q_{e,max}$ is much lower

especially for the liquid inventory of 57%. The results in Figures 4.3 - 4.5 indicate

that only at the liquid inventory of 75% the CPL heat transfer performance for the

type-1 pin fin block is better than the grooved block.

Finally, the effects of the relative height between the evaporator and condenser

on the CPL performance with the pin fin and plane fin blocks are tested. Here we only

test the type-1 pin fin block with the liquid inventory fixed at 62%. The relative height

is varied from 0cm to 10cm and the evaporator is higher than the condenser. The

results from this comparison are shown in Figures 4.6 - 4.8. It is noted that the CPL system with the pin fin block has a worse heat transfer performance than the system with the plane fin block at all relative heights tested. Figure 4.9 shows the mean temperature at the evaporator and thermal resistance variations with the power input to the evaporator for the relative height varied from 0cm – 10cm for the type-1 pin fin block. Note that the maximum allowable power input to the evaporator $Q_{e,max}$ increases with the increase in the relative height.

4.2 Installation of Heat Spreader

In examining the performance of the CPL system with the heat spreader containing the grooved channels formed by the plane fins, the liquid inventory is varied from 44% to 71% and the relative height between the evaporator and condenser ranges from 0 cm to 10 cm. It should be noted that in the test of the heat spreader effects, the volume of the whole loop available for the working fluid is larger than the previous test. The volume of each component for the loop with the heat spreader is shown in Table 4.2. The data measured from the CPL system with the heat spreader are inspected in the following.

The measured data for the variations of the mean evaporator and condenser temperatures and the temperatures at the evaporator and condenser inlets and exits along with the thermal resistances of the CPL with the power input to the evaporator are shown in Figures 4.10 - 4.16 for various liquid inventories at the relative height of 0 cm. The results indicate that in the sections where the vapor flow dominates at the evaporator outlet and condenser inlet, the measured temperatures increase significantly with the power input, so does the evaporator temperature. Besides, the measured temperatures at the condenser outlet and evaporator inlet are close to the saturated temperature of the working fluid. To illustrate the effects of the liquid

inventory on the performance of the CPL with the heat spreader, Figure 4.17 compares the data for the liquid inventory varied from 44% to 71%. The results manifest that the maximum allowable power input increases when the liquid inventory decreases from 71% to 59%, and decreases when the liquid inventory decreases further from 59% to 53%. But the maximum allowable power input increases again when the liquid inventory decreases from 53% to 47%. At the optimal liquid inventory of 47% the minimum thermal resistance is about 0.2℃/W and the maximum allowable power input is about 290W. Note that at the lower liquid inventory ranging from 44% to 53%, an unusual phenomenon of a small decrease in the mean evaporator temperature for an increase in the power input is observed at low power input. It is conjectured to be caused by a larger two-phase region in the condenser due to an insufficient liquid in the condenser.

How the relative height between the evaporator and condenser affects the performance of the CPL with the heat spreader is examined next. Figures 4.18 - 4.20 show the test results at the liquid inventory of 59% for various height differences between the evaporator and the condenser. Comparing the results in Figures 4.18-4.20 reveals that the maximum allowable power input increases substantially with the increase in the relative height (Figure 4.21). This is simply due to the fact that the liquid in the condenser flows back to the evaporator more easily at the larger relative height due to the stronger gravity effects. However, at the lower liquid inventory of 47% the data presented in Figures 4.22-4.25 show that there is no significant effect of the relative height on $Q_{e,max}$. The anomaly at the lower liquid inventory discussed above reduces the effect of the relative height.

Finally, the present data for the CPL system with the heat spreader installed in the evaporator are compared with the previous study without using heat spreader [34]. The results from this comparison are shown in Figure 4.26 for various liquid

inventories for the relative height of 0 cm. Note that the system installed with the heat spreader has a much higher $Q_{e,max}$ at all liquid inventories. We further compare the results for the case of optimal liquid inventories for the systems with and without the heat spreader in Figure 4.27. The results show that at the optimal liquid inventories of 47% and 62% respectively for the systems with and without the heat spreader, $Q_{e,max}$ is increased by nearly 100% simply by using the heat spreader. The effects of heat spreader at the relative heights between evaporator and condenser of 5 cm and 10 cm are shown in Figures 4.28 and 4.29.

4.3 The Effects of Roughing the Surfaces of Grooved Channels

The effects of roughing the vertical and bottom surfaces of the grooved channels on the CPL performance are examined in this section. The heat spreader containing the grooved channels formed by the plane fins is installed in the evaporator in this test.

The measured data from this test are shown in Figures 4.30 - 4.34 for various liquid inventories for the relative height fixed at 0 cm. It is clearly noted that the maximum allowable power input increases when the liquid inventory decreases from 59% to 50%, and decreases when the liquid inventory decreases further from 50% to 47%. The maximum allowable power input at the inventory of 50% is about 325W and the minimum thermal resistance is about 0.17 ℃/W. Note that the anomaly at the lower liquid inventory discussed in section 4.2 is also observed in Figures 4.30 and 4.31.

Comparison of the CPL performance for the grooved channels with and without surface roughing is shown in Figure 4.35. The results indicate that roughing the surfaces of the vapor channels can effectively improve the heat transfer performance. We further compare the results for the case of optimal liquid inventories for the

44

systems with and without the surface roughing for the vapor channels in Figure 4.36. The enhancement for $Q_{e,max}$ about 10% can be obtained.

Finally, the test results about the relative height at the optimum liquid inventory of 50% are presented in Figures 4.37 - 4.40. The maximum allowable power input $Q_{e,max}$ also increases with the increase in the relative height. But it can be noted from Figure 4.40 that the enhancement is small at the optimum liquid inventory. Selected test data at other liquid inventories are shown in Figures 4.41 – 4.48. Note that at the other liquid inventories the increase in the relative height between the evaporator and condenser can also noticeably enhance the maximum allowable power input to the evaporator with the surface roughing on the grooved channels. The more effects of vapor channels with surface roughing at the relative heights between evaporator and condenser of 5 cm and 10 cm are shown in Figures 4.49 and 4.50.

In order to simulate cooling a CPU chip, the results presented above are for the cases that the tests are terminated when the mean evaporator temperature reachs 80℃. The test results for the terminating T_{evap} increased to 85℃ and 90℃ for various liquid inventories are shown in Figures 4.51 – 4.54. Quantitatively, the data show that for the terminating T_{evap} raised from 80℃ to 90℃ the maximum allowable power input to the evaporator can be increased by about 20% on an average (Figure 4.54). It is noted that the maximum allowable power input to the evaporator is increased noticeably for a rise in the terminating T_{evap}. Besides, the thermal resistance almost maintains at a constant for each liquid inventories when the power input is larger than 300W.

Table 4.1 Volume of each component in the CPL system without heat spreader

Component		Volume (cm^3)
Evaporator	liquid storage	7.5
	grooved channel	2
Condenser		5.5
Liquid line		12.5
Vapor line		12.5
Total		40

Table 4.2 Volume of each component in the CPL system with heat spreader in evaporator.

| Component		Volume (cm^3)
Evaporator	liquid storage	46.5
	grooved channel	8
Condenser		5.5
Liquid line		12.5
Vapor line		12.5
Total		85
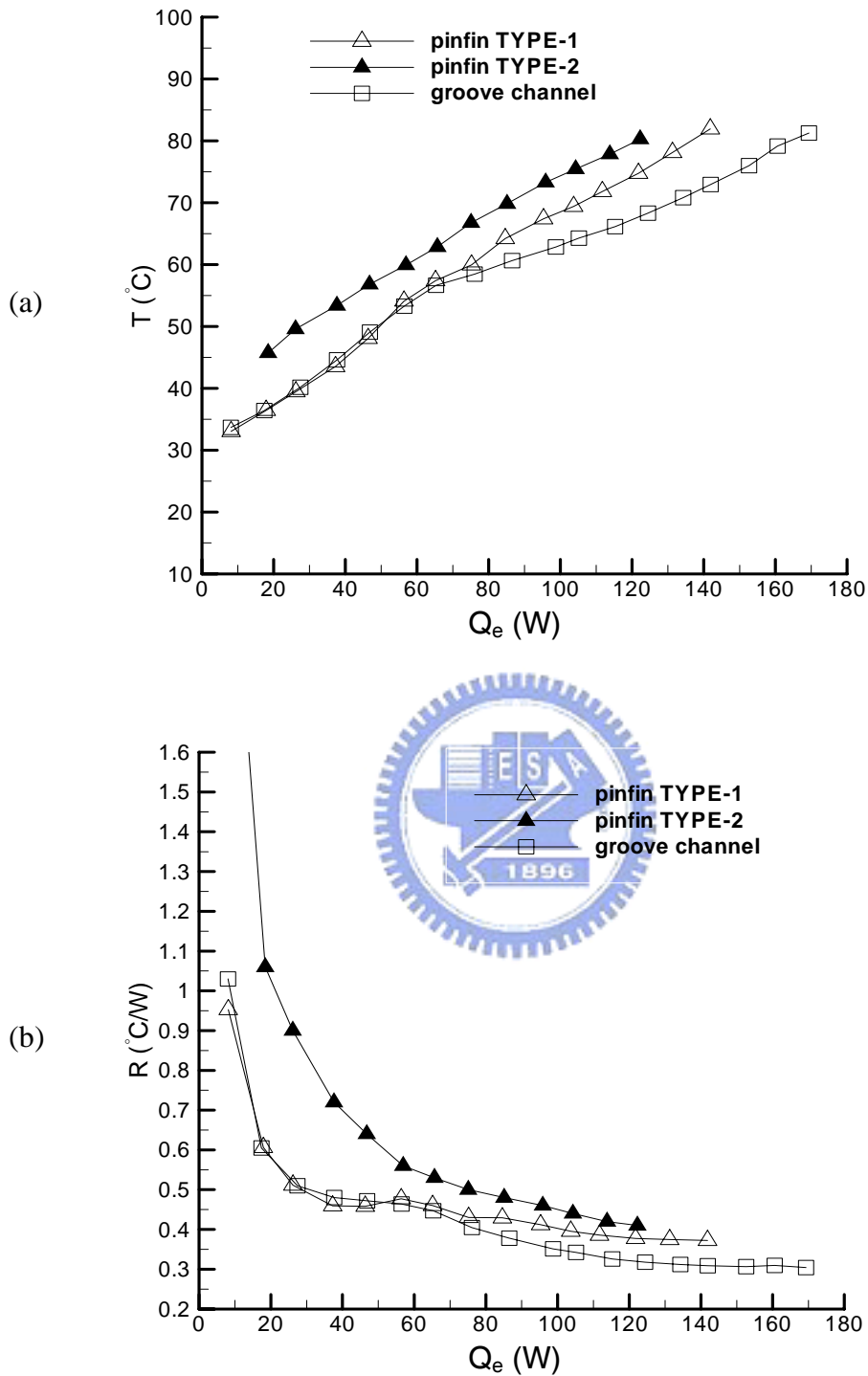
Figure 4.1 Variations of mean evaporator temperature (a) and thermal resistance of the CPL (b) with the input power to the evaporator for the liquid inventory of 62% and relative height between condenser and evaporator of 0 cm for CPL with pin fin and plane fin blocks.
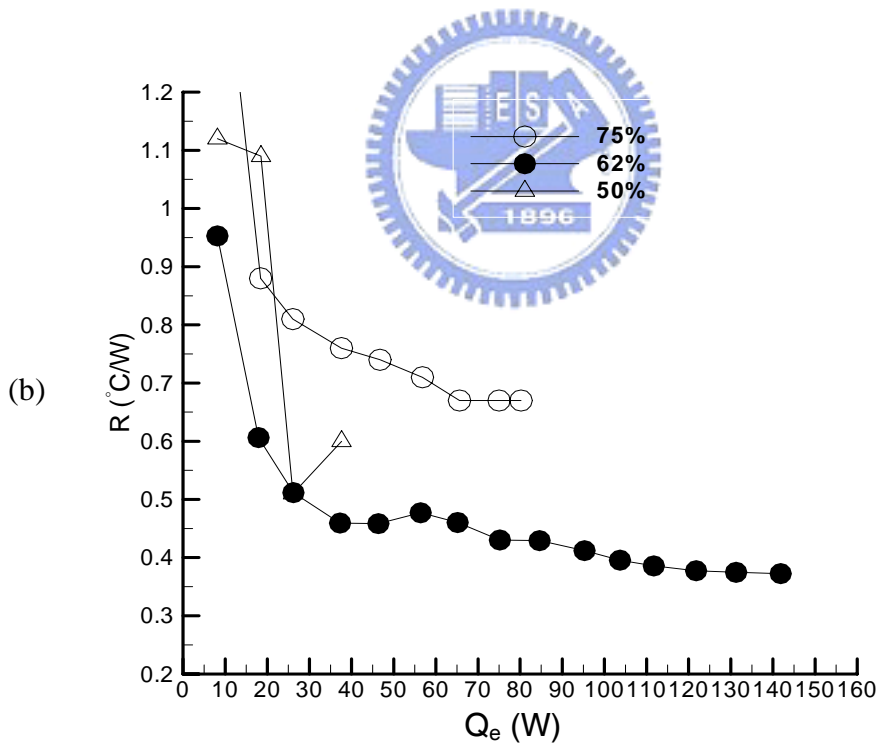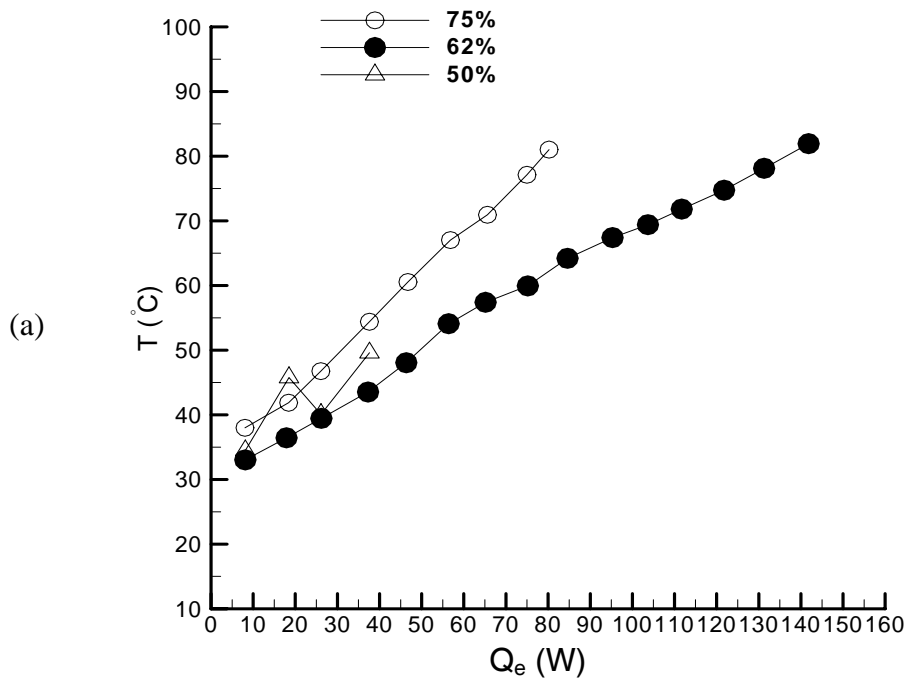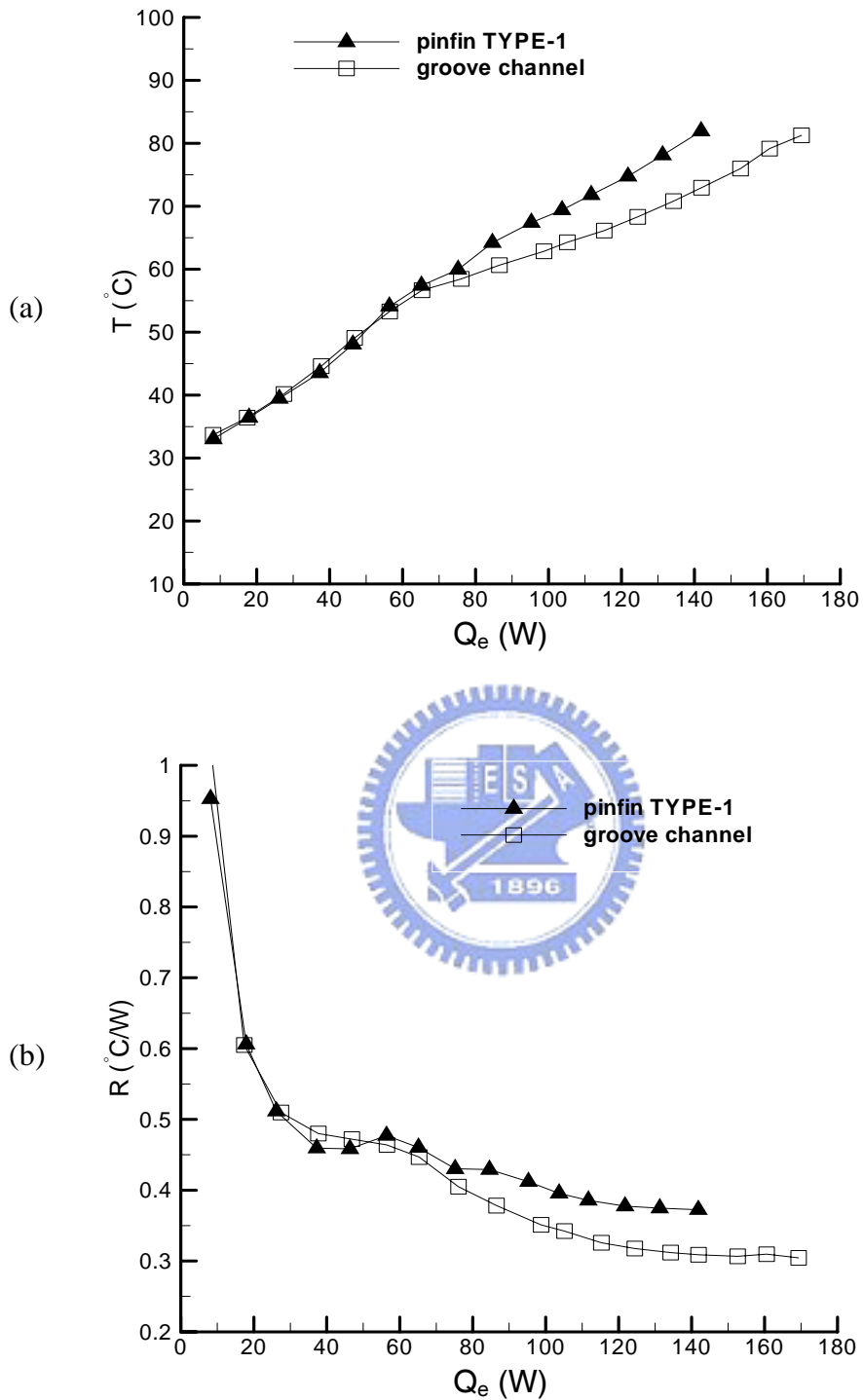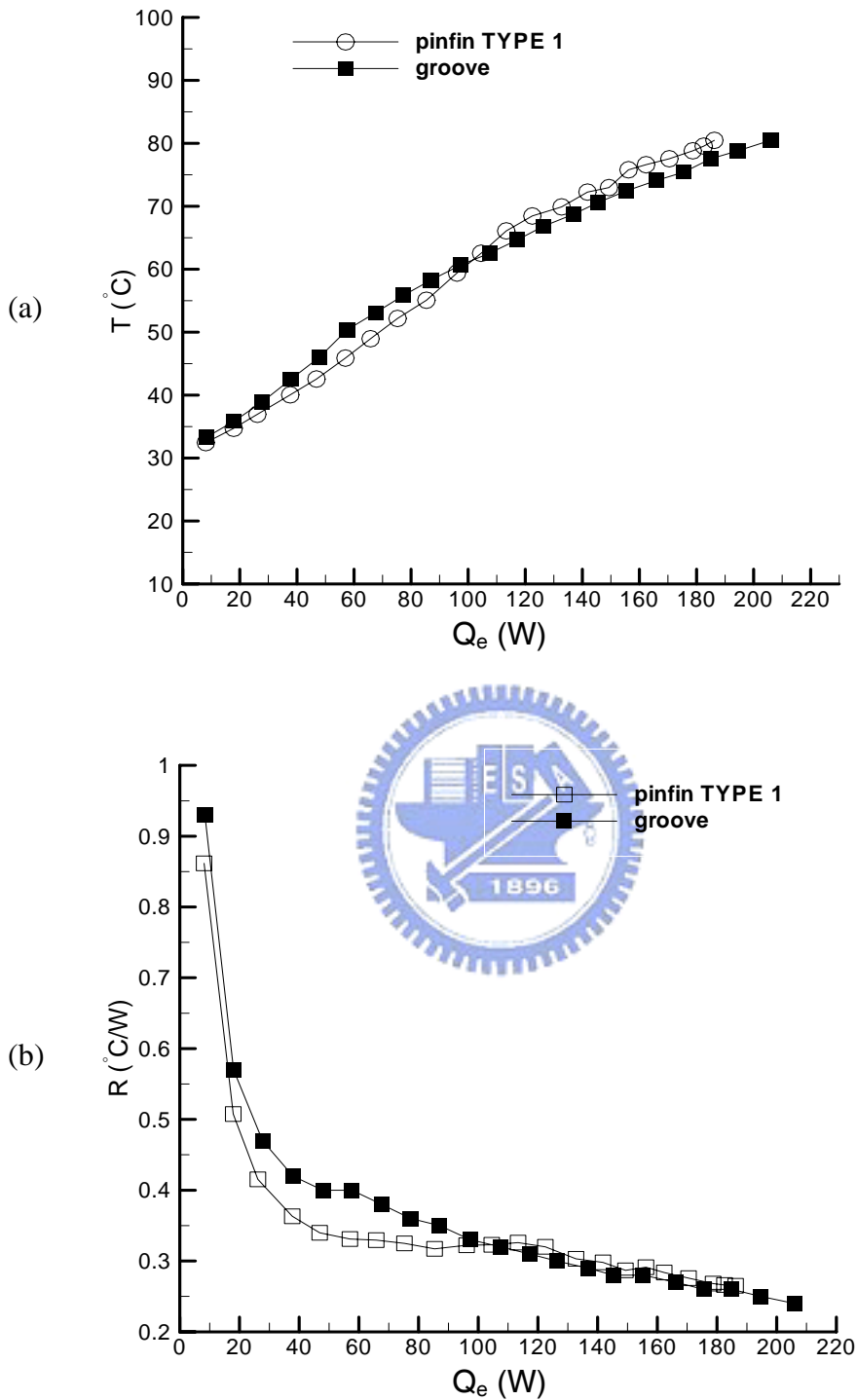
Figure 4.2 Variations of mean evaporator temperature (a) and thermal resistance of the CPL (b) with the input power to the evaporator using type-1 pin fin block for relative height between condenser and evaporator of 0 cm.
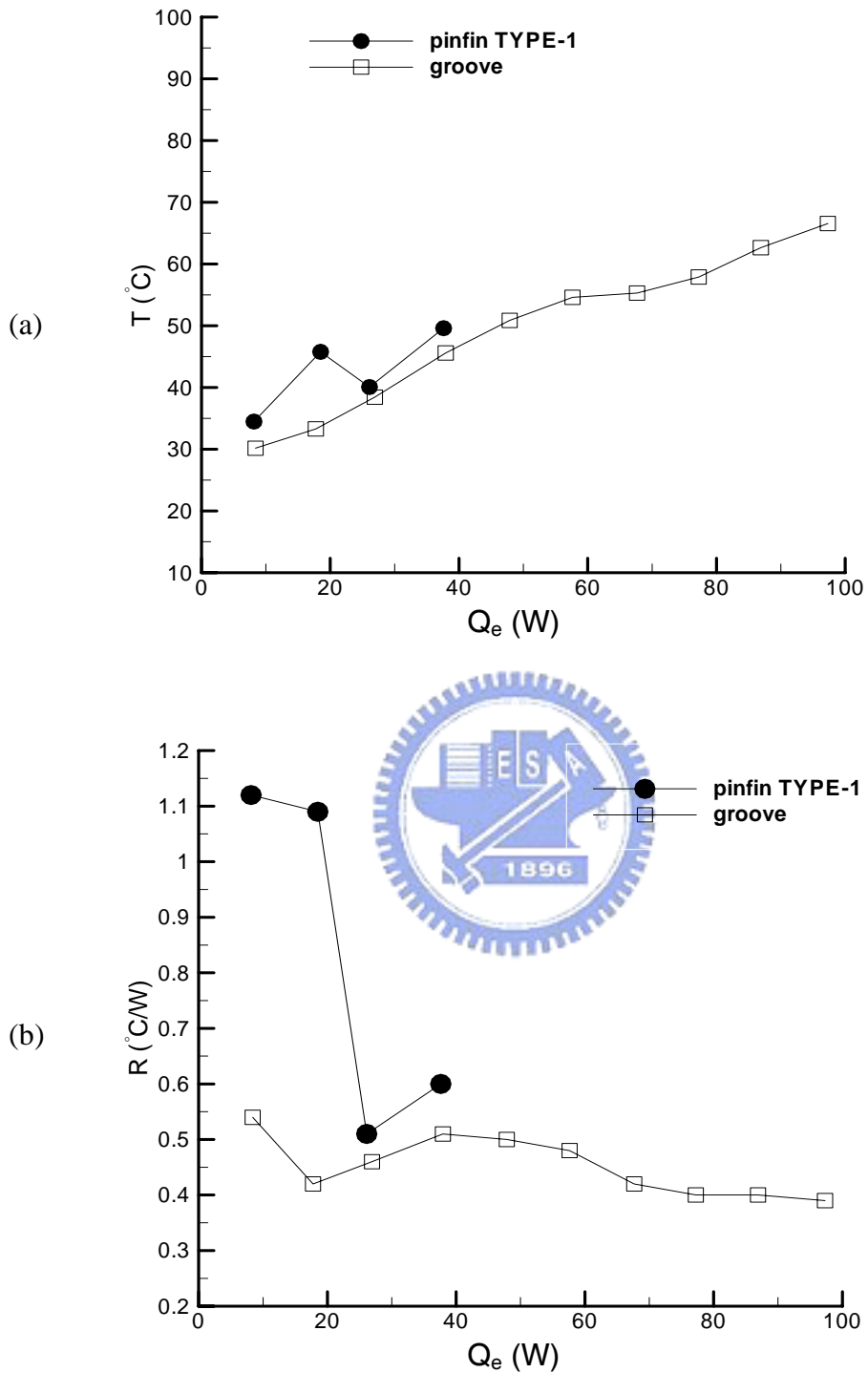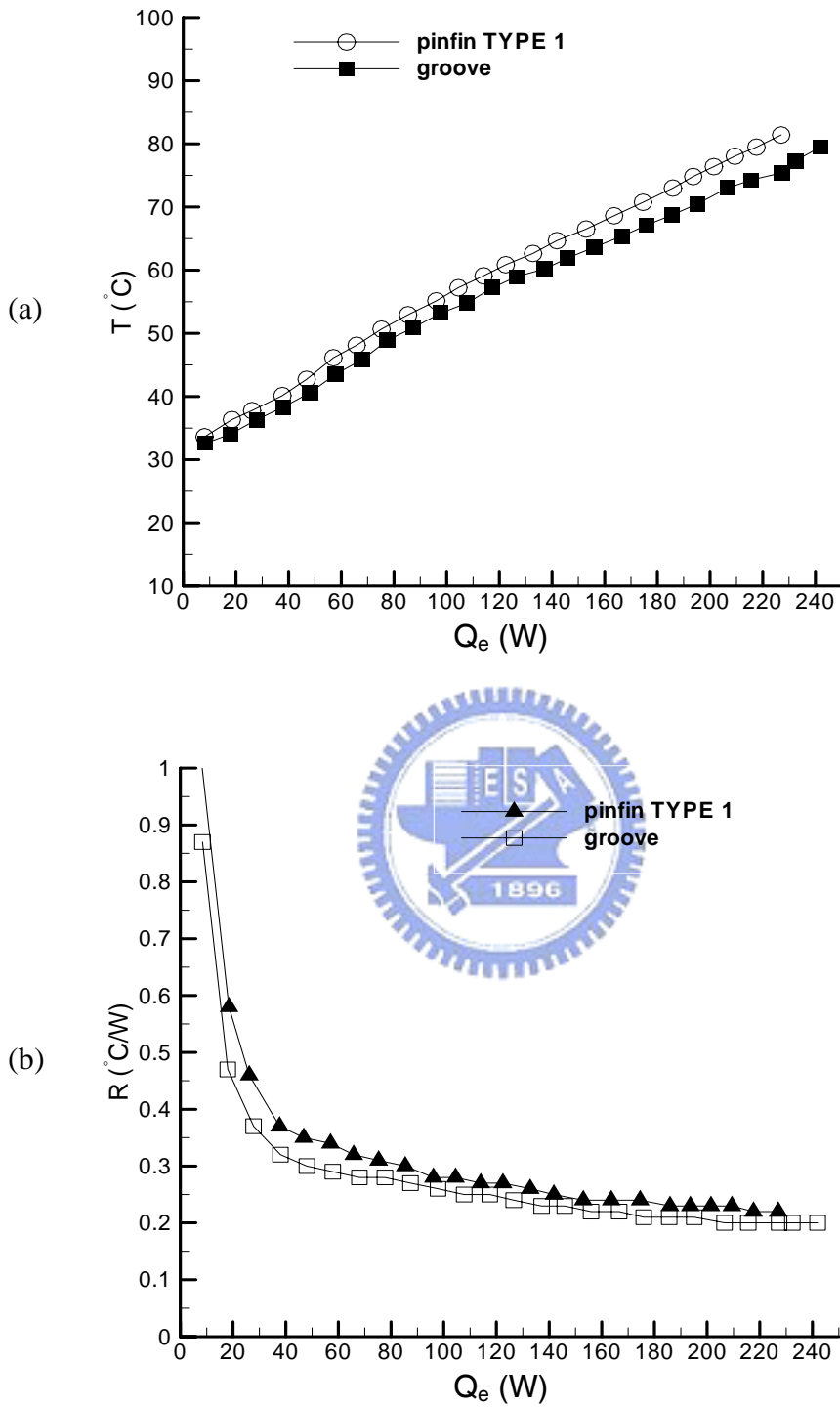
Fig 4.3 Variations of mean evaporator temperature (a) and thermal resistance of the CPL (b) with the input power to the evaporator using type-1 pin fin block for liquid inventory of 50% and relative height between condenser and evaporator of 0 cm.

(a)

(b)
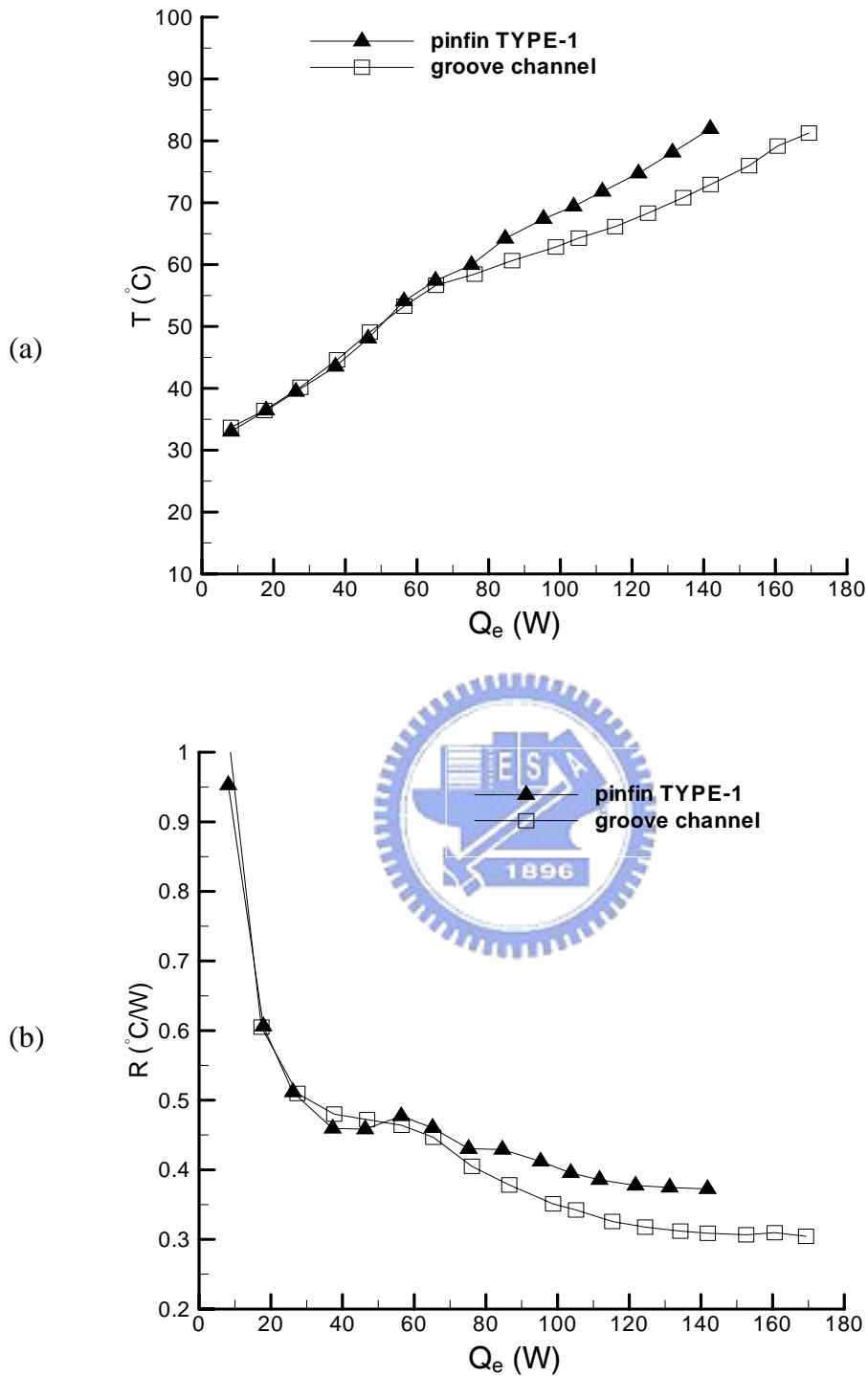
Fig 4.4 Variations of mean evaporator temperature (a) and thermal resistance of the CPL (b) with the input power to the evaporator using type-1 pin fin block for liquid inventory of 62% and relative height between condenser and evaporator of 0 cm.
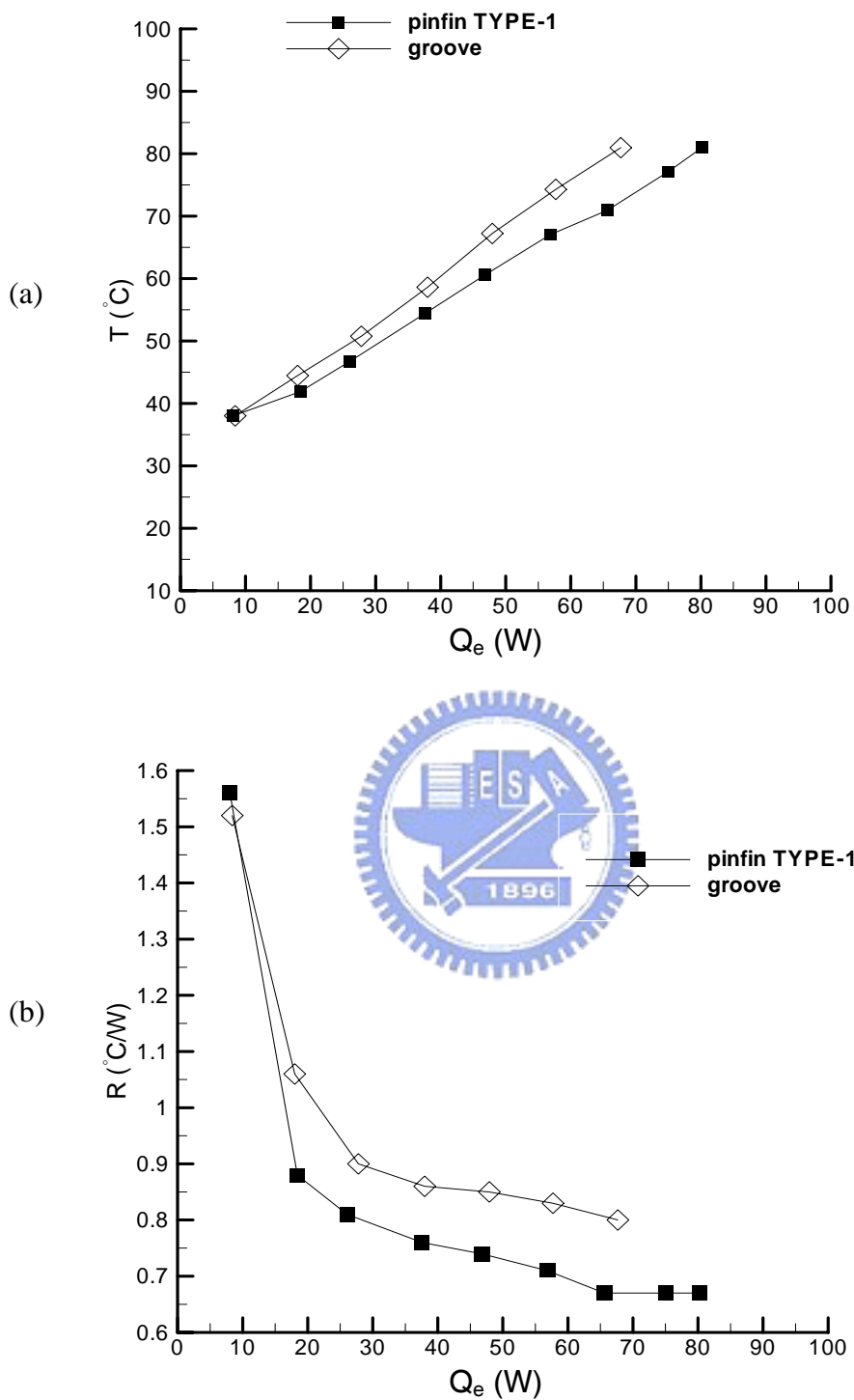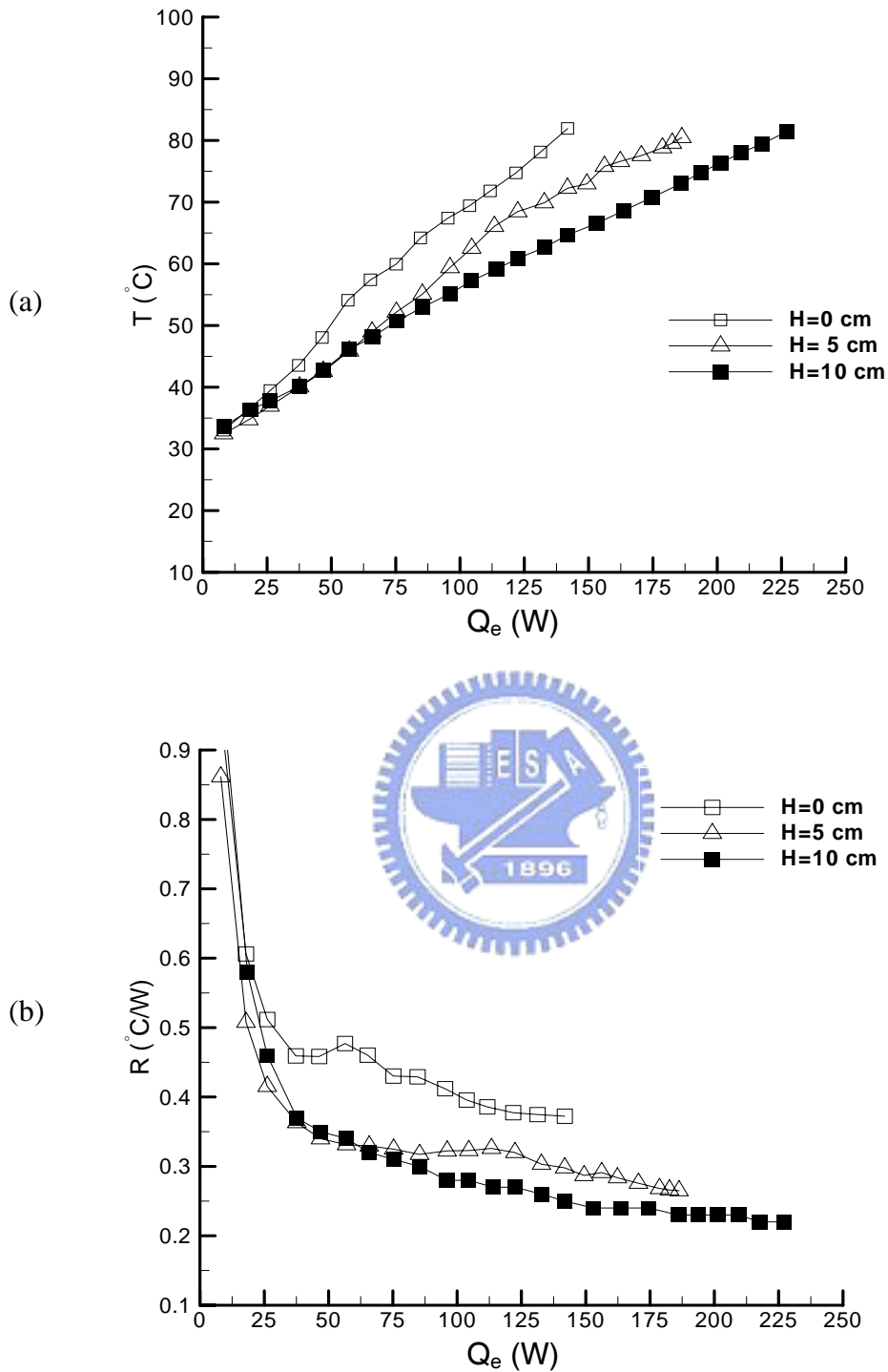
Fig 4.5 Variations of mean evaporator temperature (a) and thermal resistance of the CPL (b) with the input power to the evaporator using type-1 pin fin block for liquid inventory of 75% and relative height between condenser and evaporator of 0 cm.

Fig 4.6 Variations of mean evaporator temperature (a) and thermal resistance of the CPL (b) with the input power to the evaporator using type-1 pin fin block for liquid inventory of 62% and relative height between condenser and evaporator of 0 cm.

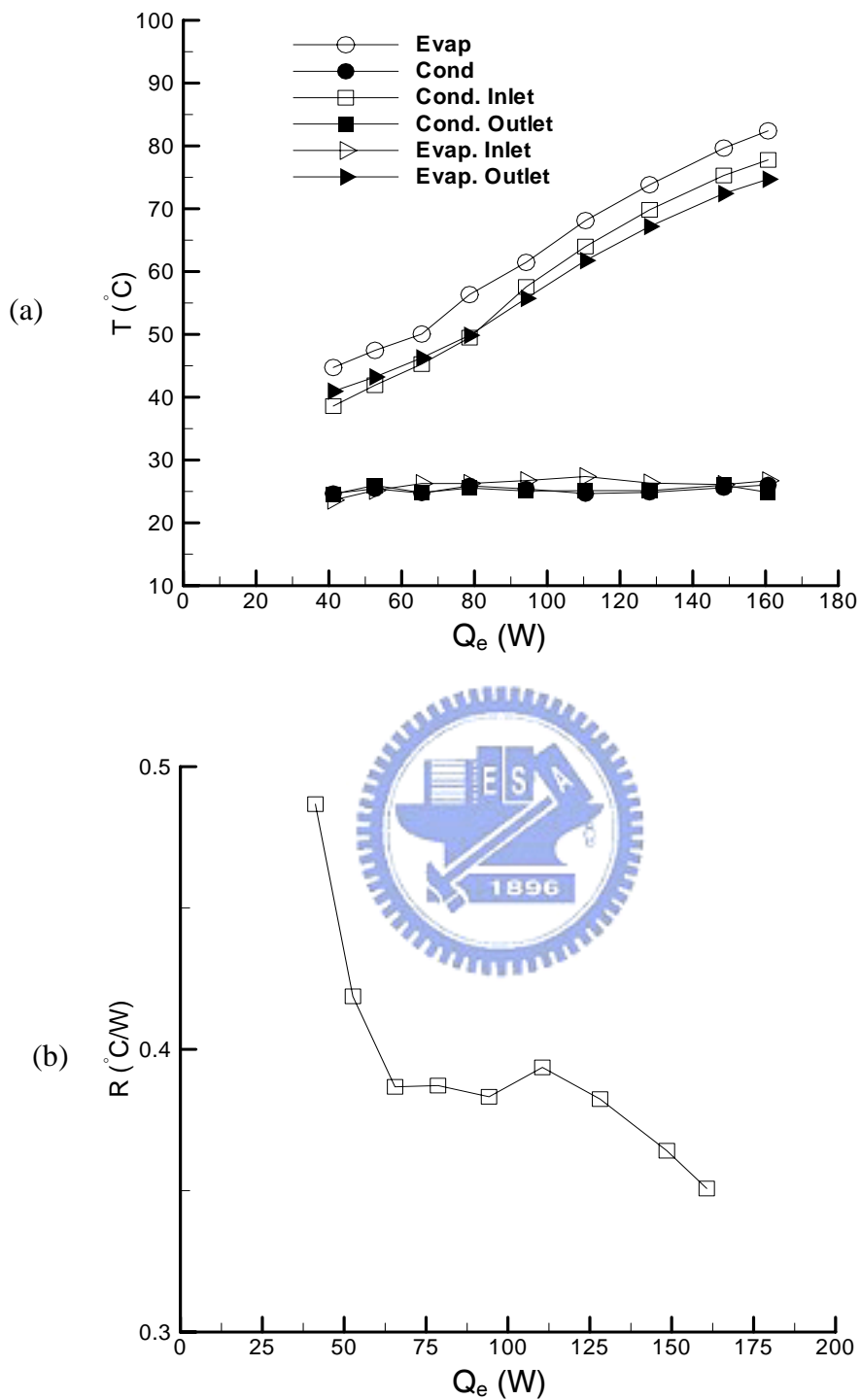Fig 4.7 Variations of mean evaporator temperature (a) and thermal resistance of the CPL (b) with the input power to the evaporator using type-1 pin fin block for liquid inventory of 62% and relative height between condenser and evaporator of 5 cm.
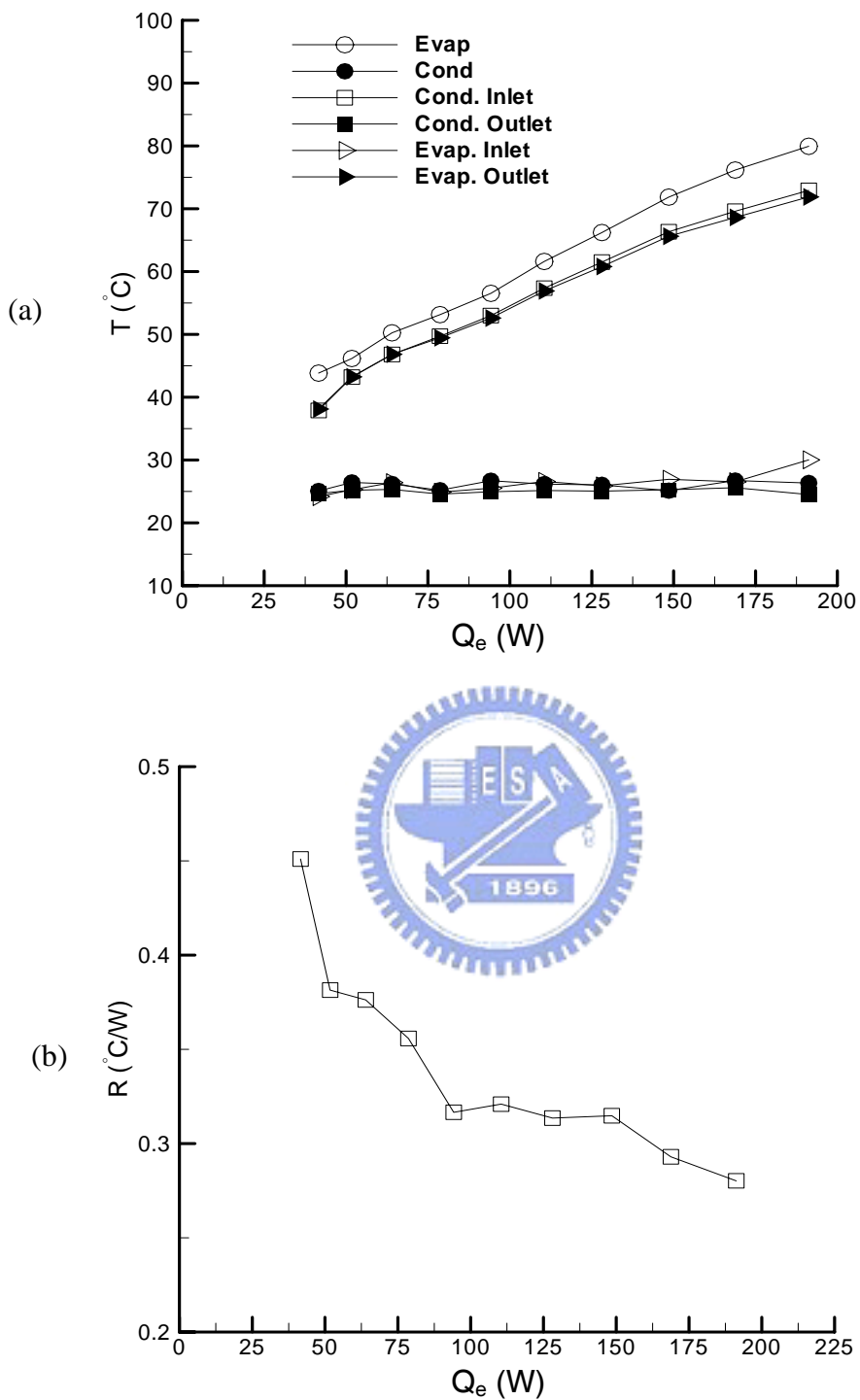
Fig 4.8 Variations of mean evaporator temperature (a) and thermal resistance of the CPL (b) with the input power to the evaporator using type-1 pin fin block for liquid inventory of 62% and relative height between condenser and evaporator of 10 cm.

Figure 4.9 Variations of mean evaporator temperature (a) and thermal resistance of the CPL (b) with the input power to the evaporator using type-1 pin fin block for liquid inventory of 62% for different relative heights between evaporator and condenser.
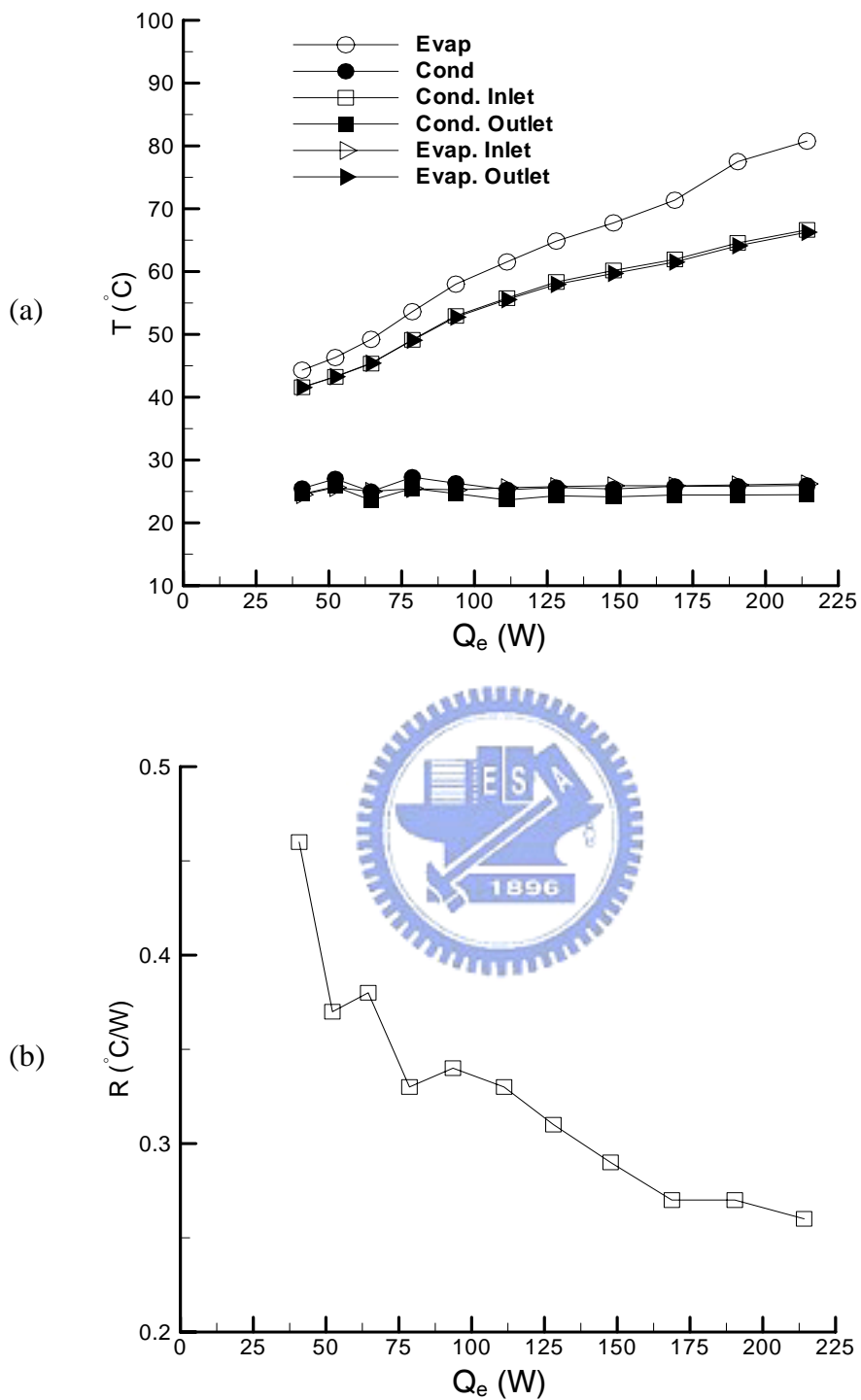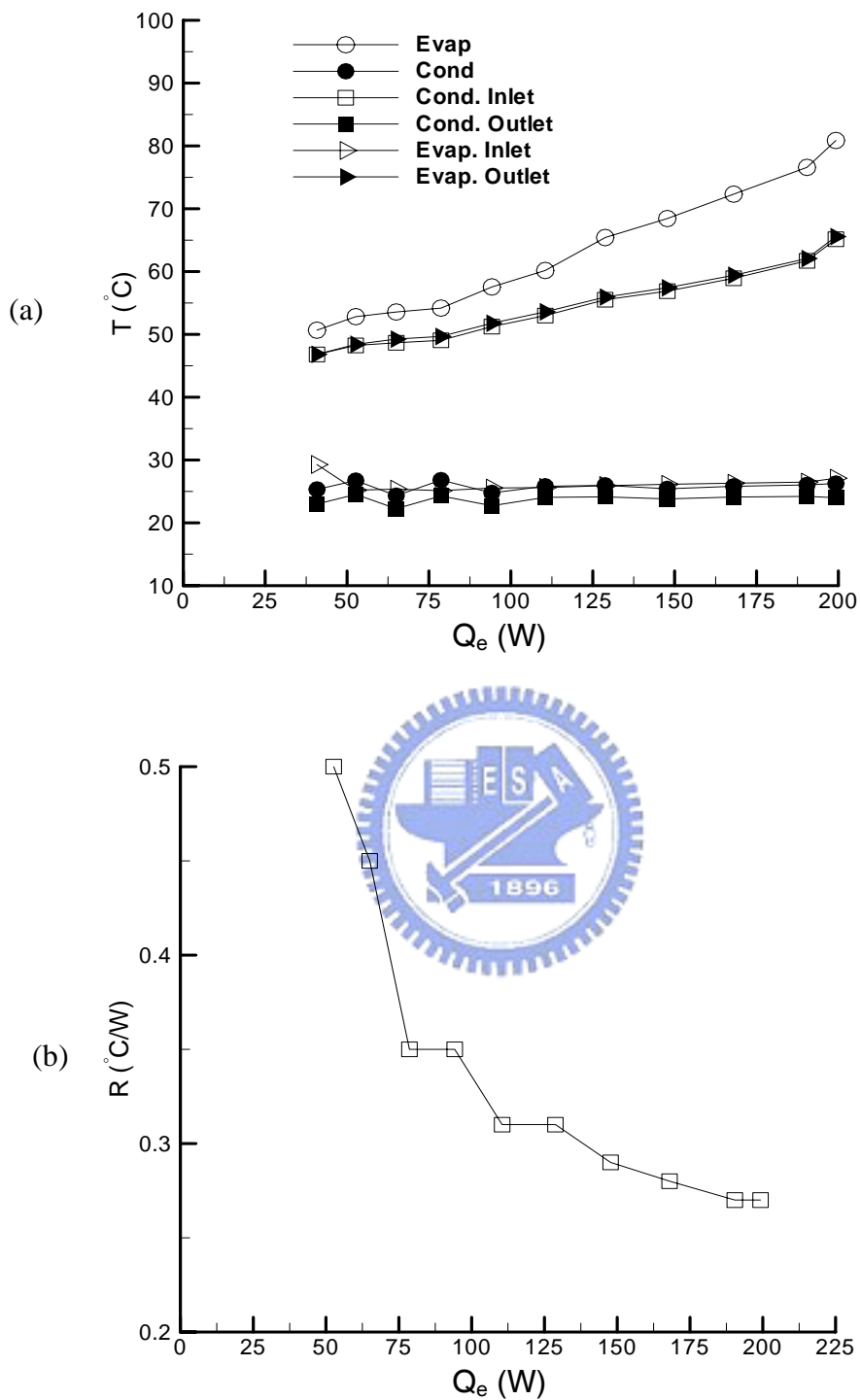
Fig 4.10 Variations of temperatures at selected locations (a) and thermal resistance of the CPL (b) with the input power to the evaporator using heat spreader for liquid inventory of 71% and relative height between condenser and evaporator of 0 cm.

Fig 4.11 Variations of temperatures at selected locations (a) and thermal resistance of the CPL (b) with the input power to the evaporator using heat spreader for liquid inventory of 65% and relative height between condenser and evaporator of 0 cm.
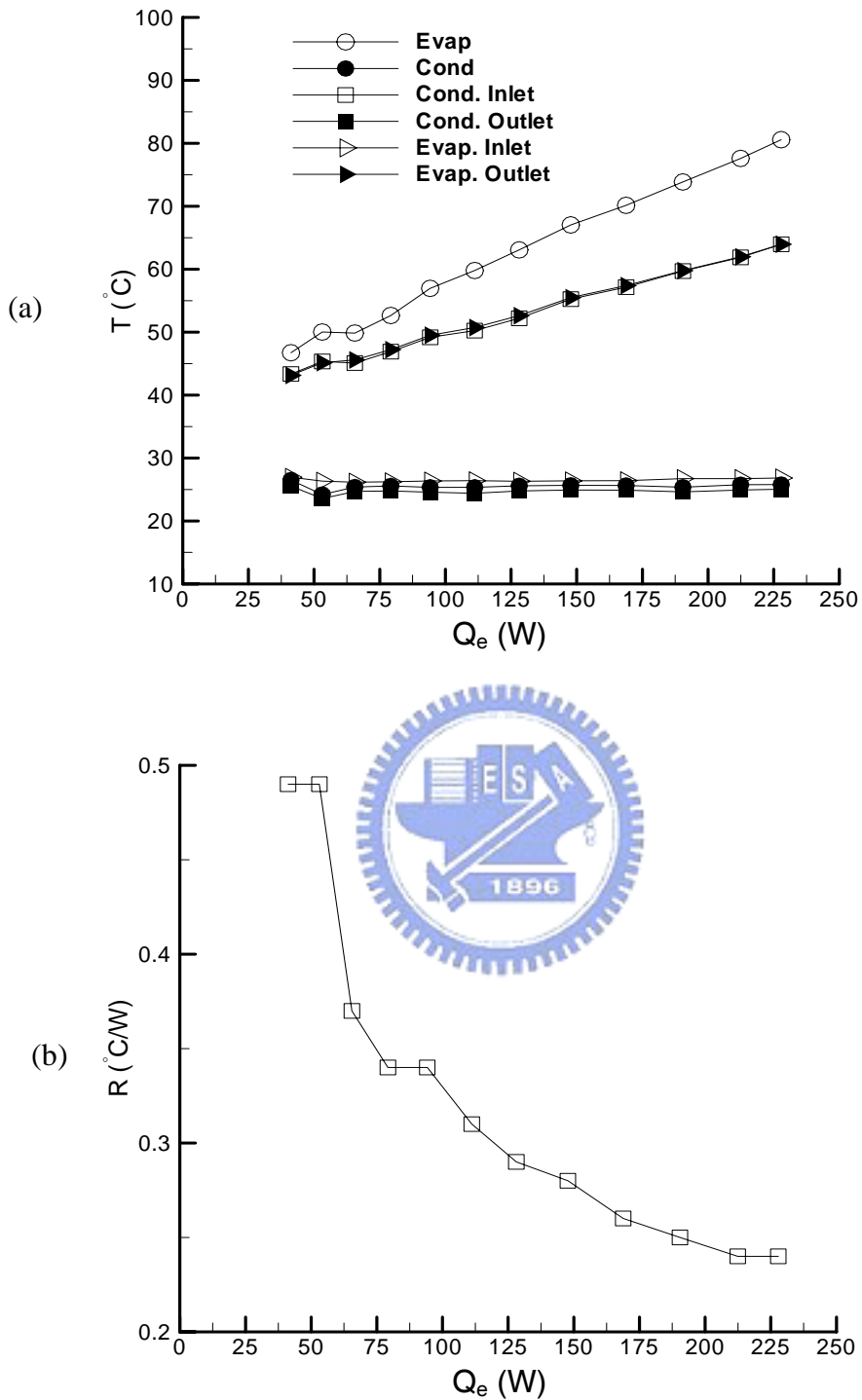
Fig 4.12 Variations of temperatures at selected locations (a) and thermal resistance of the CPL (b) with the input power to the evaporator using heat spreader for liquid inventory of 59% and relative height between condenser and evaporator of 0 cm.
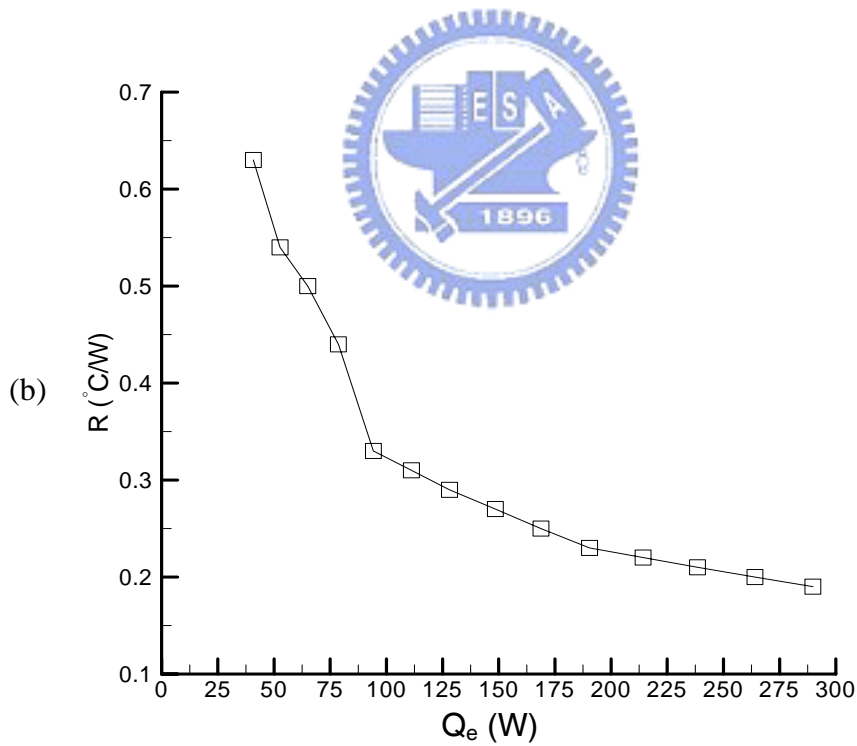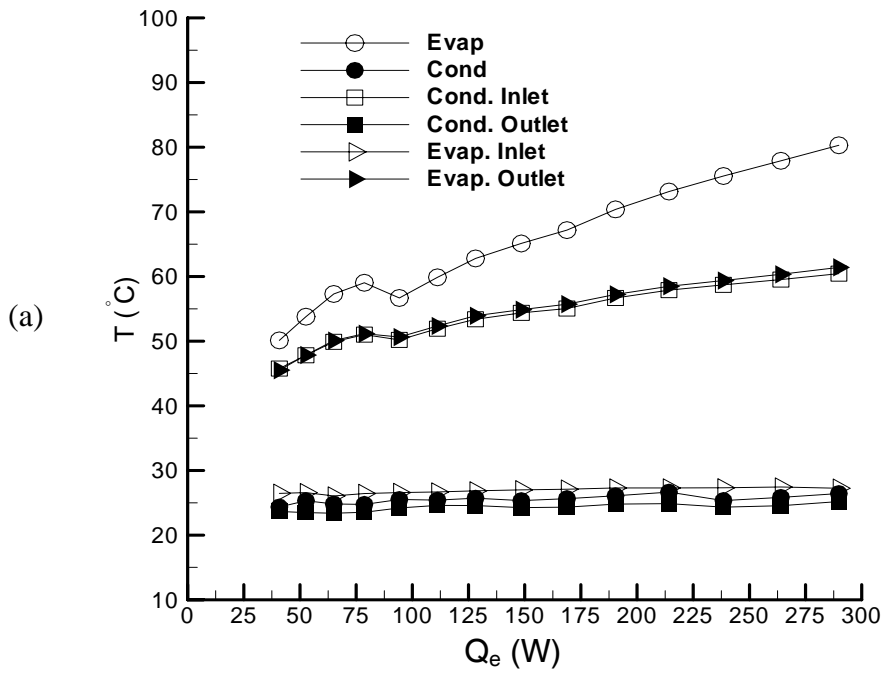
Fig 4.13 Variations of temperatures at selected locations (a) and thermal resistance of the CPL (b) with the input power to the evaporator using heat spreader for liquid inventory of 53% and relative height between condenser and evaporator of 0 cm.
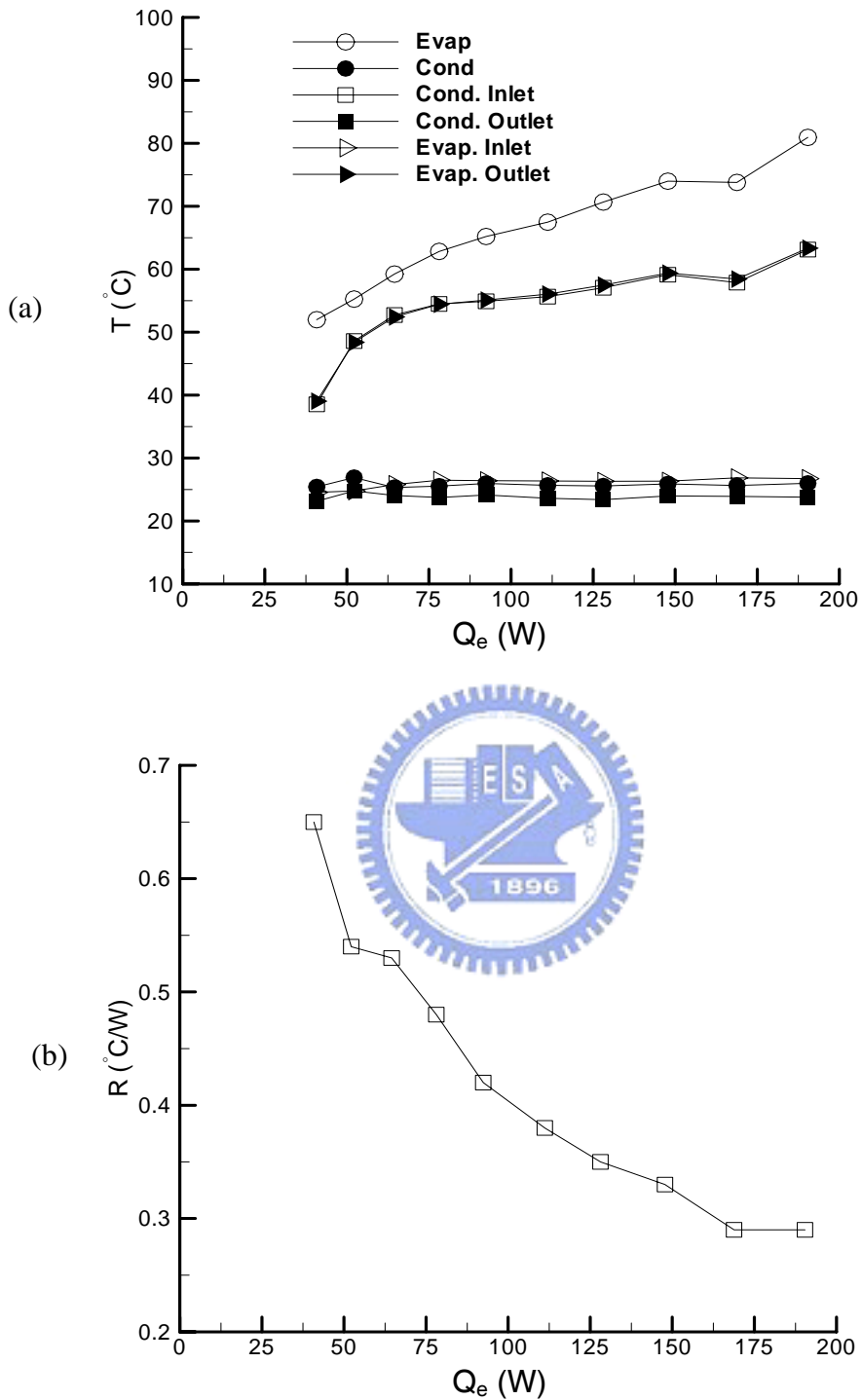
Fig 4.14 Variations of temperatures at selected locations (a) and thermal resistance of the CPL (b) with the input power to the evaporator using heat spreader for liquid inventory of 50% and relative height between condenser and evaporator of 0 cm.

Fig 4.15 Variations of temperatures at selected locations (a) and thermal resistance of the CPL (b) with the input power to the evaporator using heat spreader for liquid inventory of 47% and relative height between condenser and evaporator of 0 cm.

Fig 4.16 Variations of temperatures at selected locations (a) and thermal resistance of the CPL (b) with the input power to the evaporator using heat spreader for liquid inventory of 44% and relative height between condenser and evaporator of 0 cm.
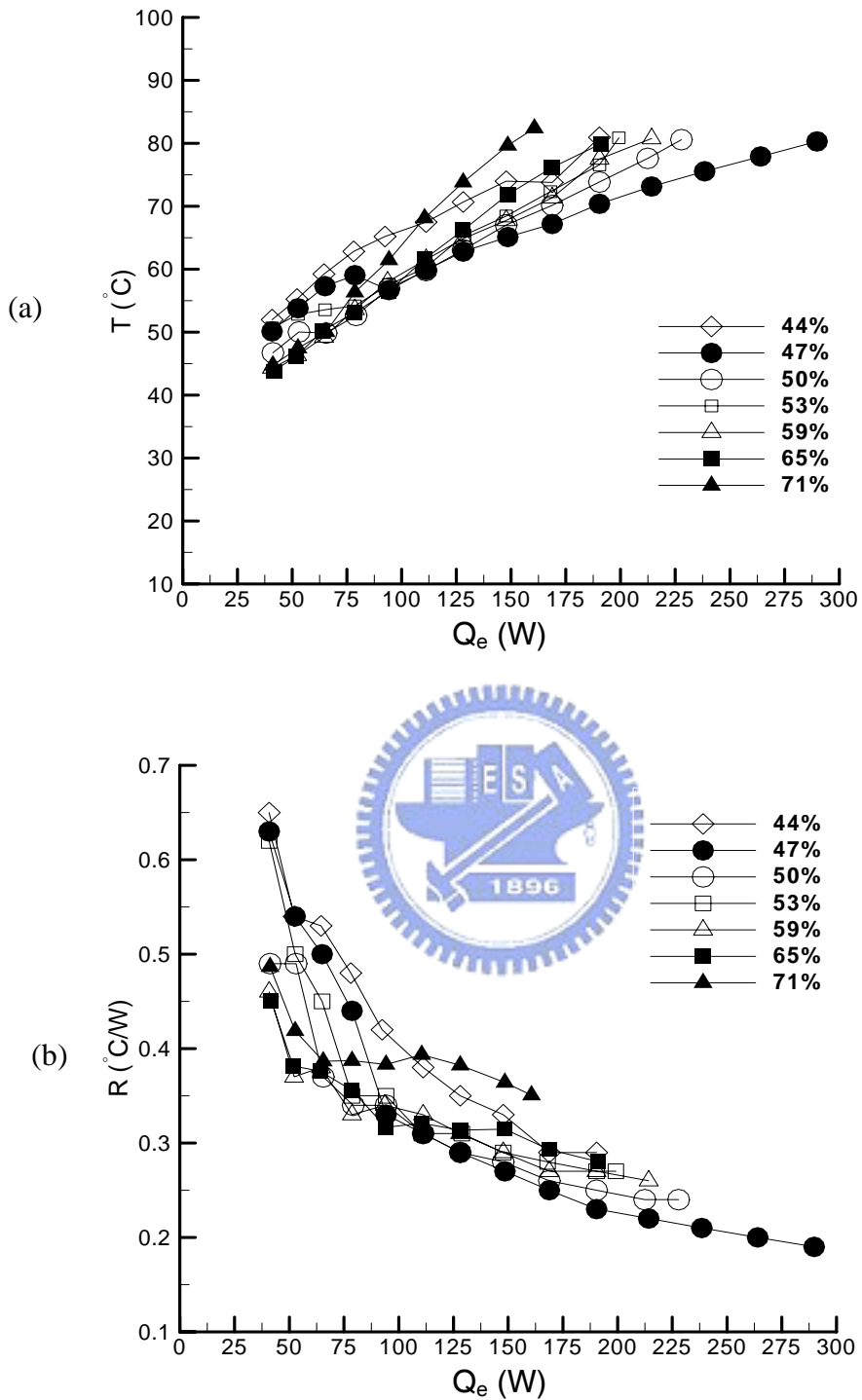
Fig 4.17 Variations of mean evaporator temperature (a) and thermal resistance of the CPL (b) with the input power to the evaporator using heat spreader for various liquid inventories for relative height between condenser and evaporator of 0 cm.
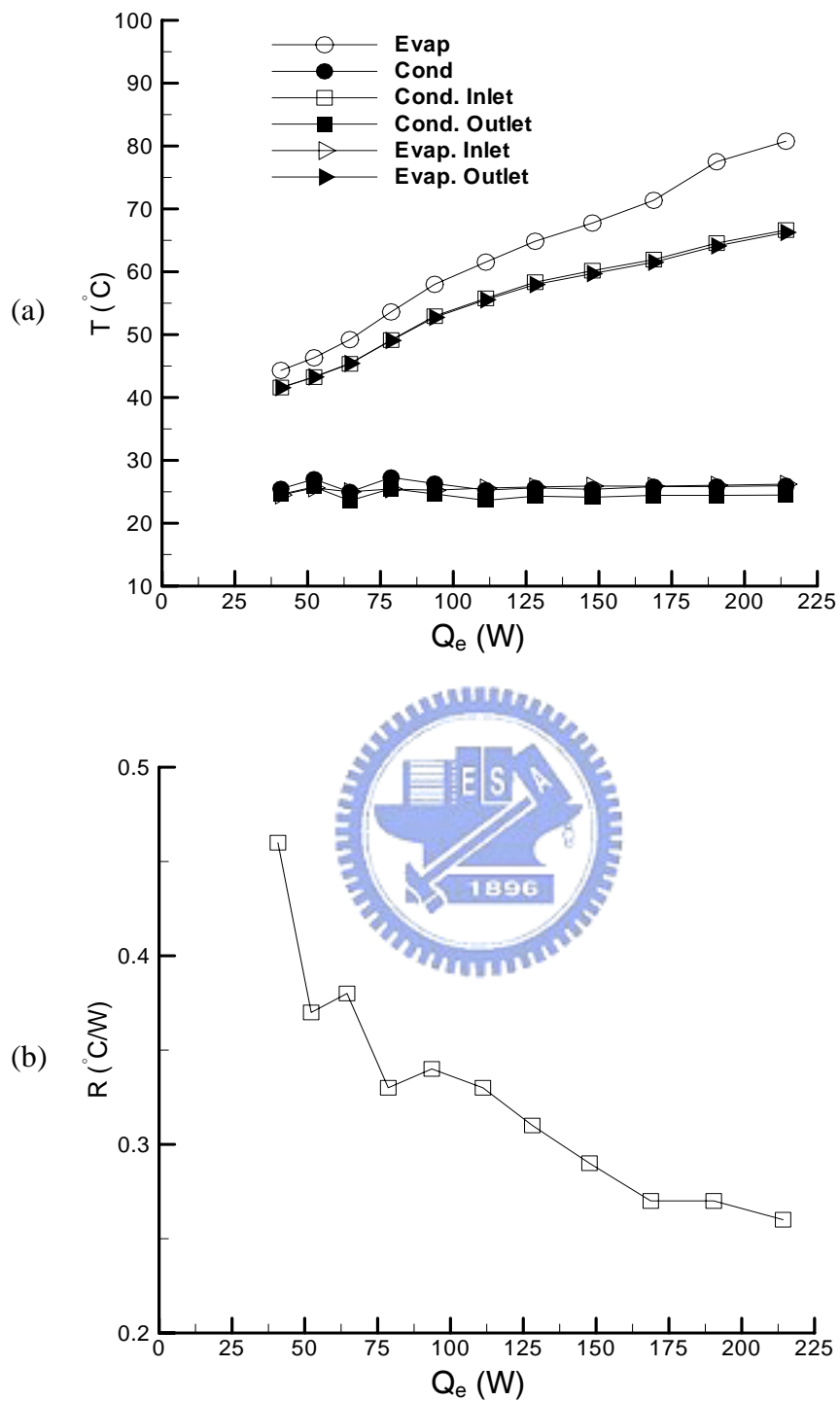
Fig 4.18 Variations of temperatures at selected locations (a) and thermal resistance of the CPL (b) with the input power to the evaporator using heat spreader for liquid inventory of 59% and relative height between condenser and evaporator of 0 cm.
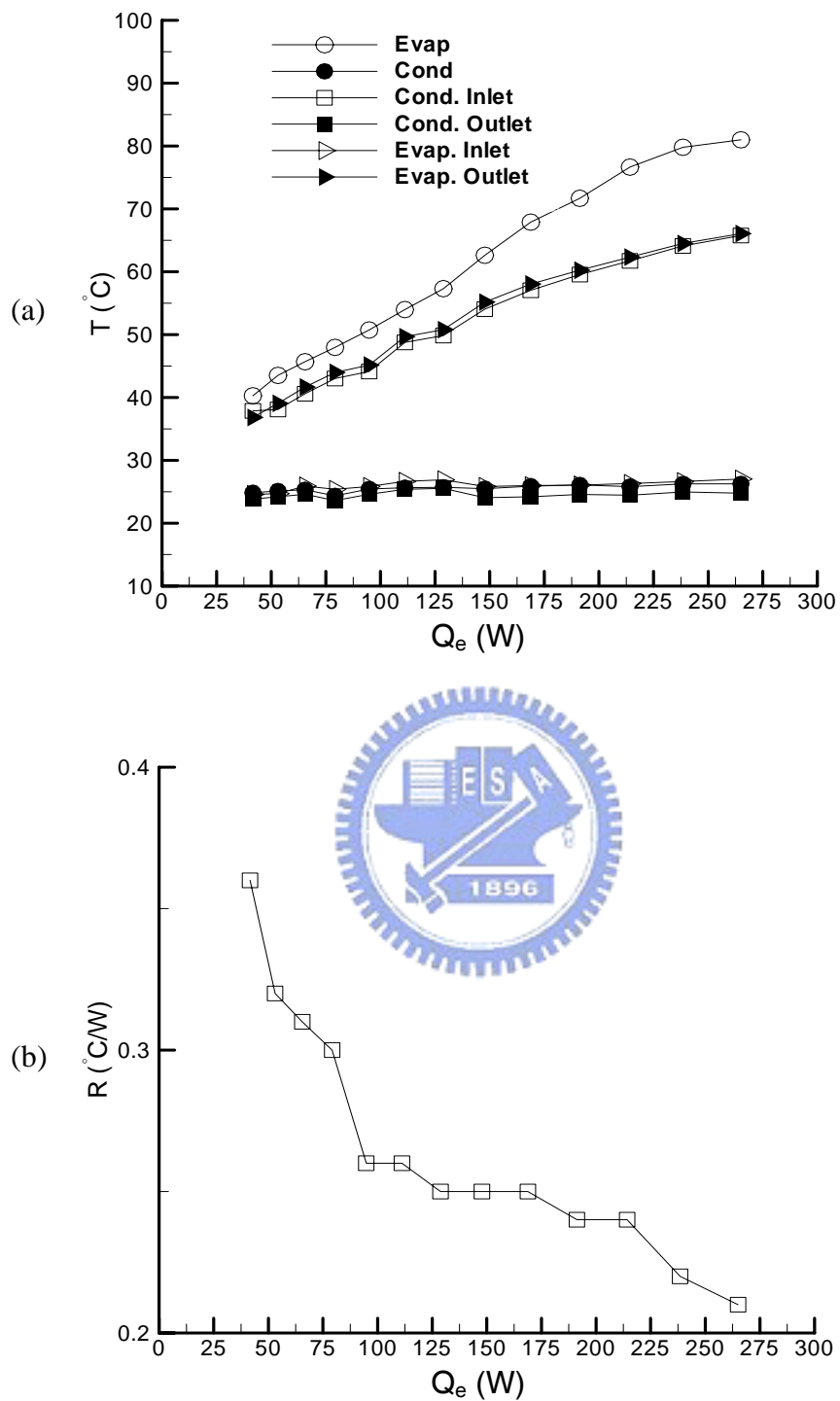
Fig 4.19 Variations of temperatures at selected locations (a) and thermal resistance of the CPL (b) with the input power to the evaporator using heat spreader for liquid inventory of 59% and relative height between condenser and evaporator of 5 cm.
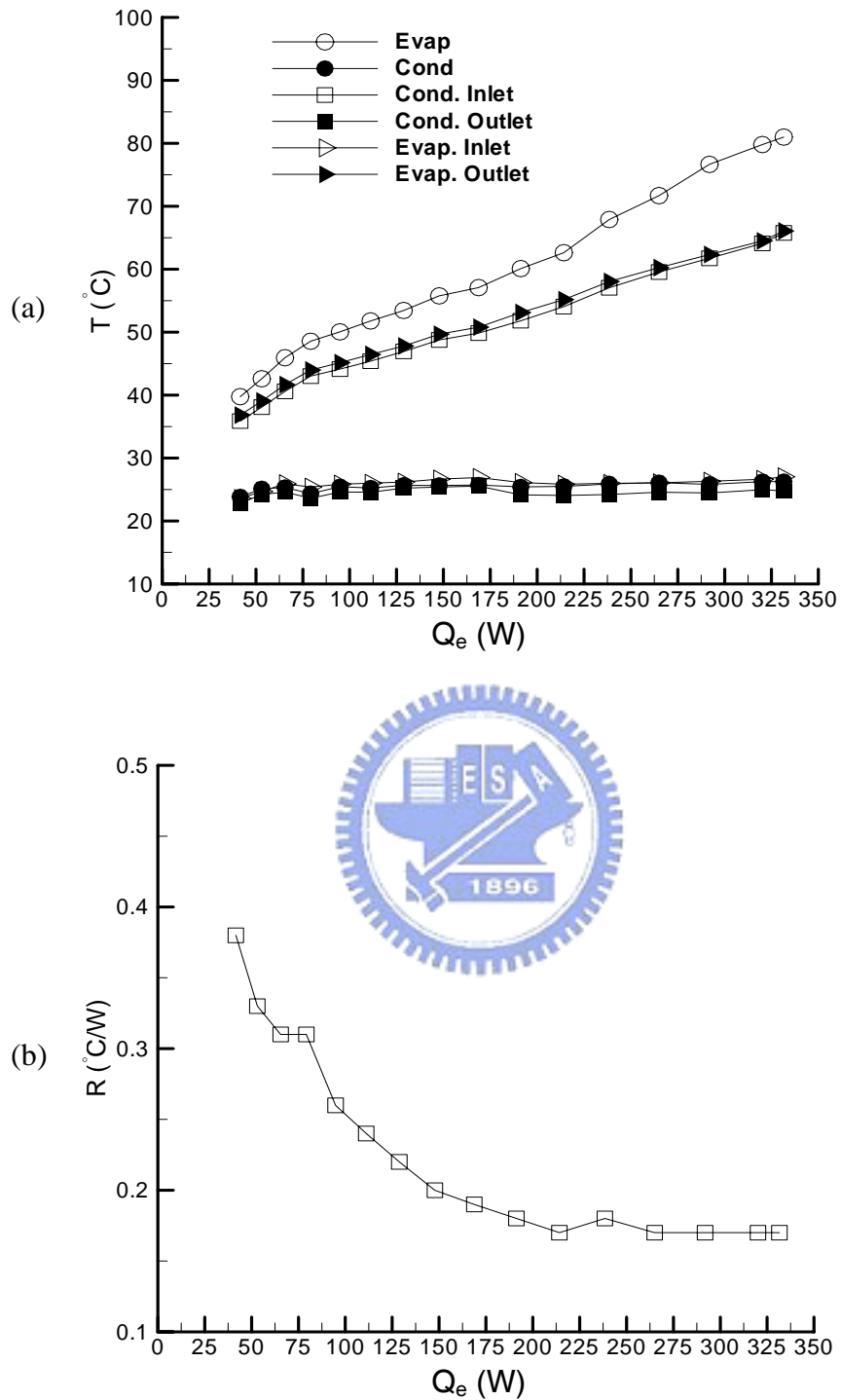
Fig 4.20 Variations of temperatures at selected locations (a) and thermal resistance of the CPL (b) with the input power to the evaporator using heat spreader for liquid inventory of 59% and relative height between condenser and evaporator of 10 cm.
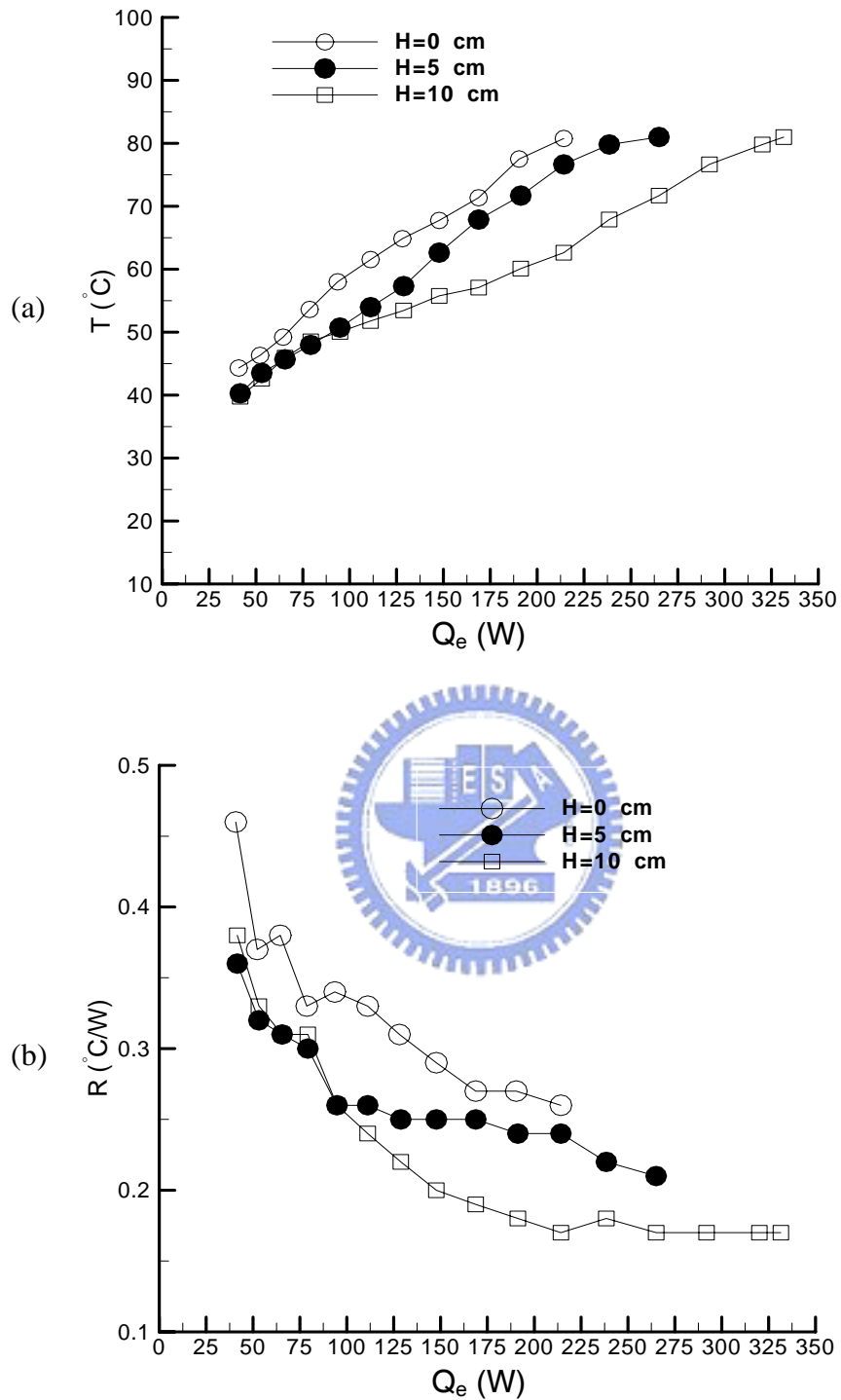
Fig 4.21 Variations of mean evaporator temperature (a) and thermal resistance of the CPL (b) with the input power to the evaporator using heat spreader for various relative heights between evaporator and condenser for liquid inventory of 59%.
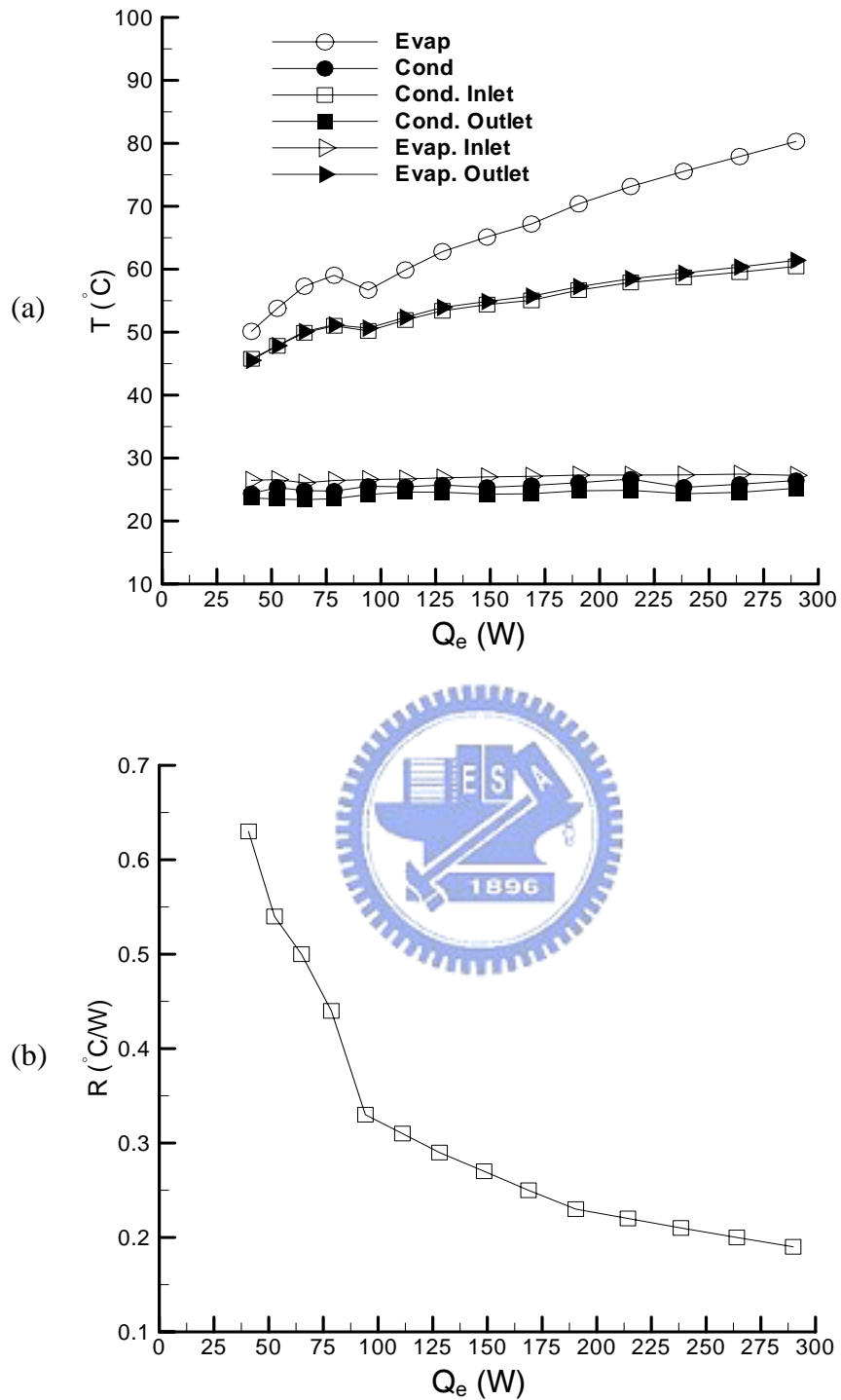
Fig 4.22 Variations of temperatures at selected locations (a) and thermal resistance of the CPL (b) with the input power to the evaporator using heat spreader for liquid inventory of 47% and relative height between condenser and evaporator of 0cm.
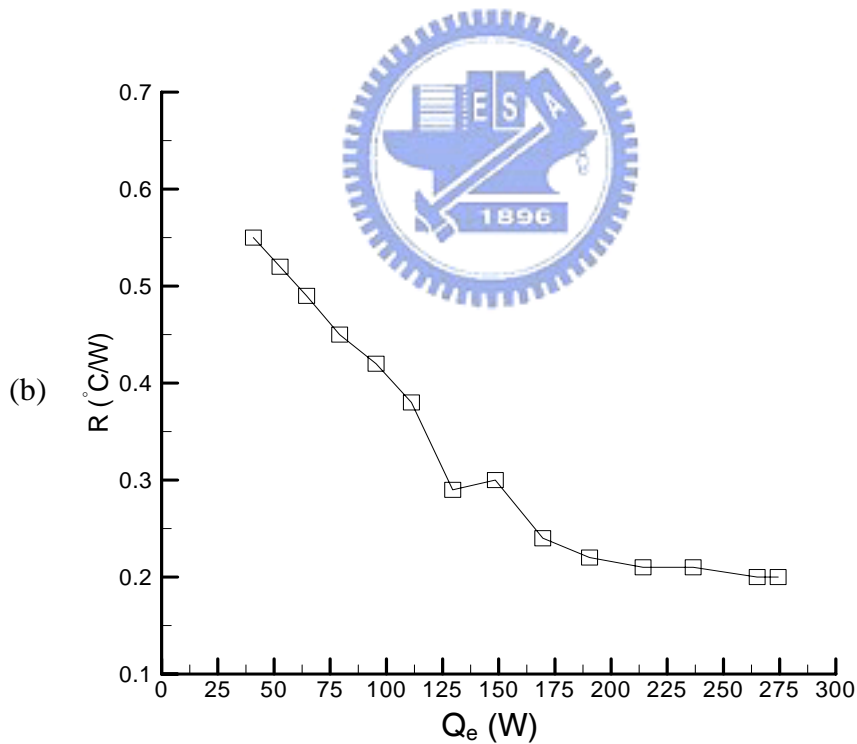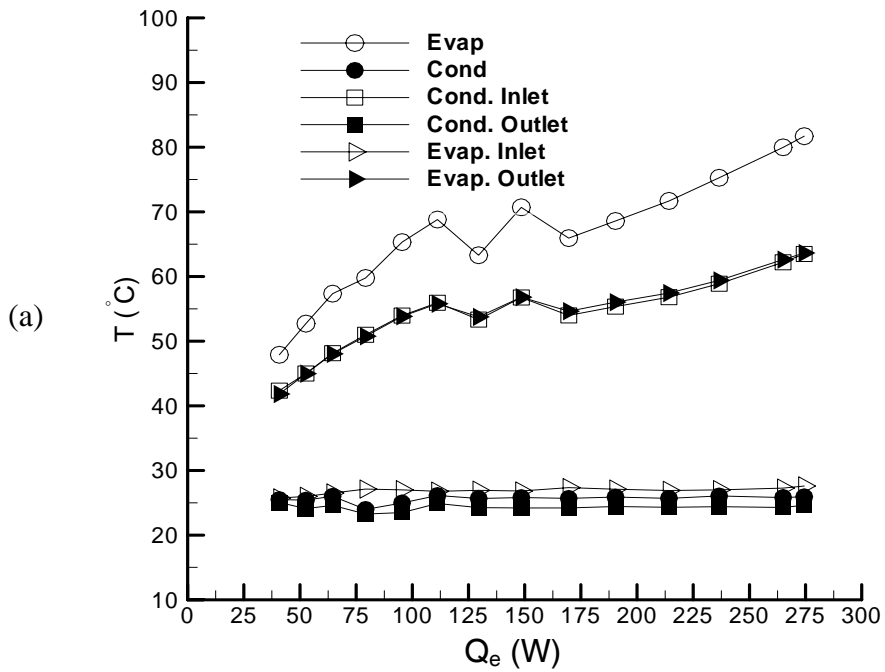
Fig 4.23 Variations of temperatures at selected locations (a) and thermal resistance of the CPL (b) with the input power to the evaporator using heat spreader for liquid inventory of 47% and relative height between condenser and evaporator of 5cm.
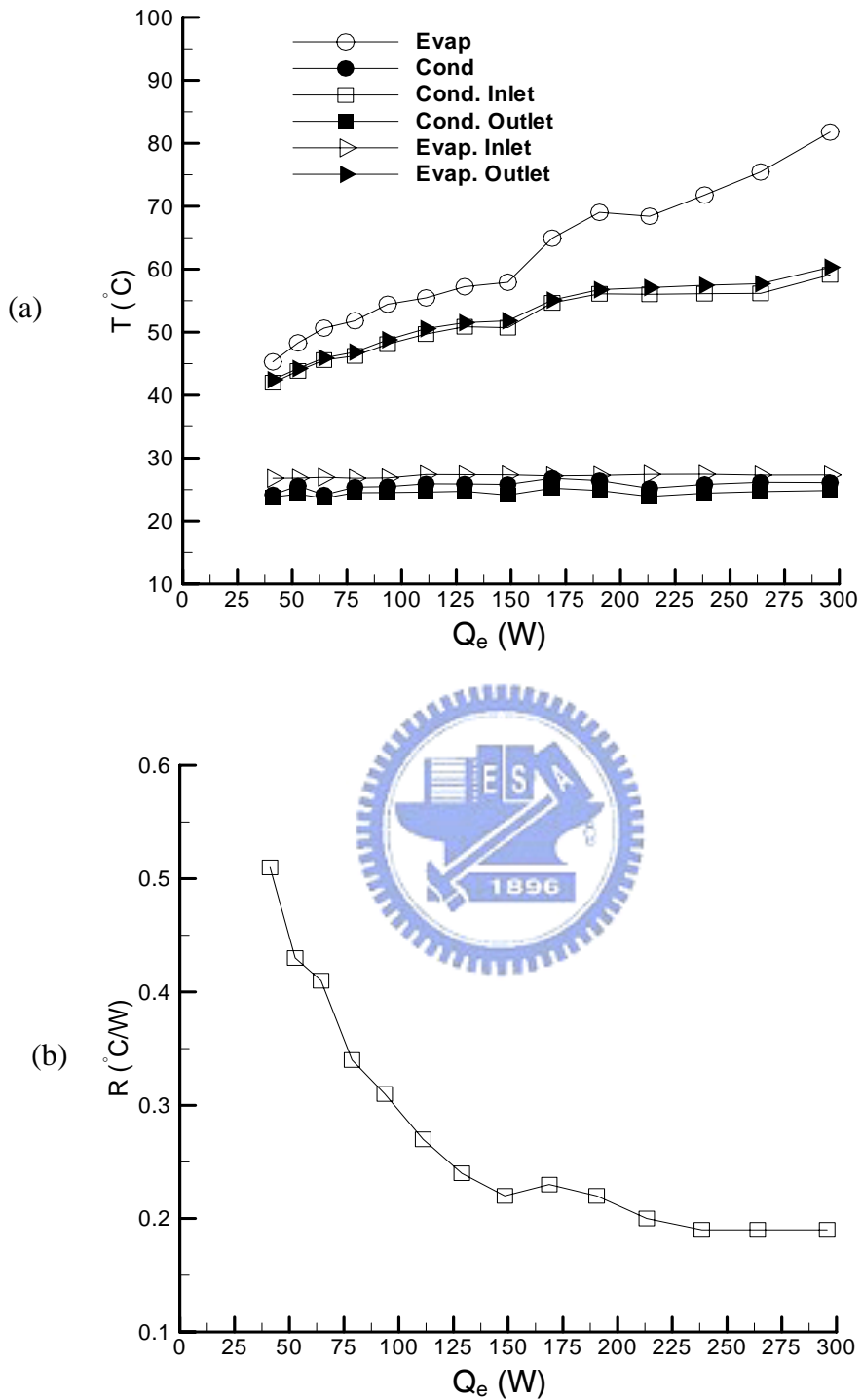
Fig 4.24 Variations of temperatures at selected locations (a) and thermal resistance of the CPL (b) with the input power to the evaporator using heat spreader for liquid inventory of 47% and relative height between condenser and evaporator of 10cm.
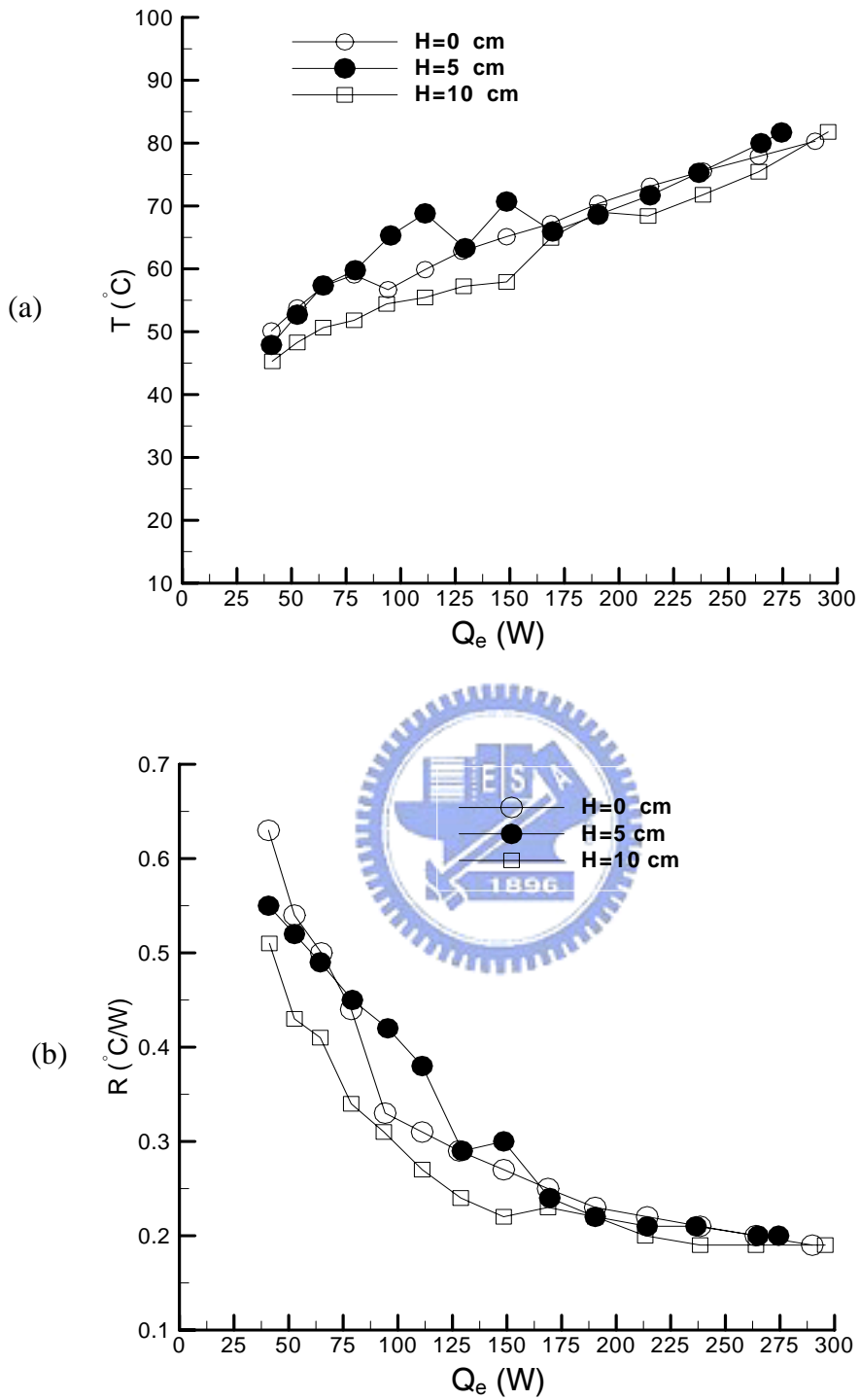
Fig 4.25 Variations of mean evaporator temperature (a) and thermal resistance of the CPL (b) with the input power to the evaporator using heat spreader for various relative heights between evaporator and condenser for liquid inventory of 47%.
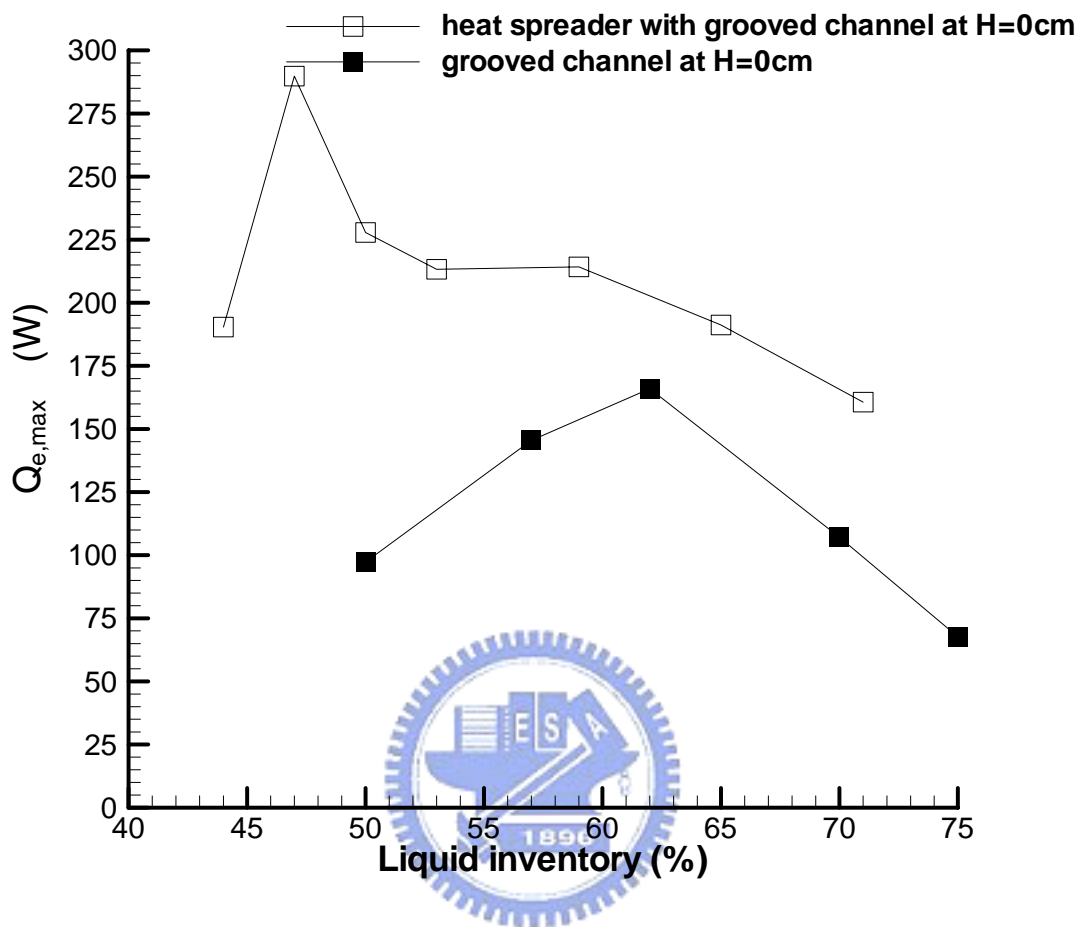
Fig 4.26 Variations of the maximum allowable power input with the liquid inventory for the relative height between condenser and evaporator of 0 cm for CPL with and without the heat spreader installed in the evaporator.
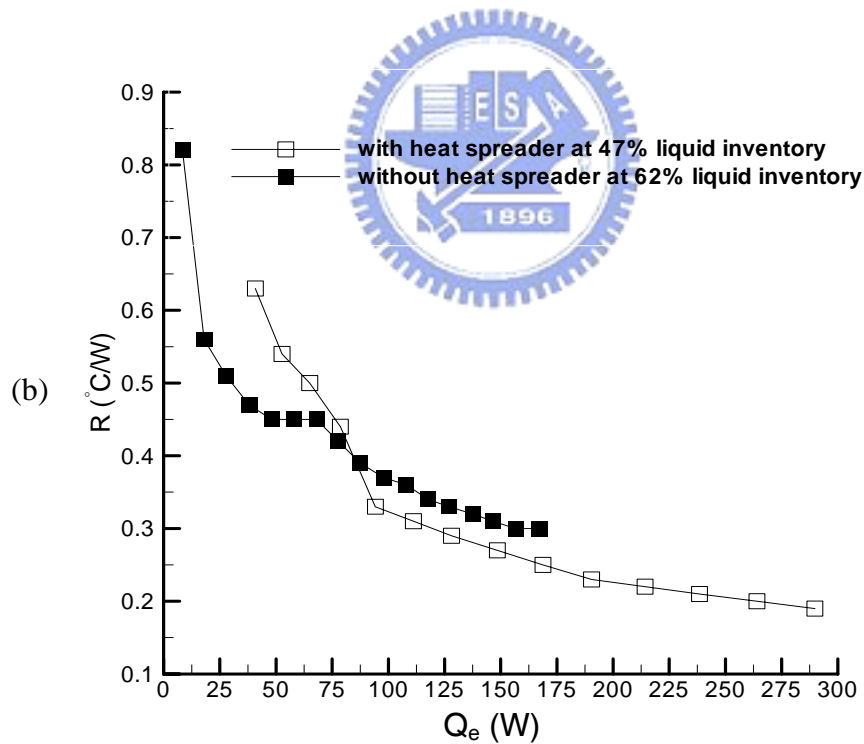
Fig 4.27 Variations of mean evaporator temperature (a) and thermal resistance of the CPL (b) with the input power for the system with and without heat spreader and relative height between condenser and evaporator of 0 cm at the optimal liquid inventory.

Fig 4.28 Variations of the maximum allowable power input with the liquid inventory
for the relative height between condenser and evaporator of 5 cm for CPL with and
without the heat spreader installed in the evaporator.
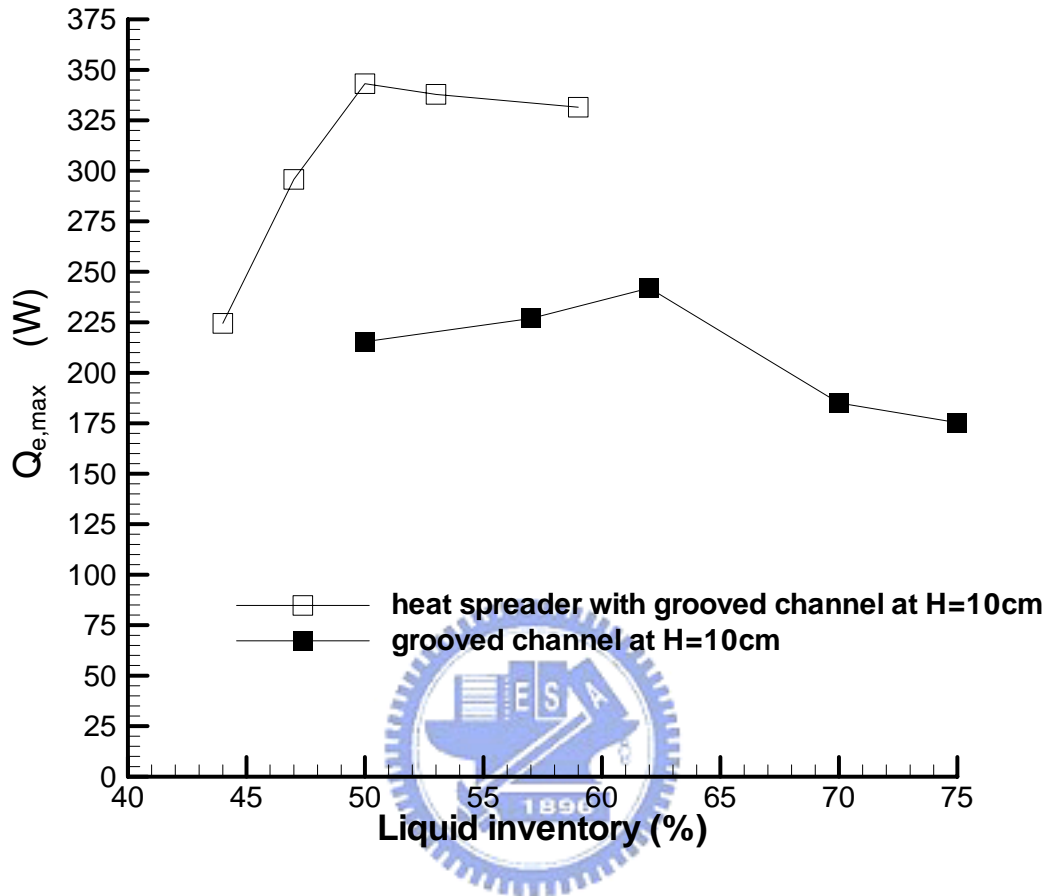
Fig 4.29 Variations of the maximum allowable power input with the liquid inventory
for the relative height between condenser and evaporator of 10 cm for CPL with and
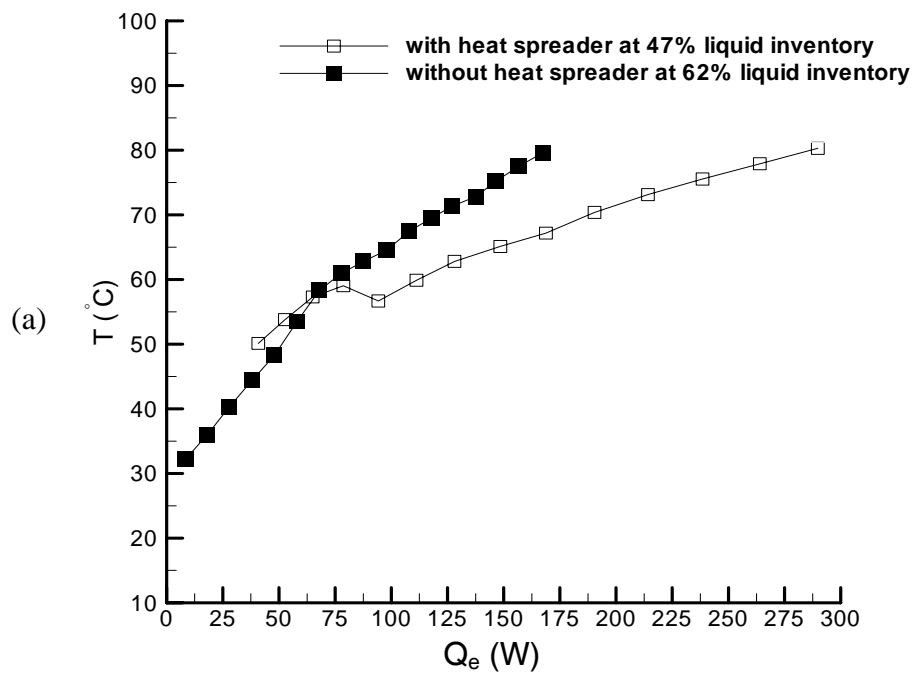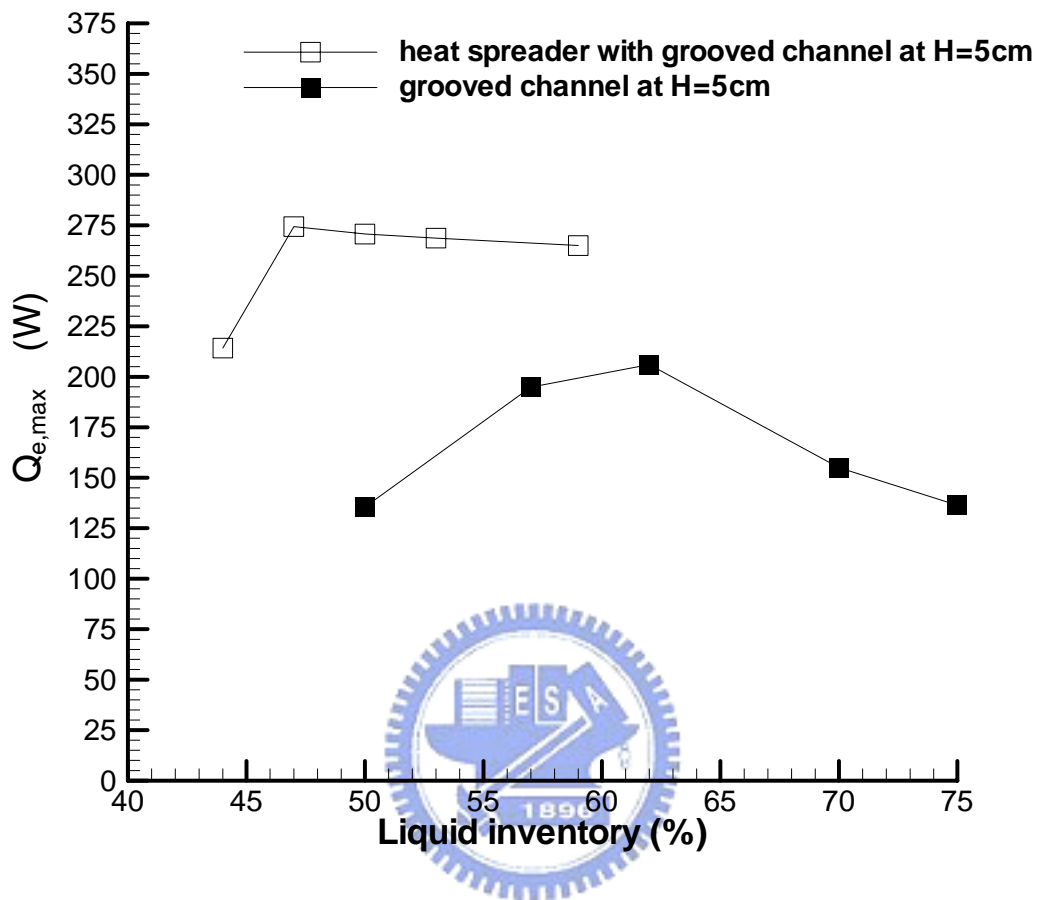without the heat spreader installed in the evaporator.

Fig 4.30 Variations of temperatures at selected locations (a) and thermal resistance of the CPL (b) with the input power to the evaporator using heat spreader with the surface roughing on the grooved channels for the liquid inventory of 47% and relative height between condenser and evaporator of 0 cm.

Fig 4.31 Variations of temperatures at selected locations (a) and thermal resistance of the CPL (b) with the input power to the evaporator using heat spreader with the surface roughing on the grooved channels for the liquid inventory of 50% and relative height between condenser and evaporator of 0 cm.
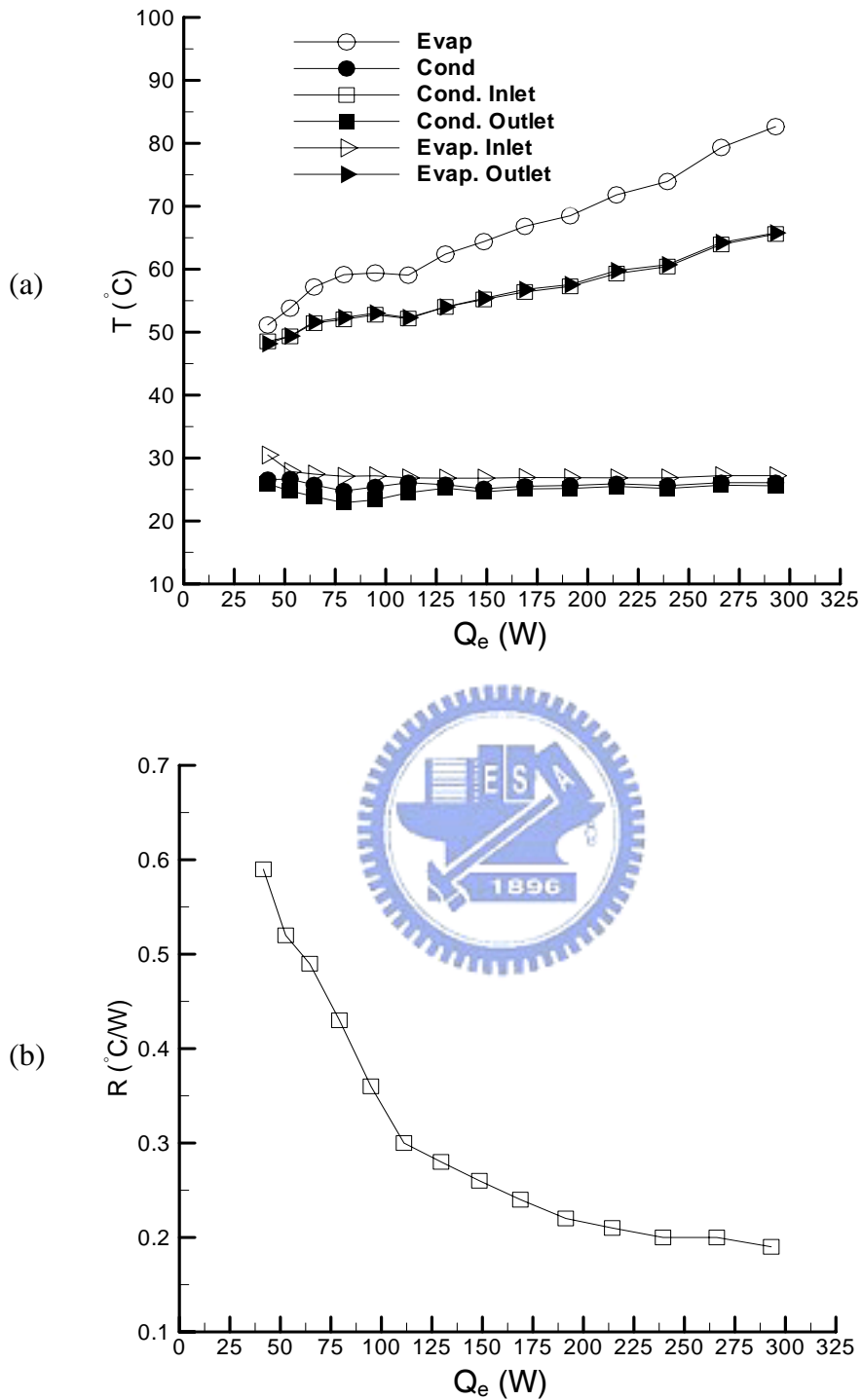
Fig 4.32 Variations of temperatures at selected locations (a) and thermal resistance of the CPL (b) with the input power to the evaporator using heat spreader with the surface roughing on the grooved channels for the liquid inventory of 53% and relative height between condenser and evaporator of 0 cm.
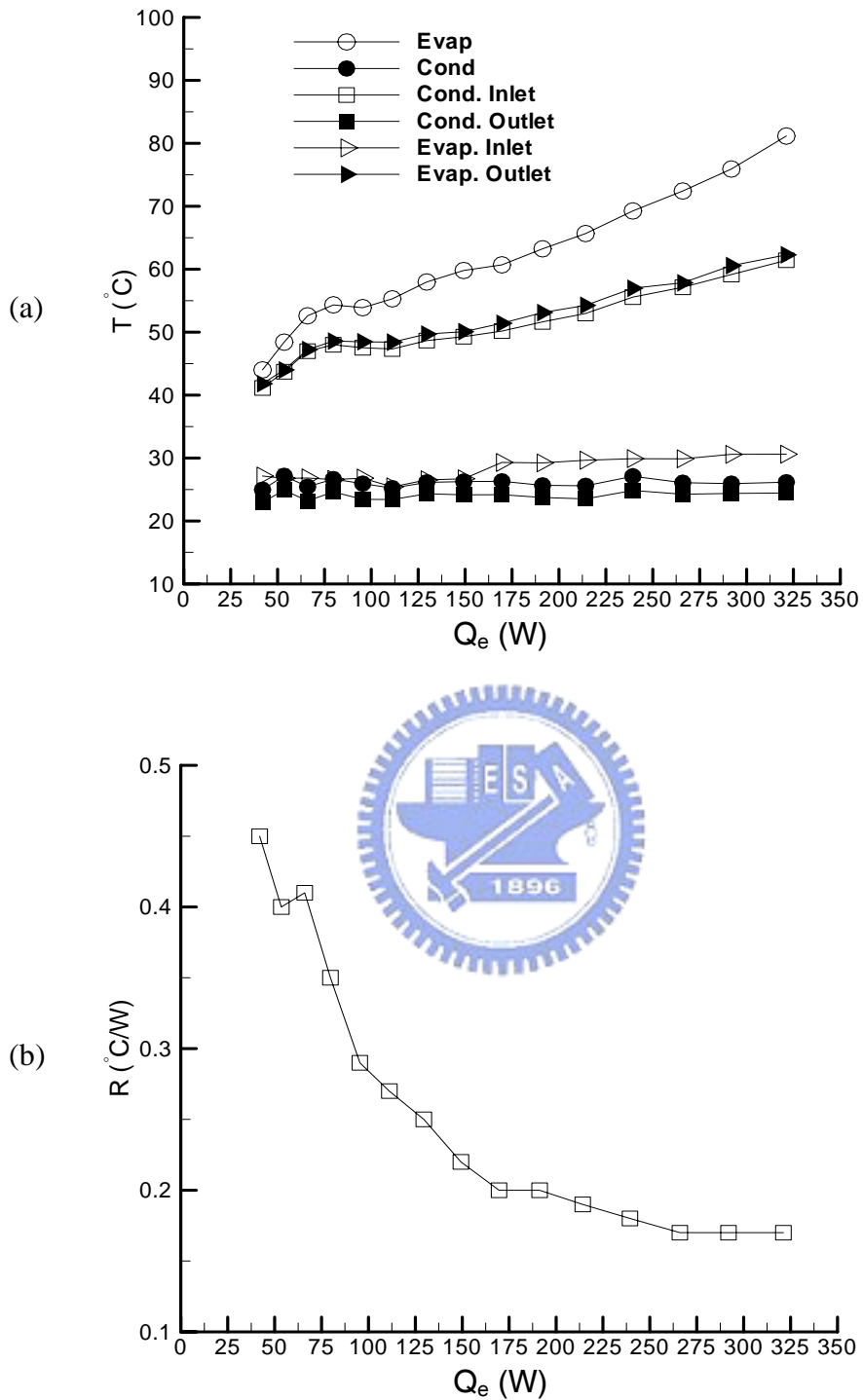
(a)

(b)

Fig 4.33 Variations of temperatures at selected locations (a) and thermal resistance of the CPL (b) with the input power to the evaporator using heat spreader with the surface roughing on the grooved channels for the liquid inventory of 59% and relative height between condenser and evaporator of 0 cm.
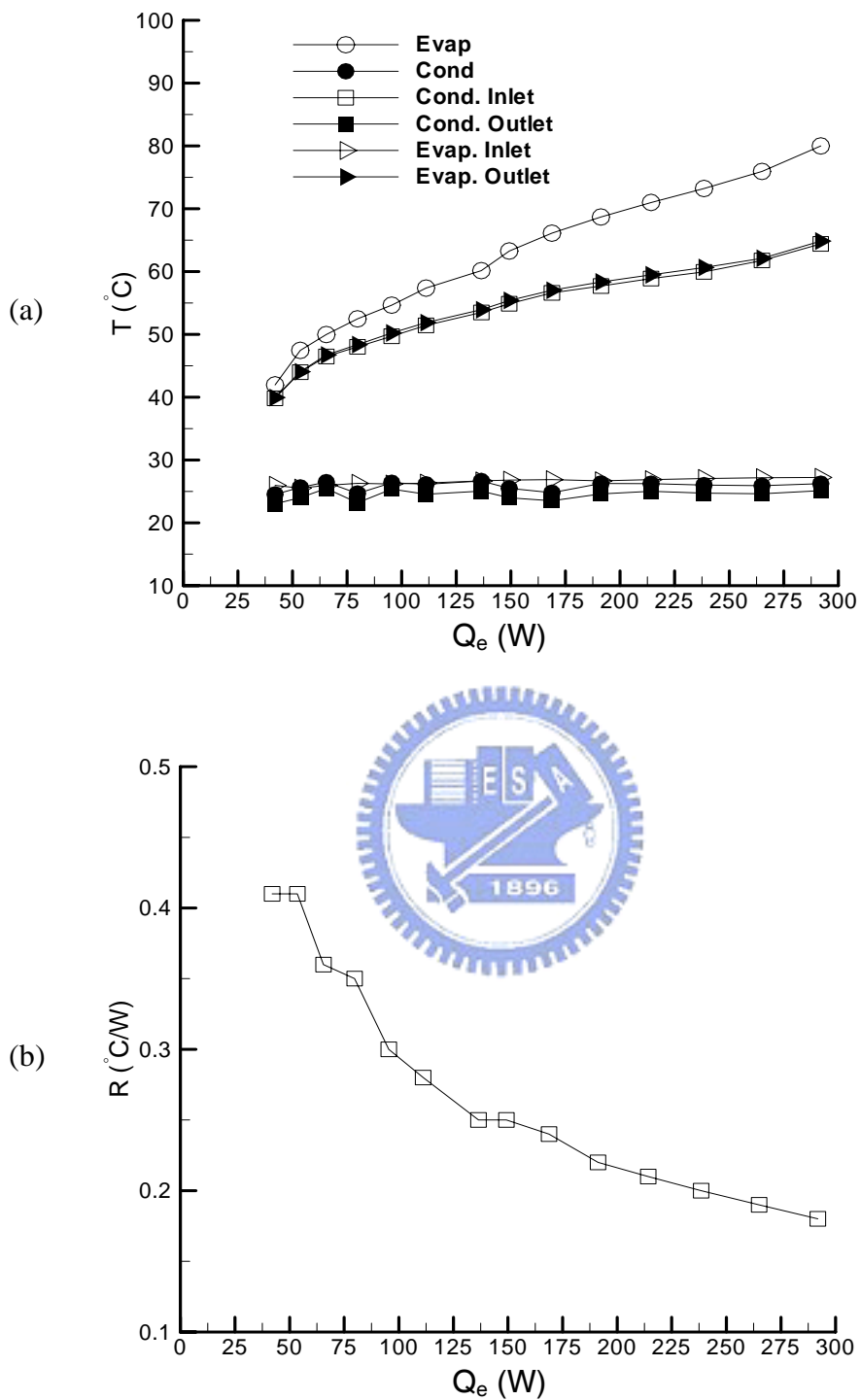
Fig 4.34 Variations of mean evaporator temperature (a) and thermal resistance of the CPL (b) with the input power to the evaporator using heat spreader with the surface roughing on the grooved channels for various liquid inventories for the relative height between condenser and evaporator of 0 cm.

Fig 4.35 Variations of the maximum allowable power input with the liquid inventory
for the relative height between condenser and evaporator of 0 cm for CPL with and
without the surface roughing on the vertical and bottom surface of the grooved
channels in the evaporator.

Fig 4.36 Variations of mean evaporator temperature (a) and thermal resistance of the CPL (b) with the input power for the relative height between condenser and evaporator of 0 cm at the optimal liquid inventories for the CPL with and without the surface roughing on the grooved channels.
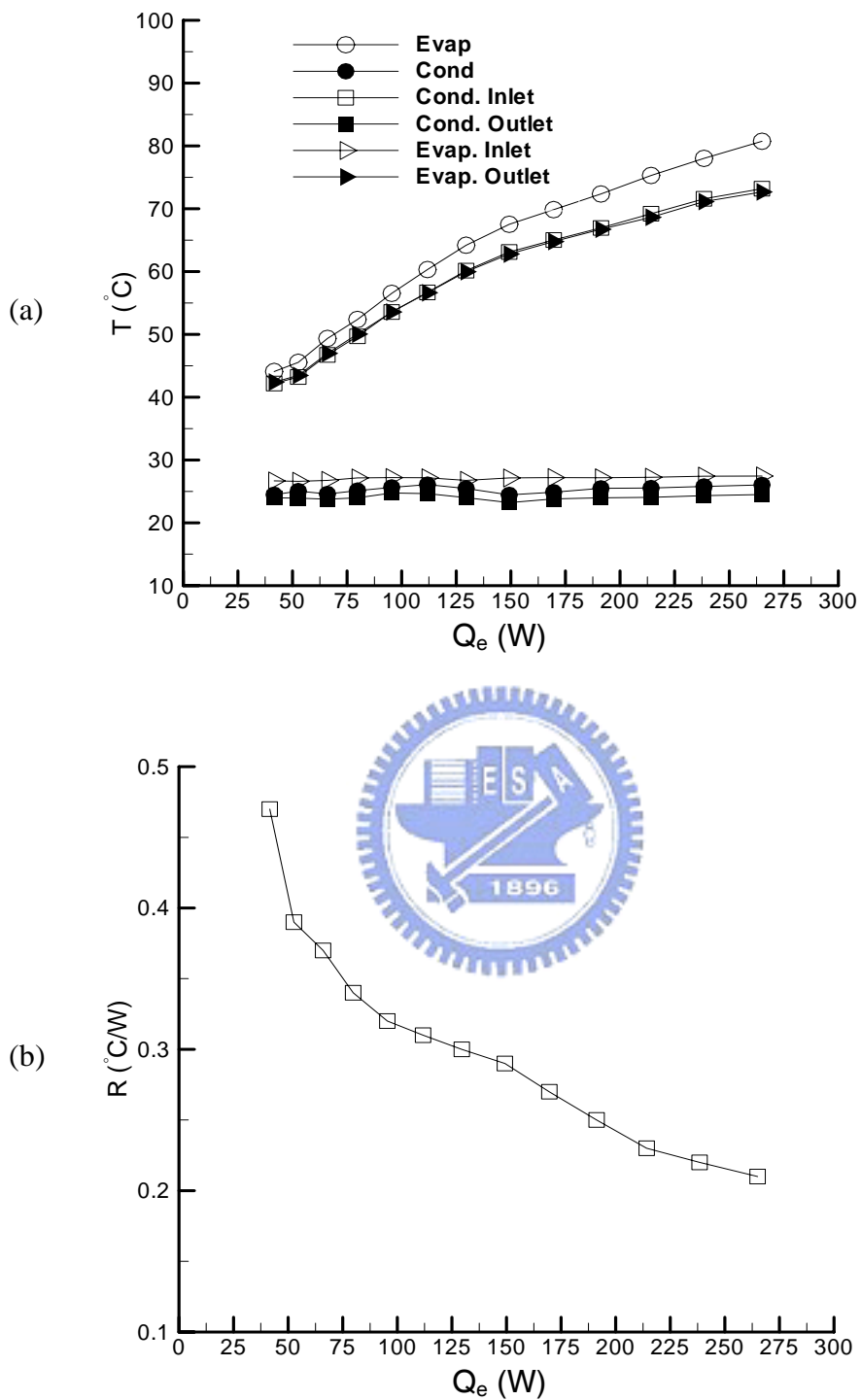
Fig 4.37 Variations of temperatures at selected locations (a) and thermal resistance of the CPL (b) with the input power to the evaporator using heat spreader with the surface roughing on the grooved channels for the liquid inventory of 50% and relative height between condenser and evaporator of 0 cm.
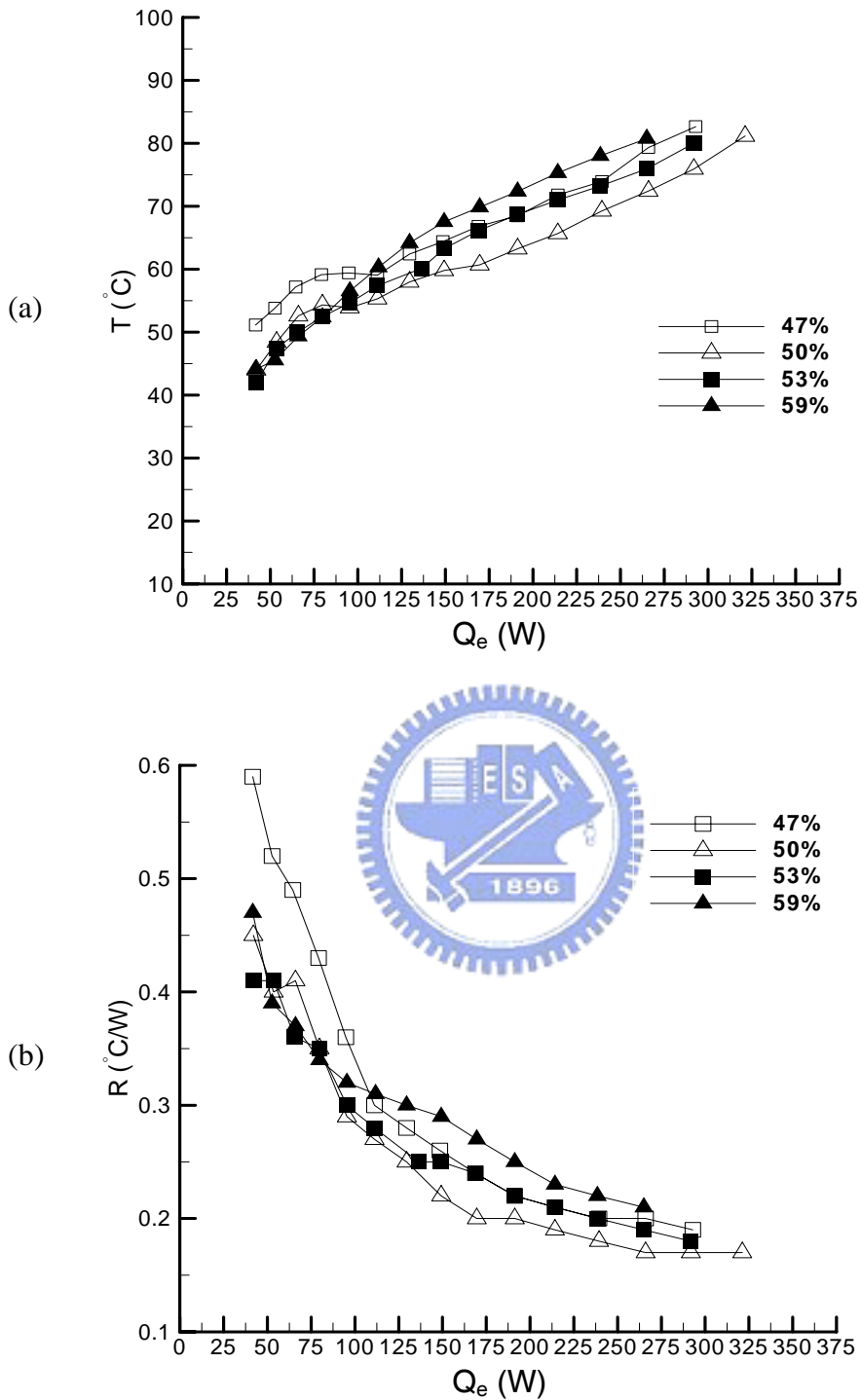
Fig 4.38 Variations of temperatures at selected locations (a) and thermal resistance of the CPL (b) with the input power to the evaporator using heat spreader with the surface roughing on the grooved channels for the liquid inventory of 50% and relative height between condenser and evaporator of 5 cm.
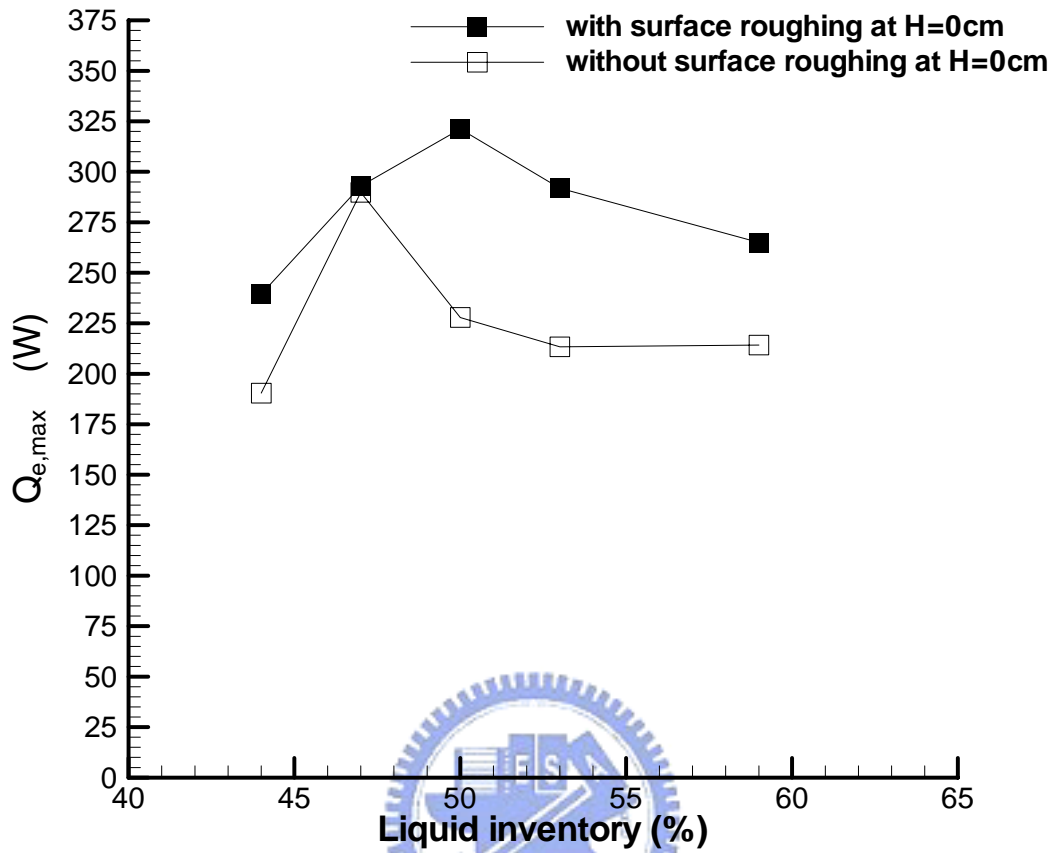
Fig 4.39 Variations of temperatures at selected locations (a) and thermal resistance of the CPL (b) with the input power to the evaporator using heat spreader with the surface roughing on the grooved channels for the liquid inventory of 50% and relative height between condenser and evaporator of 10 cm.
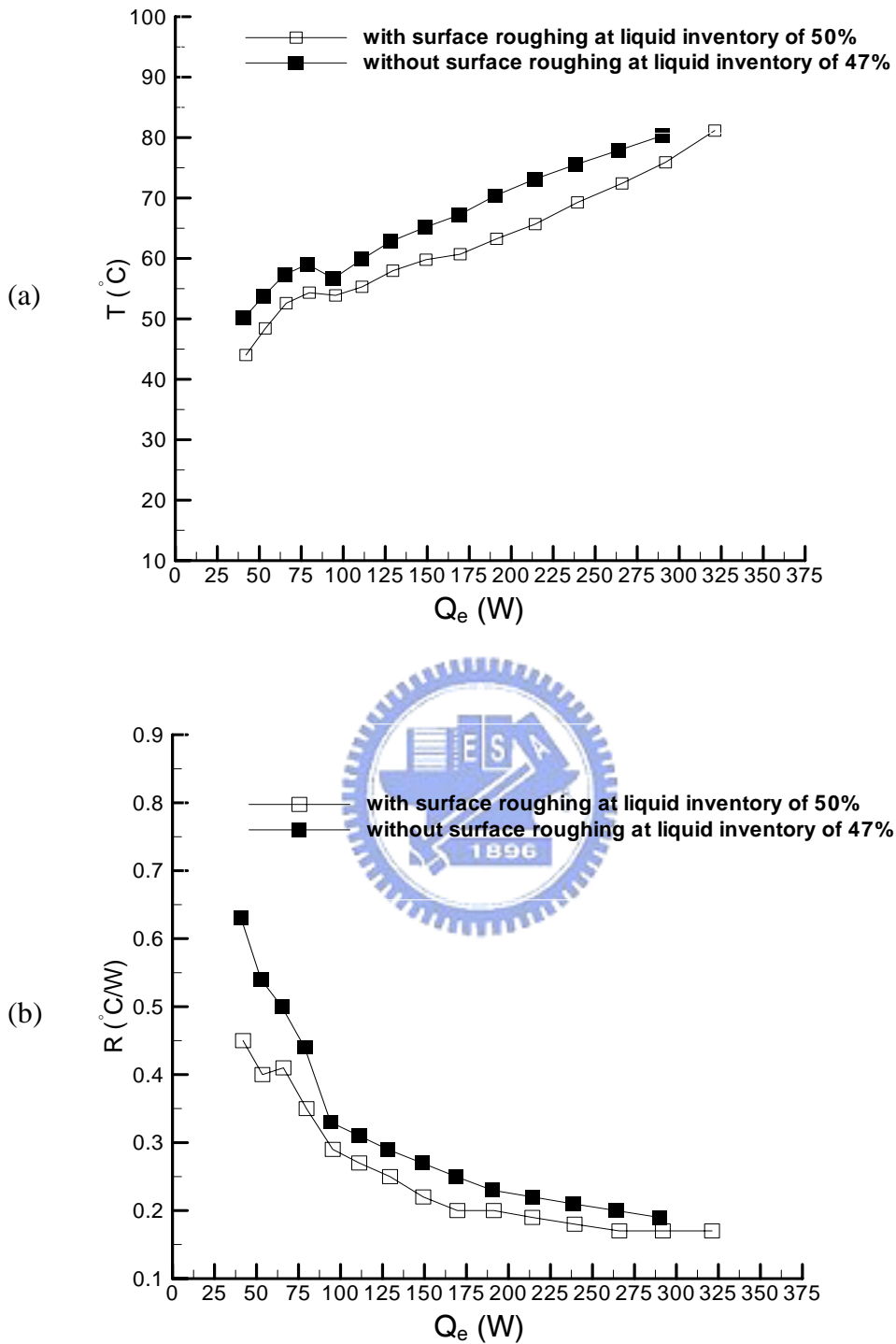
Fig 4.40 Variations of mean evaporator temperature (a) and thermal resistance of the CPL (b) with the input power to the evaporator using heat spreader with the surface roughing on the grooved channels for various relative heights between evaporator and condenser for the liquid inventory of 50%.
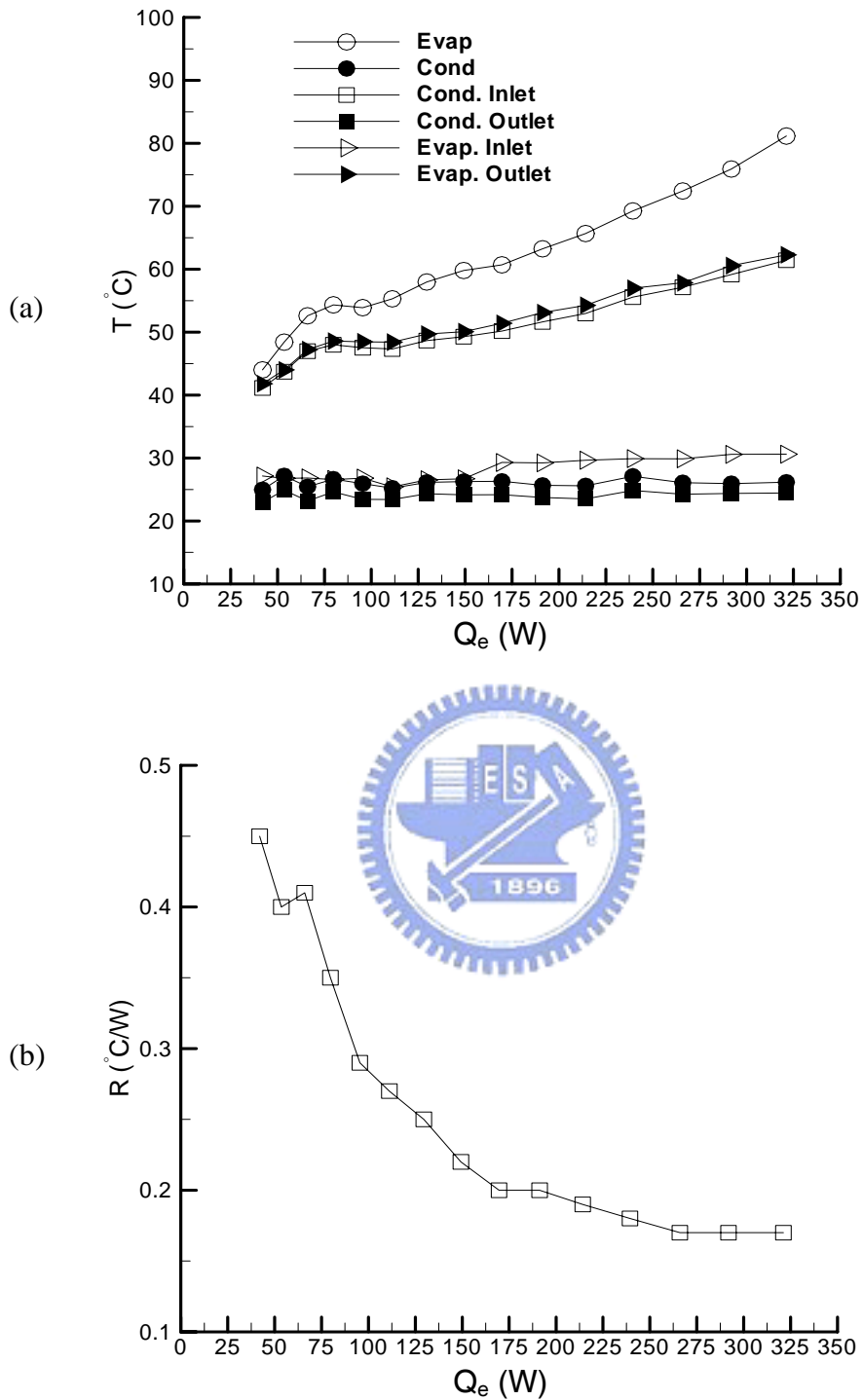
Fig 4.41 Variations of temperatures at selected locations (a) and thermal resistance of the CPL (b) with the input power to the evaporator using heat spreader with the surface roughing on the grooved channels for the liquid inventory of 47% and relative height between condenser and evaporator of 0 cm.
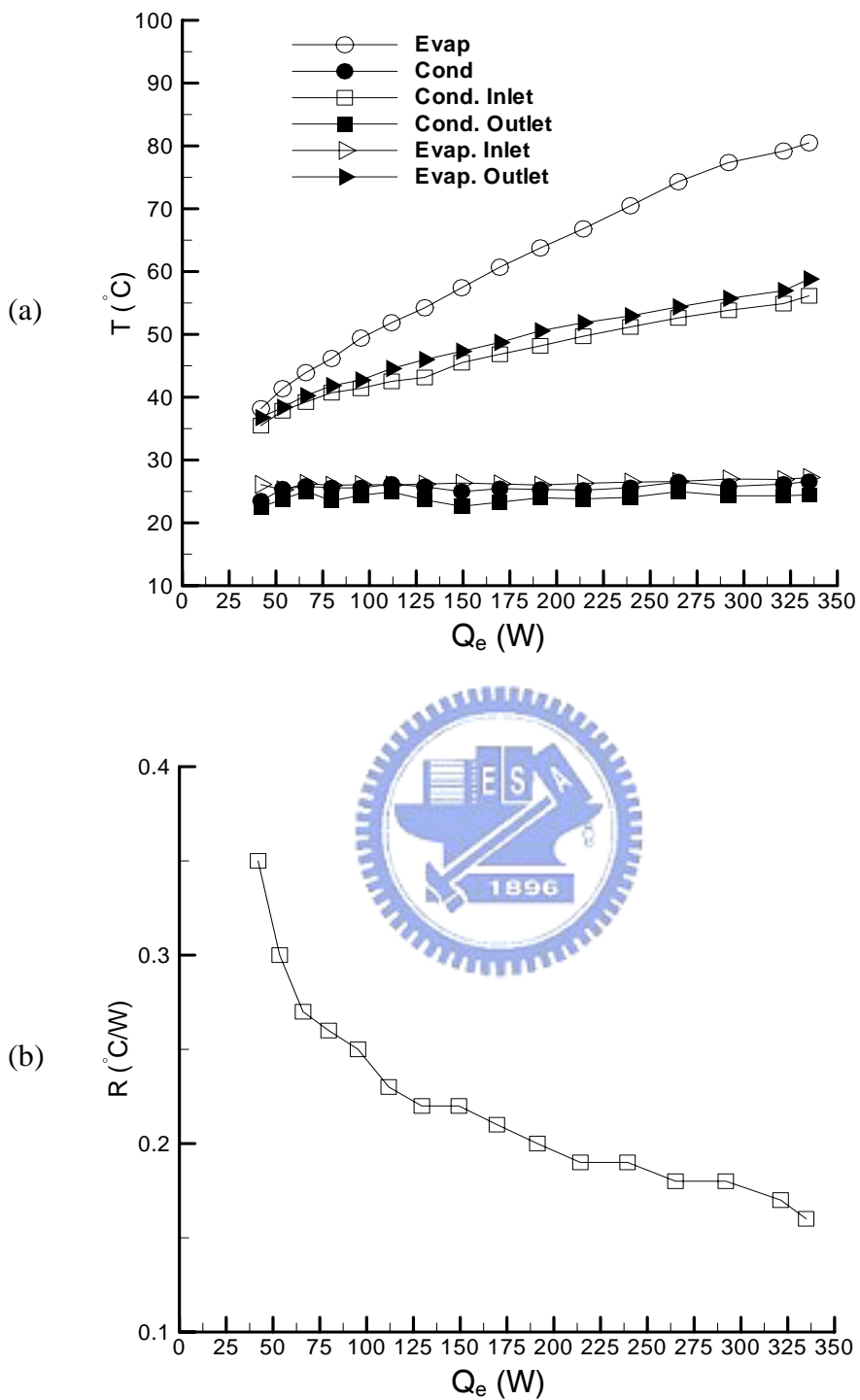
Fig 4.42 Variations of temperatures at selected locations (a) and thermal resistance of the CPL (b) with the input power to the evaporator using heat spreader with the surface roughing on the grooved channels for the liquid inventory of 47% and relative height between condenser and evaporator of 5 cm.
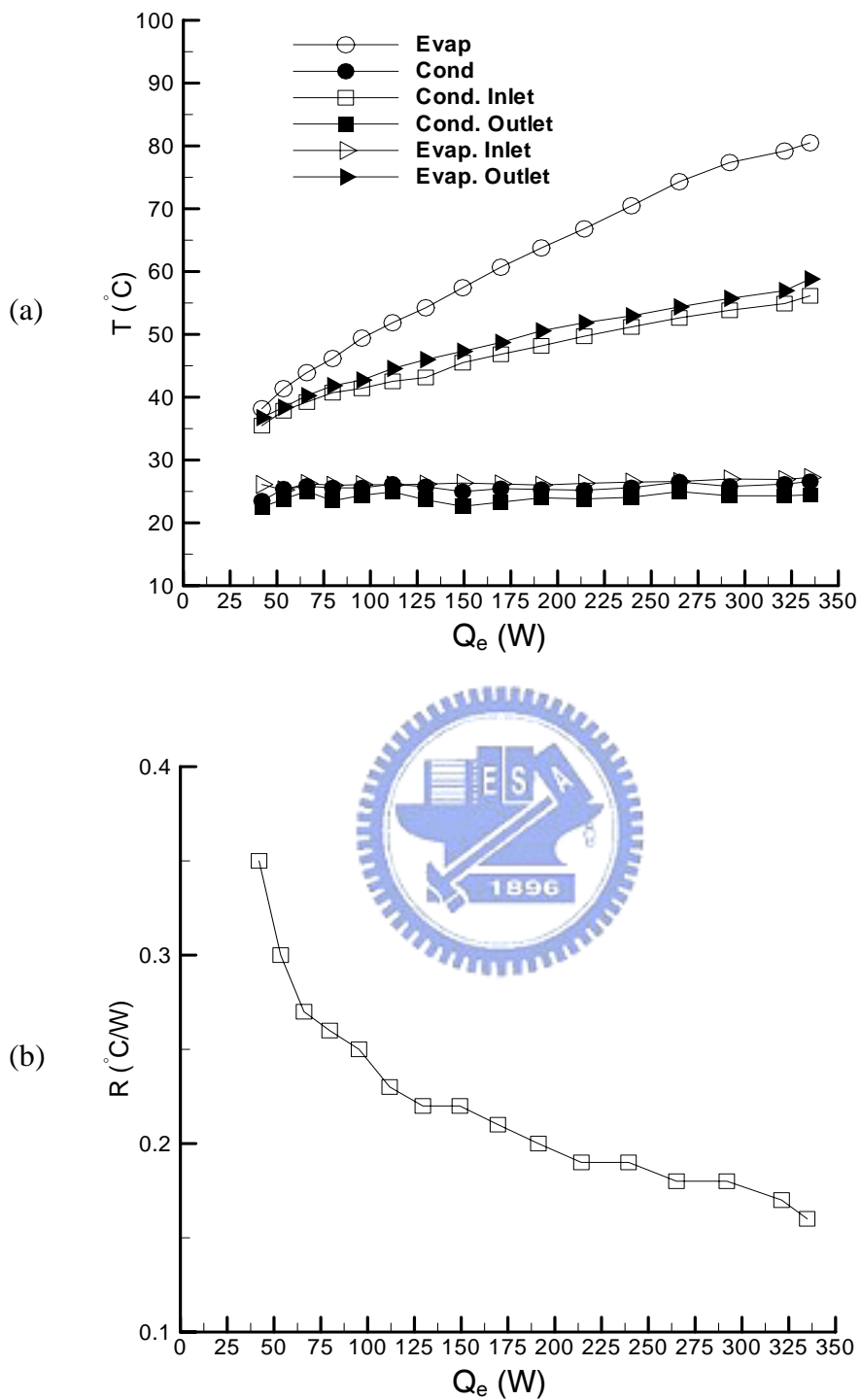
Fig 4.43 Variations of temperatures at selected locations (a) and thermal resistance of the CPL (b) with the input power to the evaporator using heat spreader with the surface roughing on the grooved channels for the liquid inventory of 47% and relative height between condenser and evaporator of 10 cm.
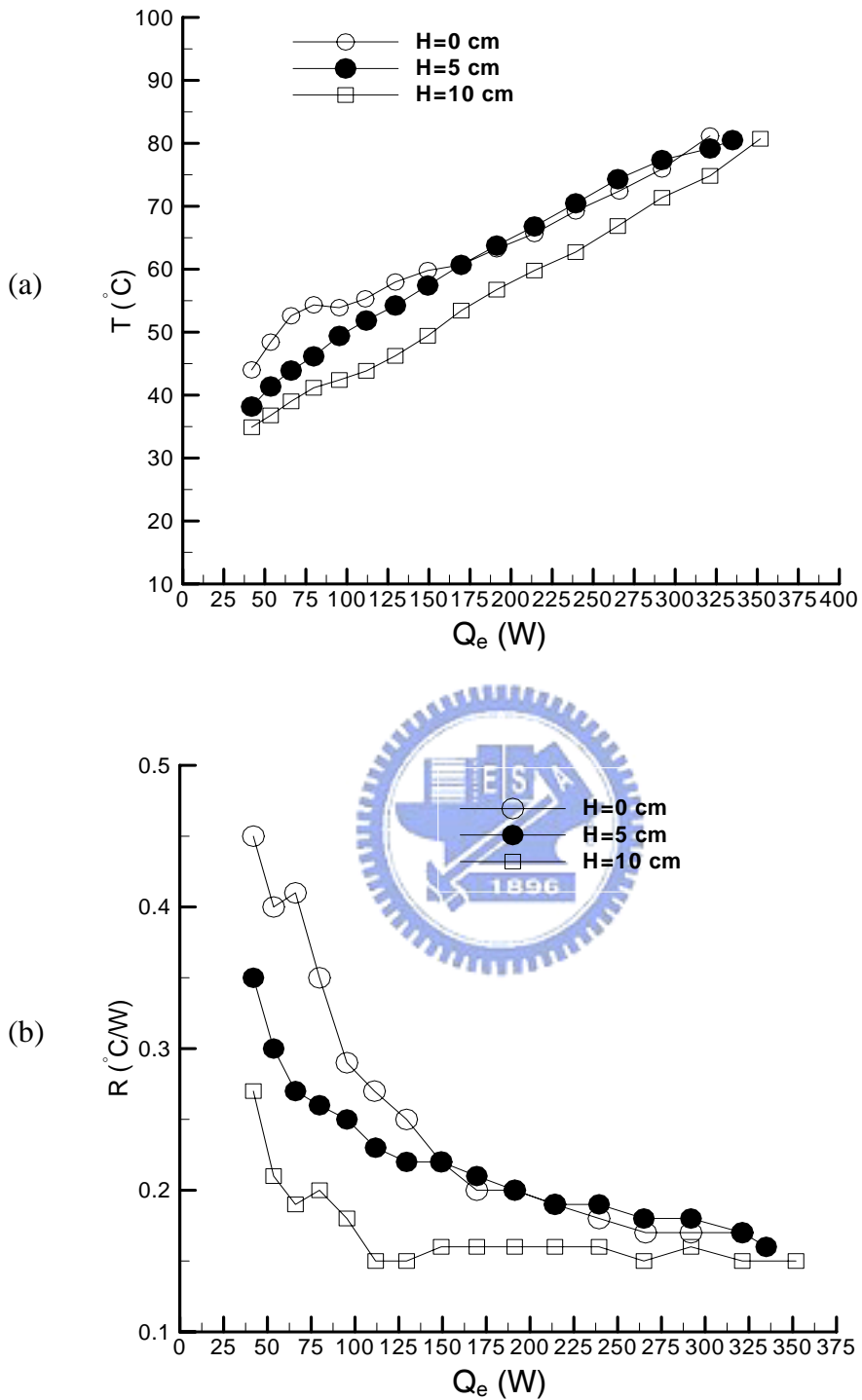
Fig 4.44 Variations of mean evaporator temperature (a) and thermal resistance of the CPL (b) with the input power to the evaporator using heat spreader with the surface roughing on the grooved channels for various relative heights between evaporator and condenser for the liquid inventory of 47%.
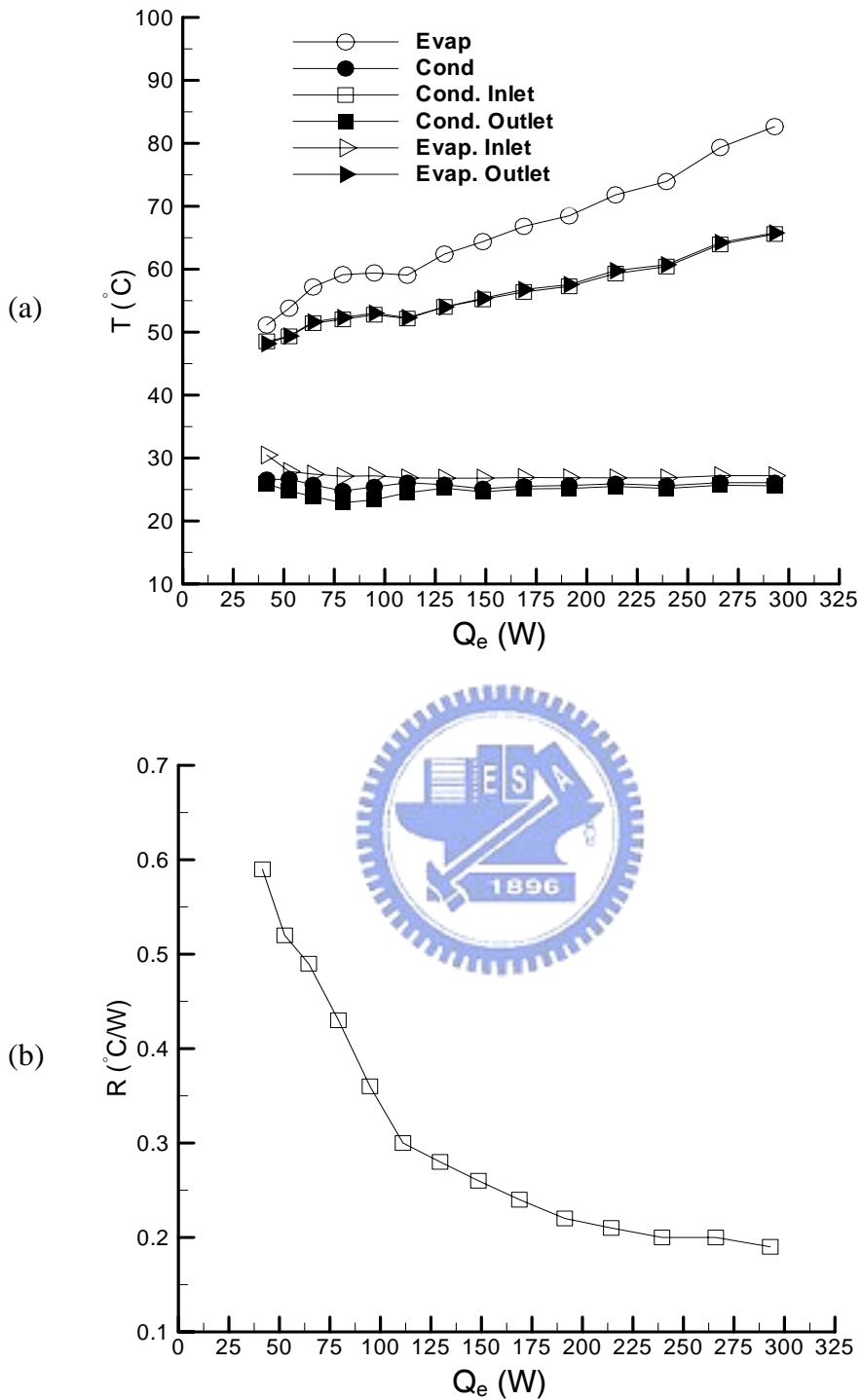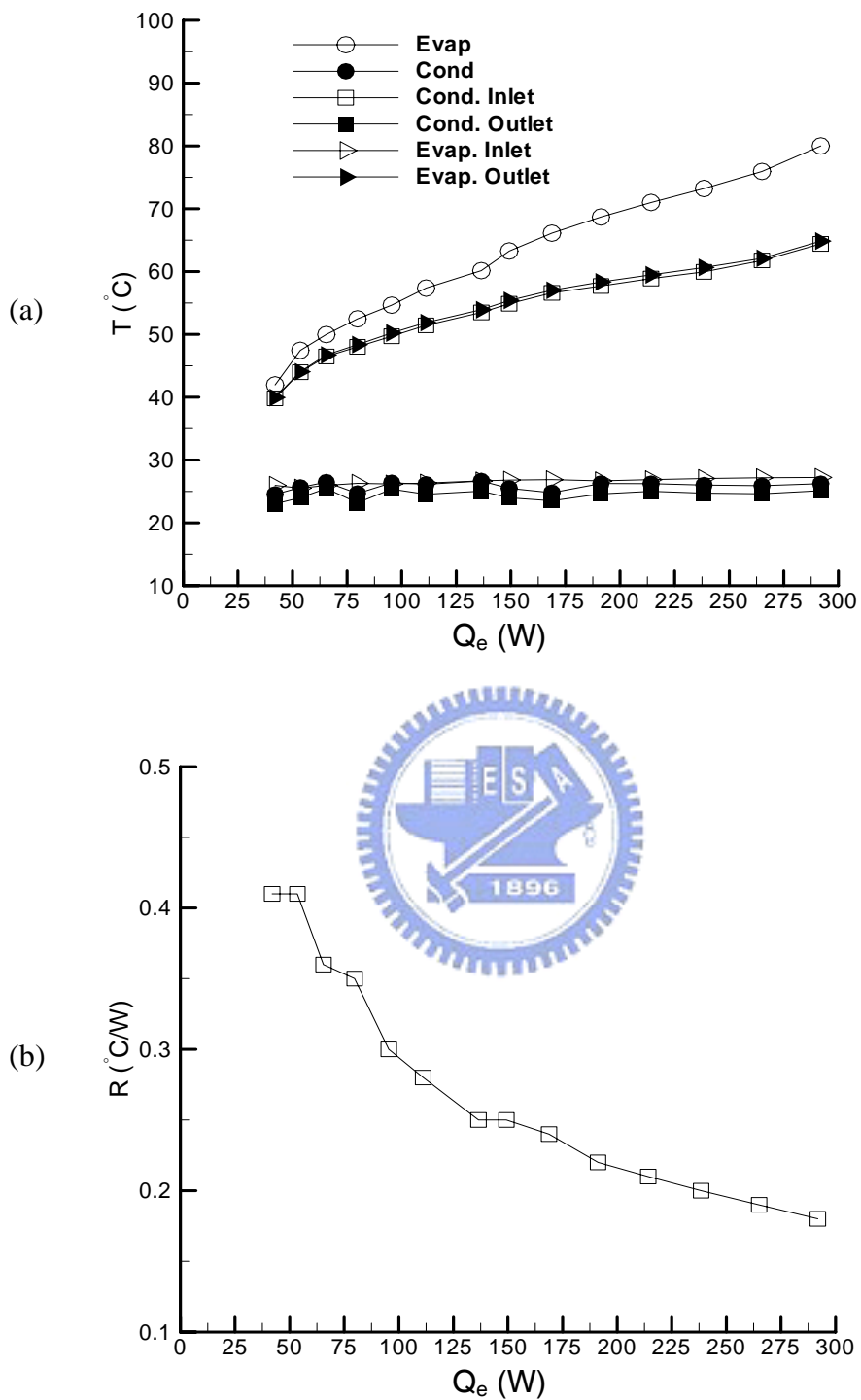
Fig 4.45 Variations of temperatures at selected locations (a) and thermal resistance of the CPL (b) with the input power to the evaporator using heat spreader with the surface roughing on the grooved channels for the liquid inventory of 53% and relative height between condenser and evaporator of 0 cm.

Fig 4.46 Variations of temperatures at selected locations (a) and thermal resistance of the CPL (b) with the input power to the evaporator using heat spreader with the surface roughing on the grooved channels for the liquid inventory of 53% and relative height between condenser and evaporator of 5 cm.
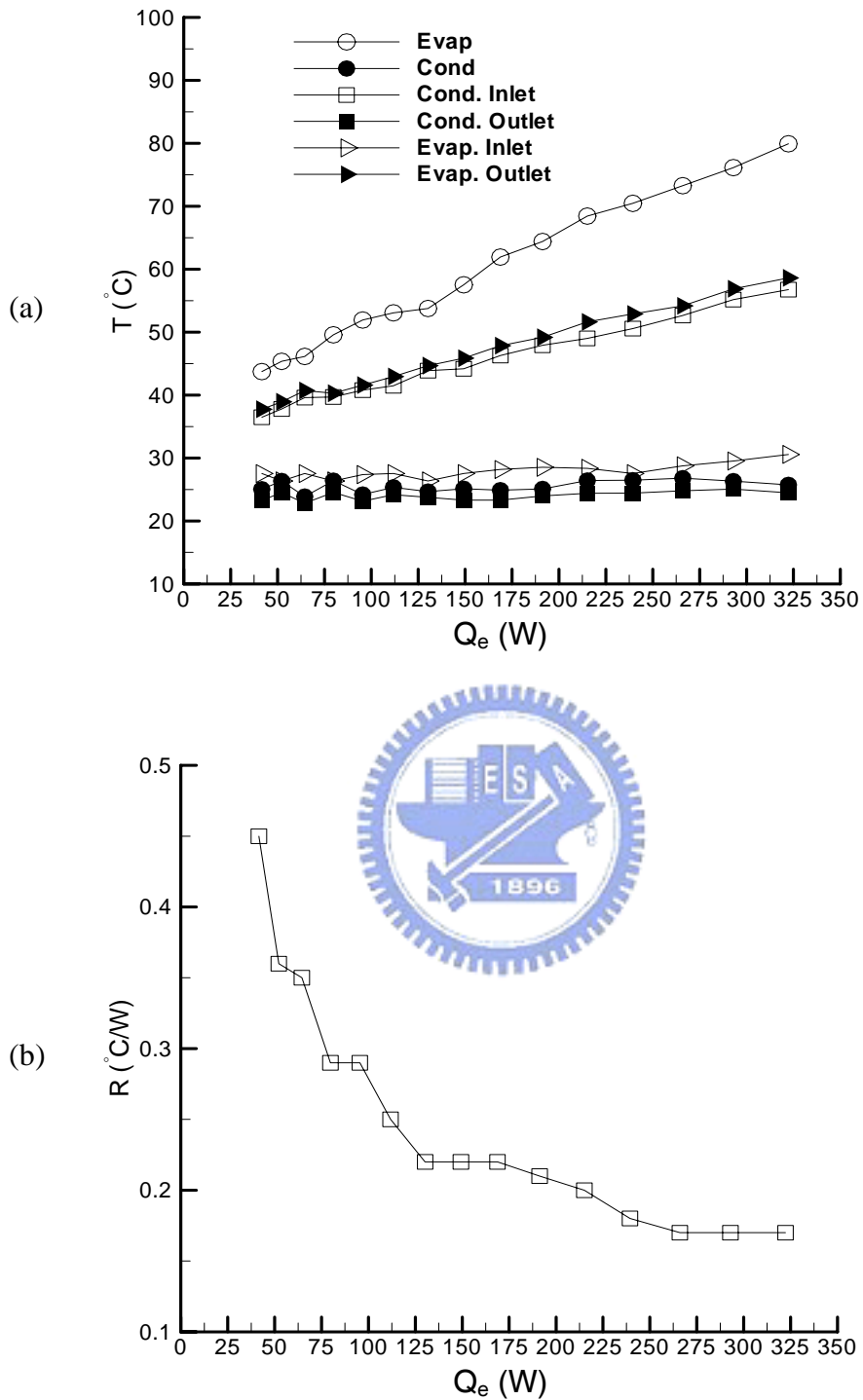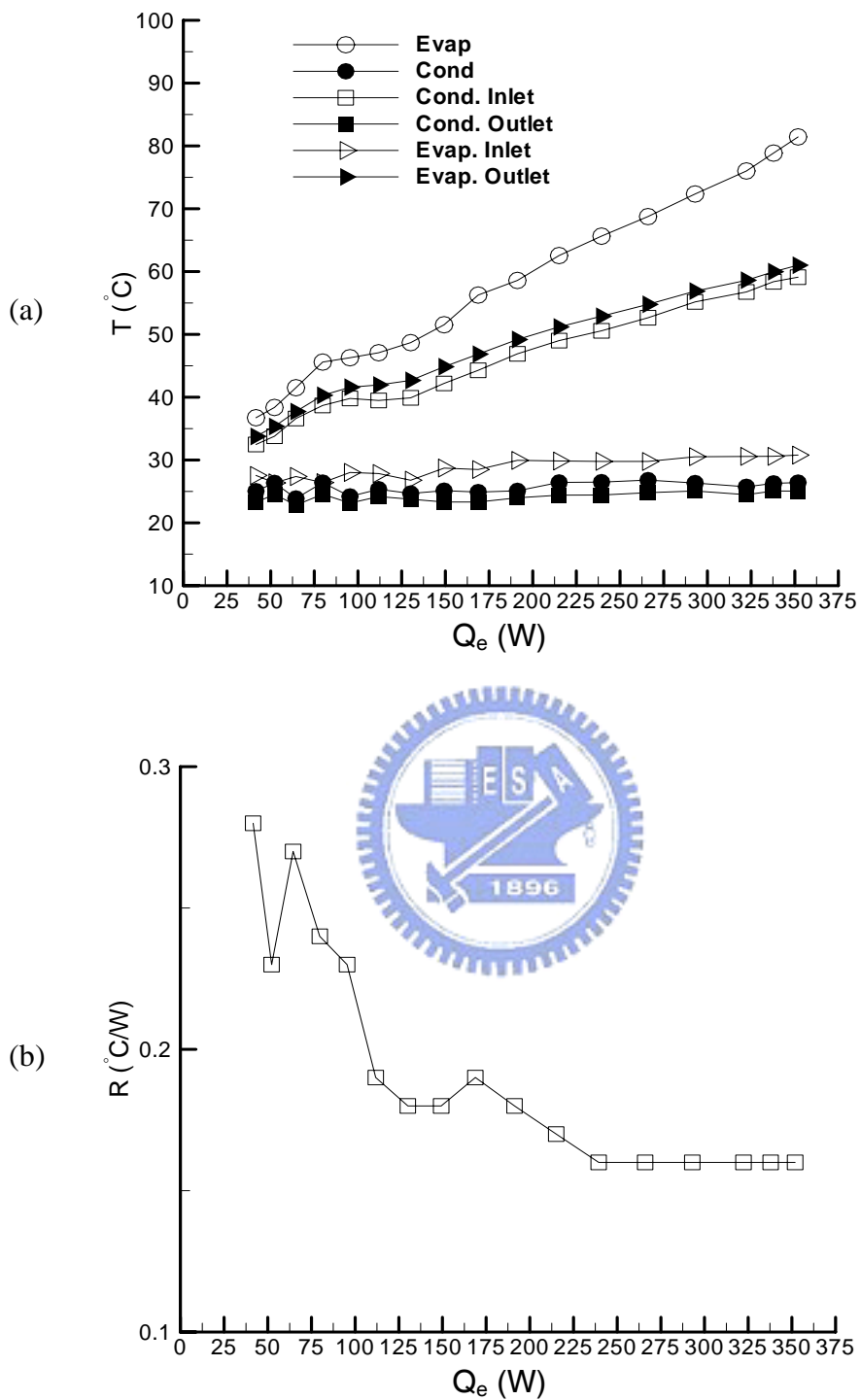
Fig 4.47 Variations of temperatures at selected locations (a) and thermal resistance of the CPL (b) with the input power to the evaporator using heat spreader with the surface roughing on the grooved channels for the liquid inventory of 53% and relative height between condenser and evaporator of 10 cm.
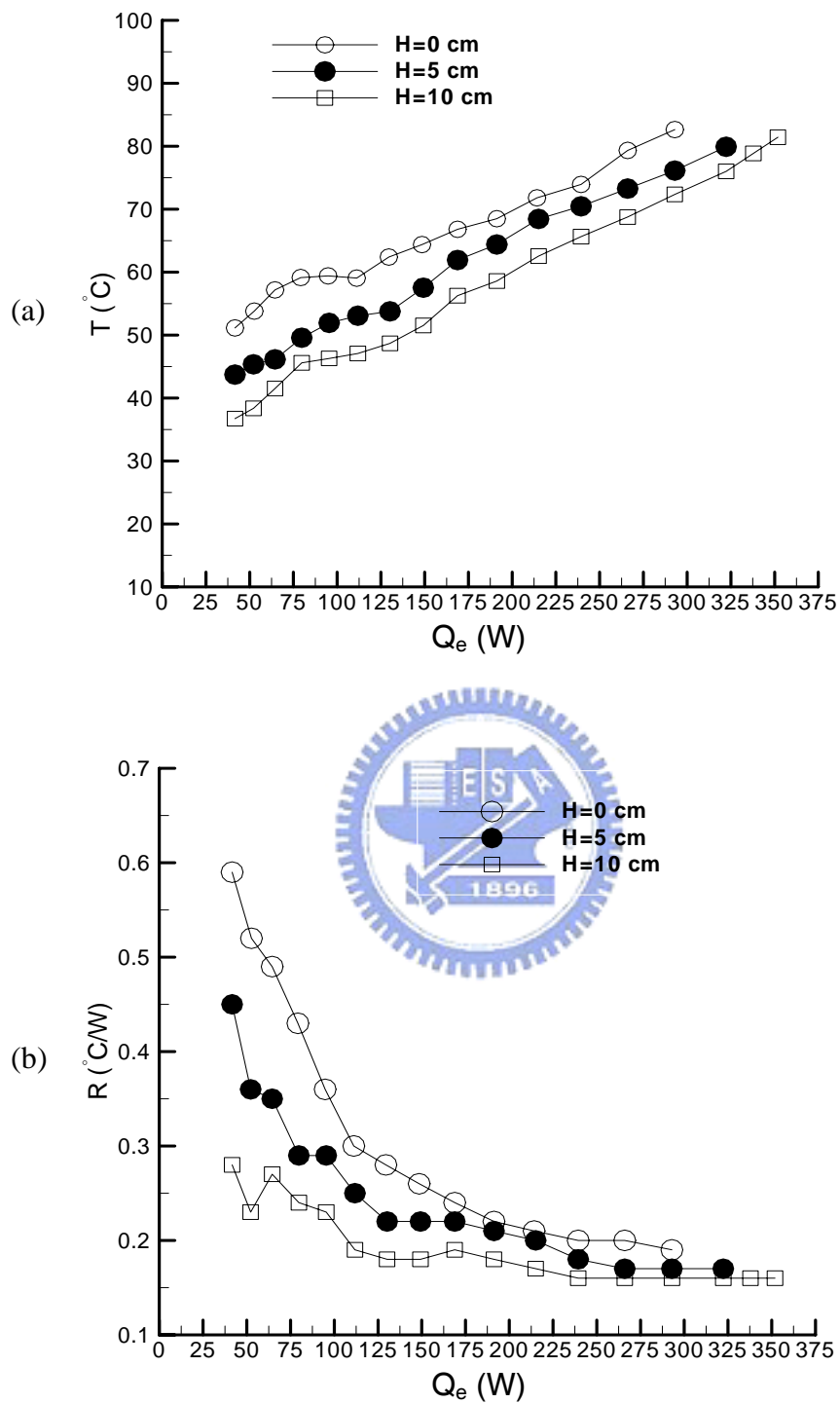
Fig 4.48 Variations of mean evaporator temperature (a) and thermal resistance of the CPL (b) with the input power to the evaporator using heat spreader with the surface roughing on the grooved channels for various relative heights between evaporator and condenser for the liquid inventory of 53%.
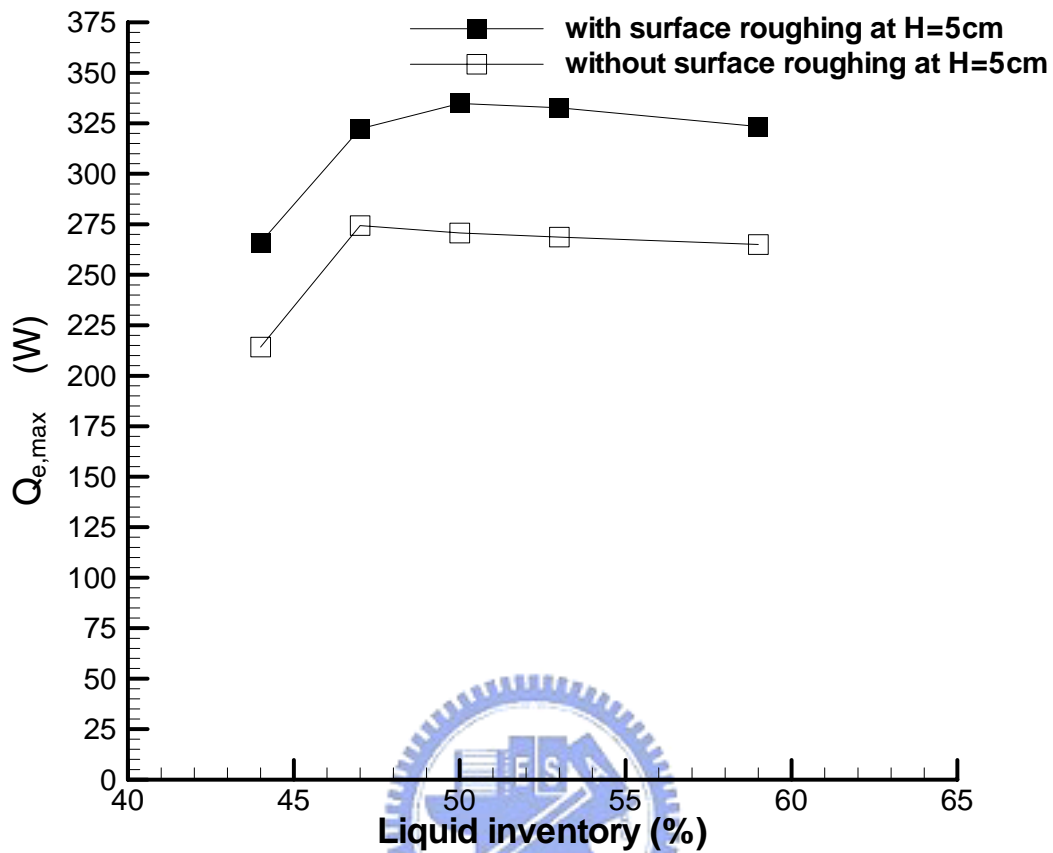
Fig 4.49 Variations of the maximum allowable power input with the liquid inventory for the relative height between condenser and evaporator of 5 cm for CPL with and without the surface roughing on the vertical and bottom surface of the grooved channels in the evaporator.
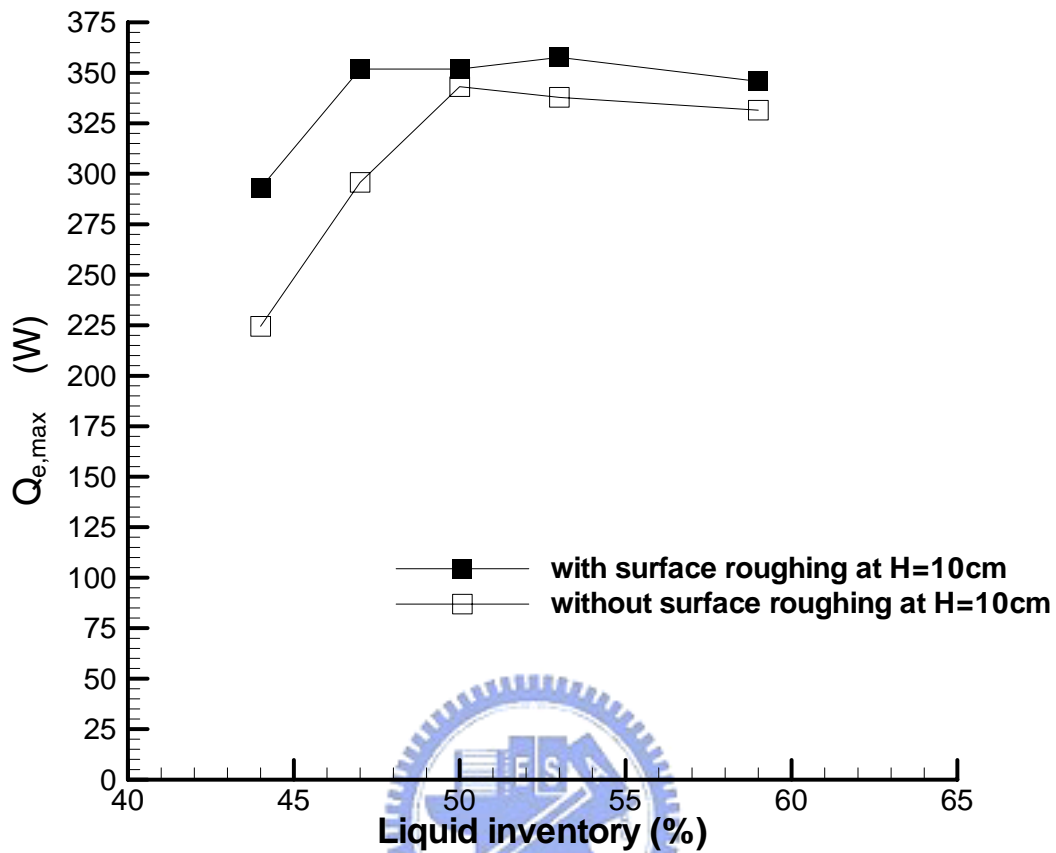
Fig 4.50 Variations of the maximum allowable power input with the liquid inventory for the relative height between condenser and evaporator of 10 cm for CPL with and without the surface roughing on the vertical and bottom surface of the grooved channels in the evaporator.
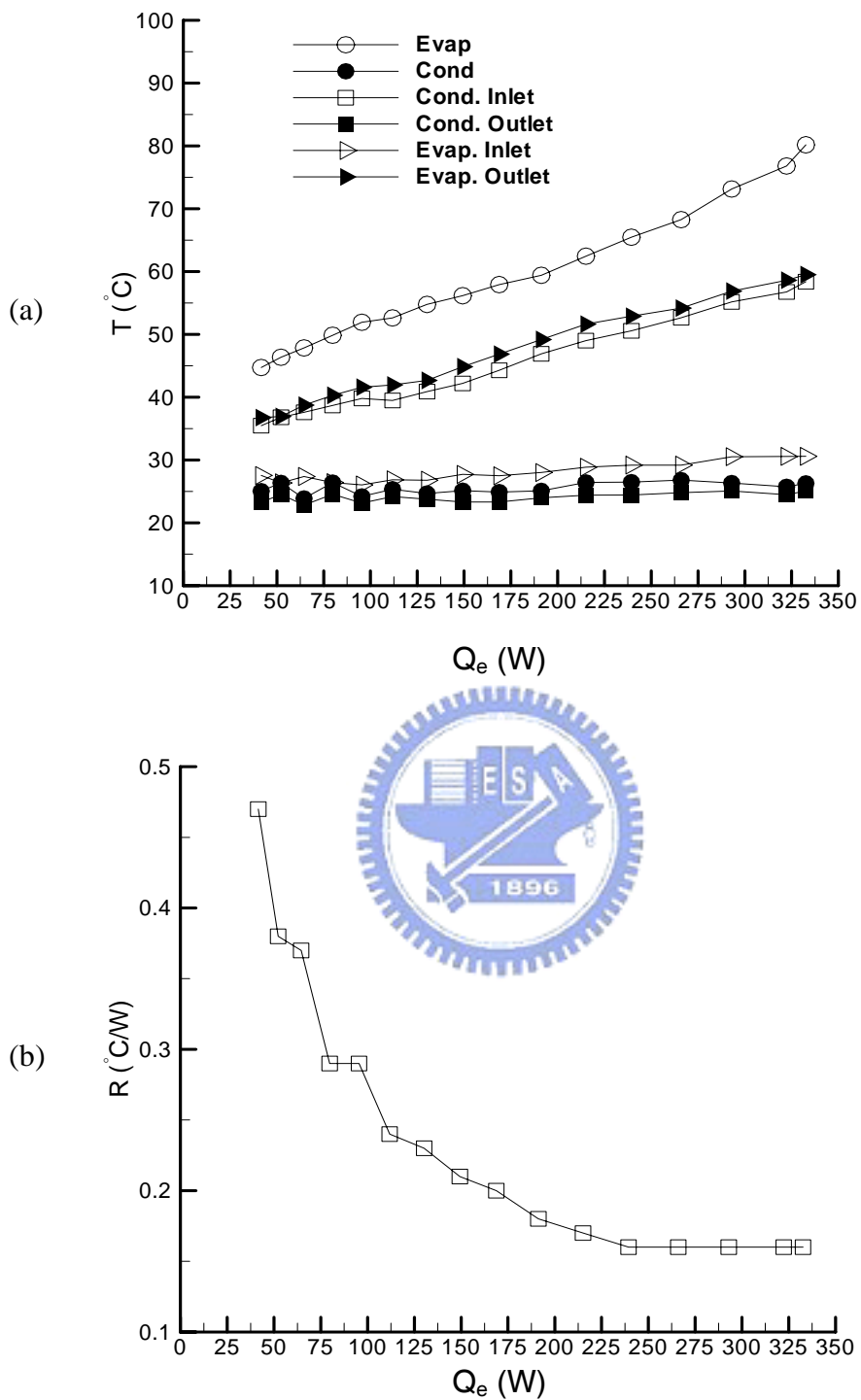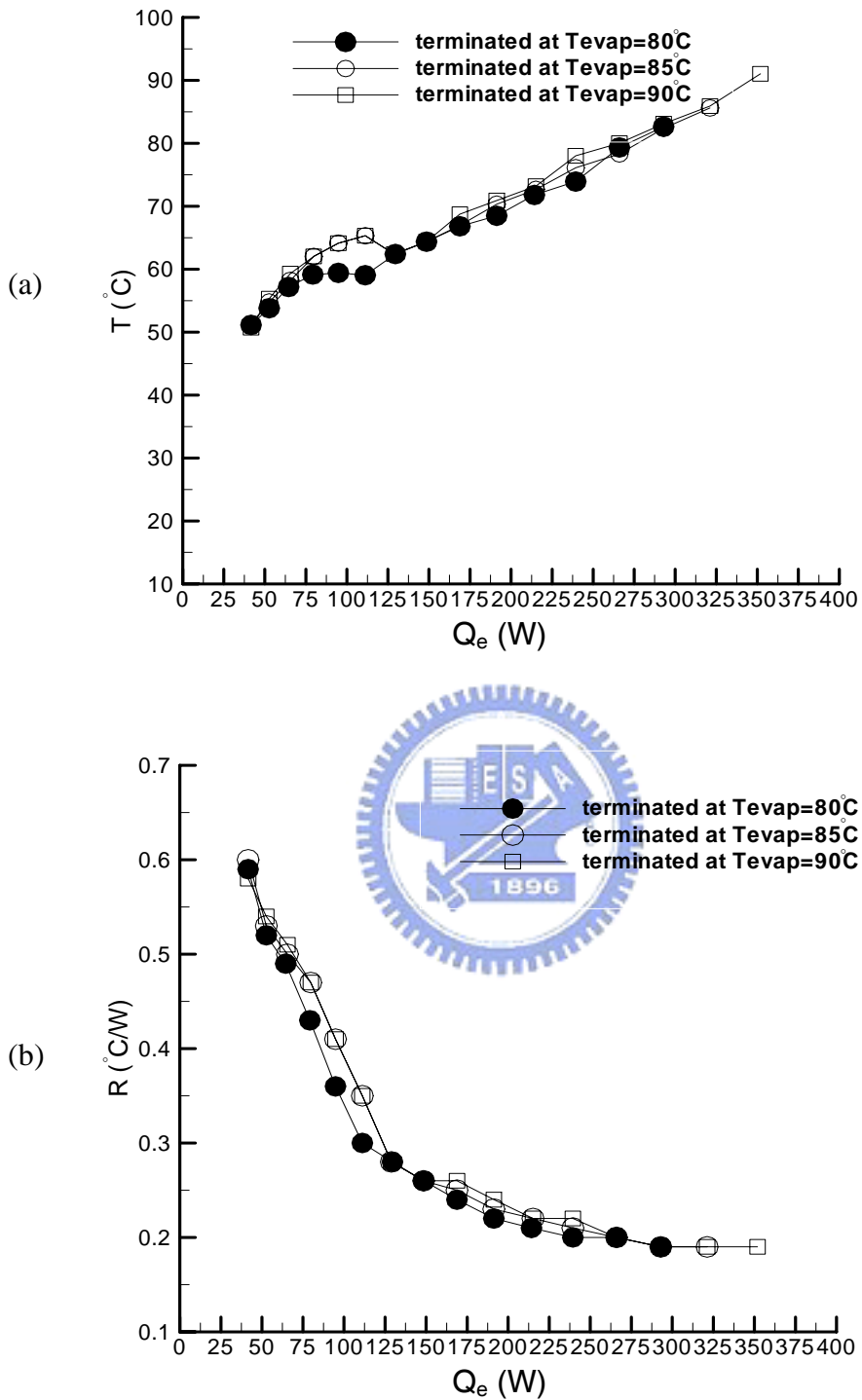
Fig 4.51 Variations of mean evaporator temperature (a) and thermal resistance of the CPL (b) with the input power to the evaporator using heat spreader with the surface roughing on the grooved channels for terminating at various T_{evap} for the liquid inventory of 47% and relative height between condenser and evaporator of 0 cm.
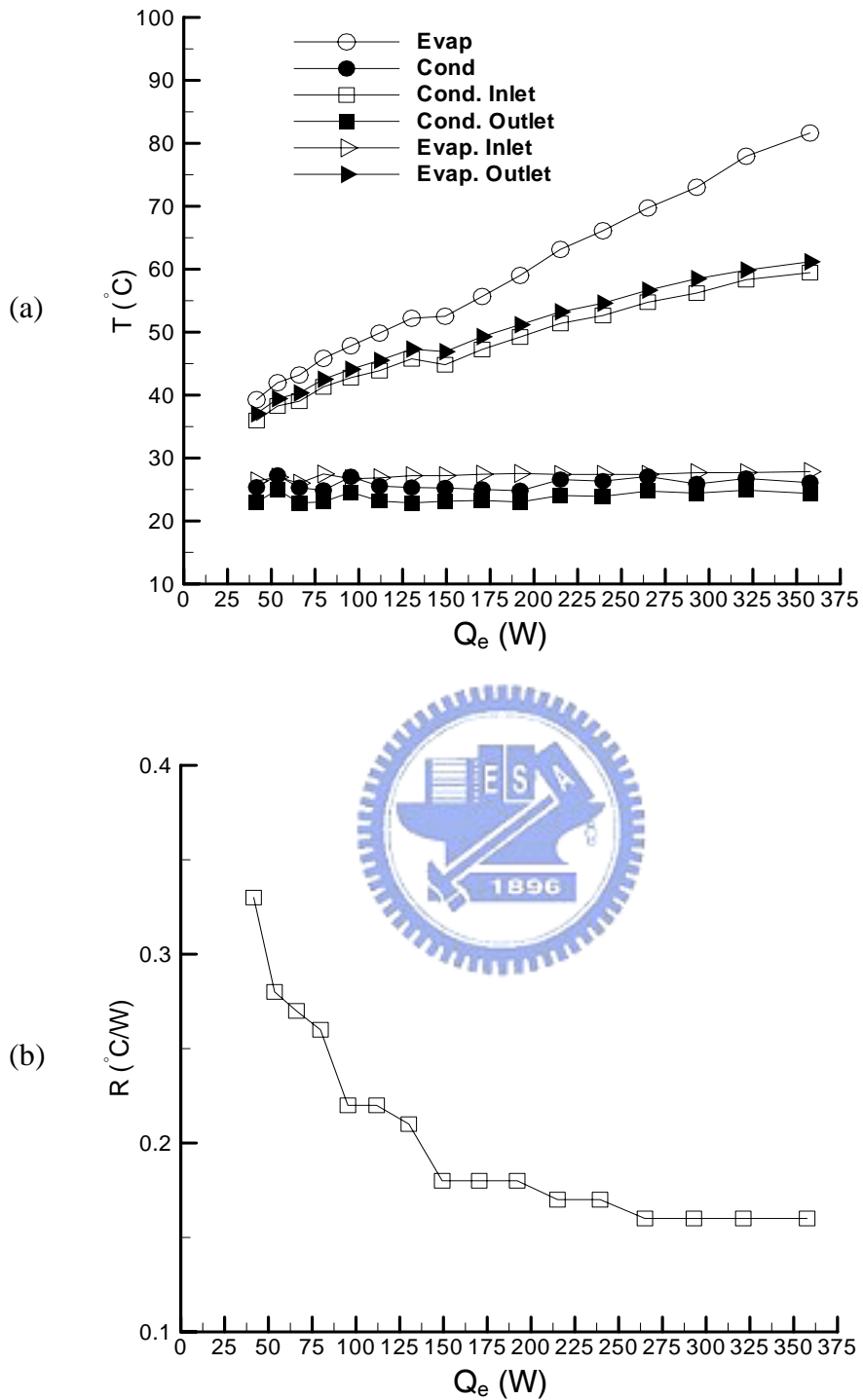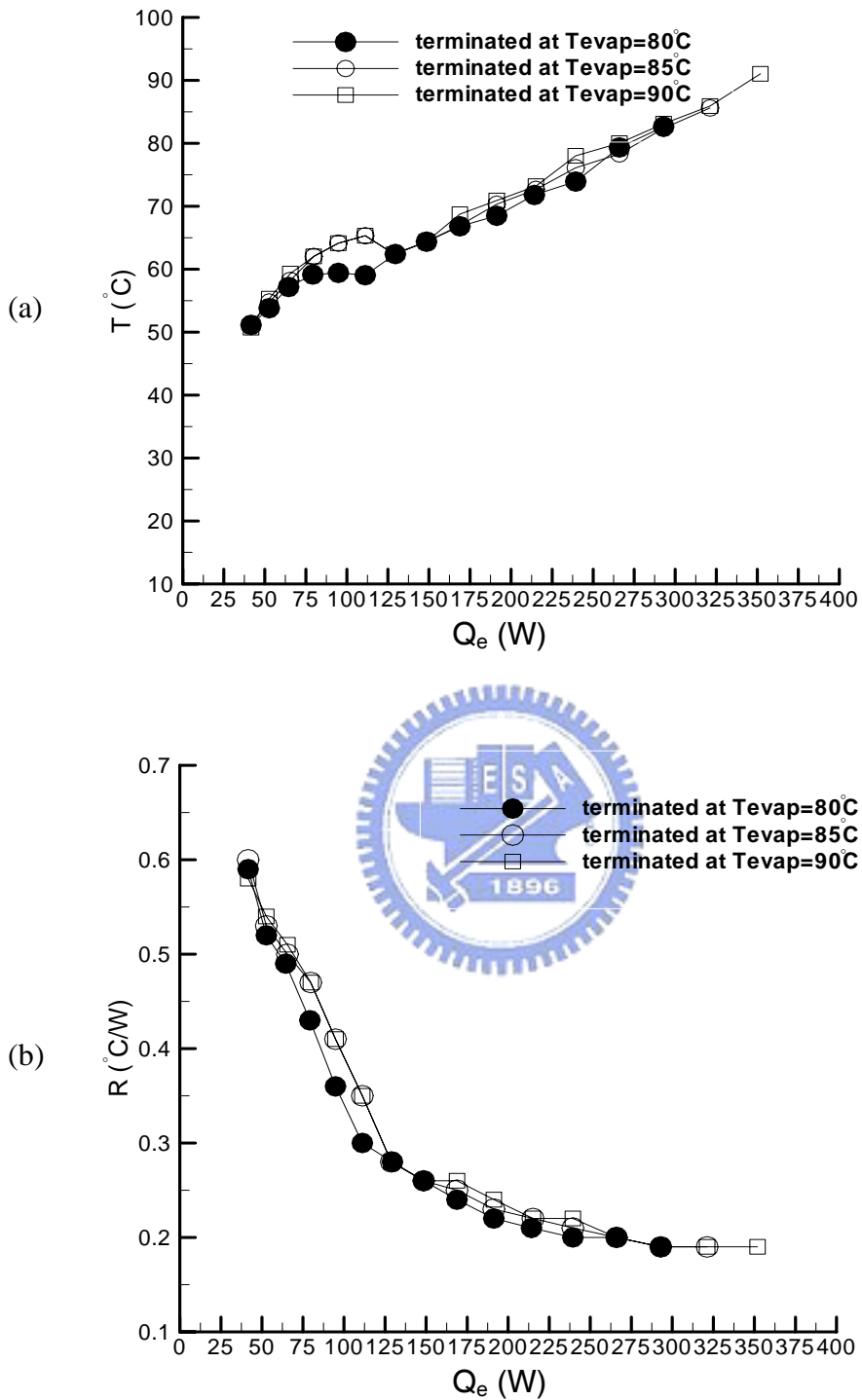
Fig 4.52 Variations of mean evaporator temperature (a) and thermal resistance of the CPL (b) with the input power to the evaporator using heat spreader with the surface roughing on the grooved channels for terminating at various T_{evap} for the liquid inventory of 50% and relative height between condenser and evaporator of 0 cm.
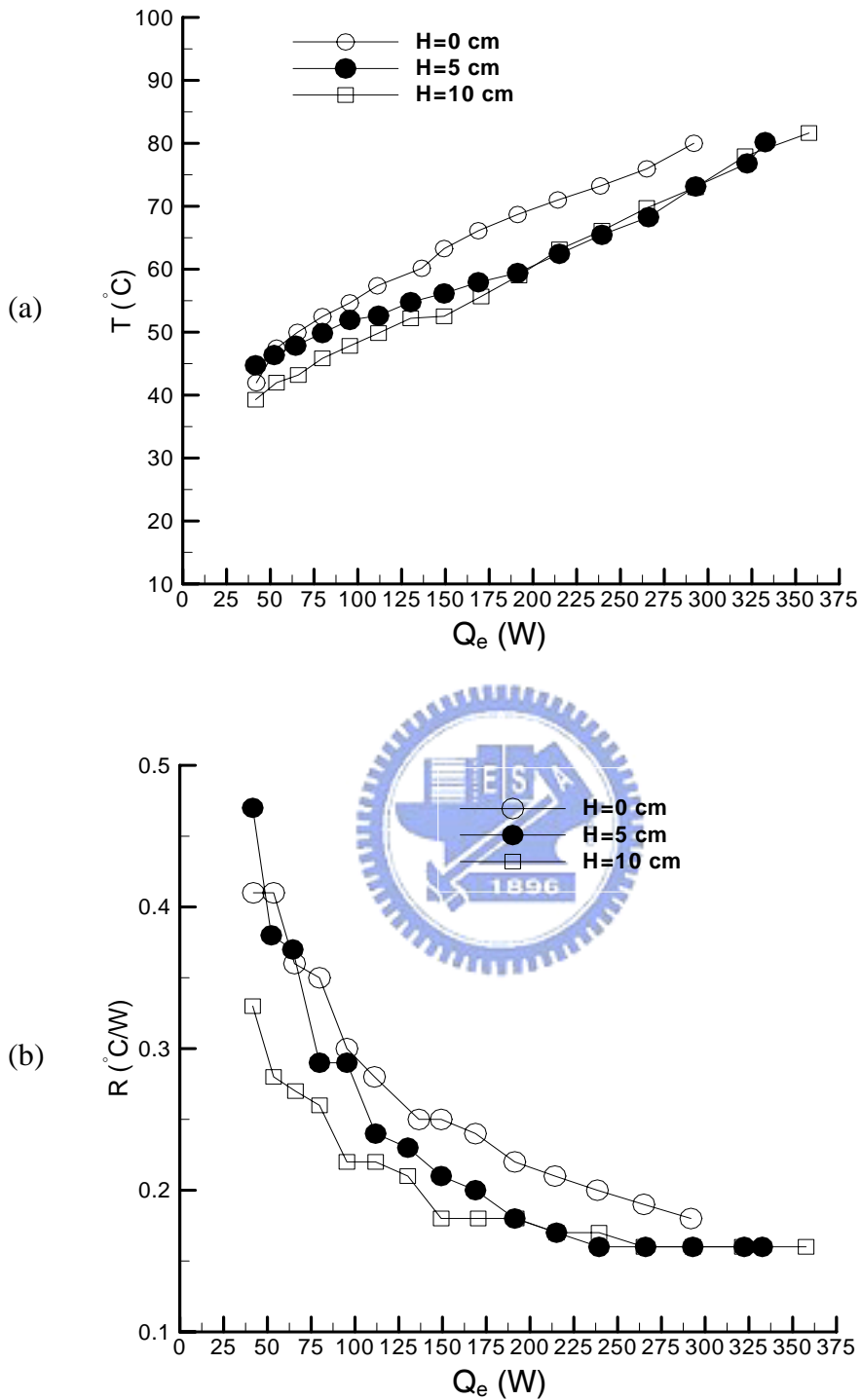
Fig 4.53 Variations of mean evaporator temperature (a) and thermal resistance of the CPL (b) with the input power to the evaporator using heat spreader with the surface roughing on the grooved channels for terminating at various T_{evap} for the liquid inventory of 53% and relative height between condenser and evaporator of 0 cm.
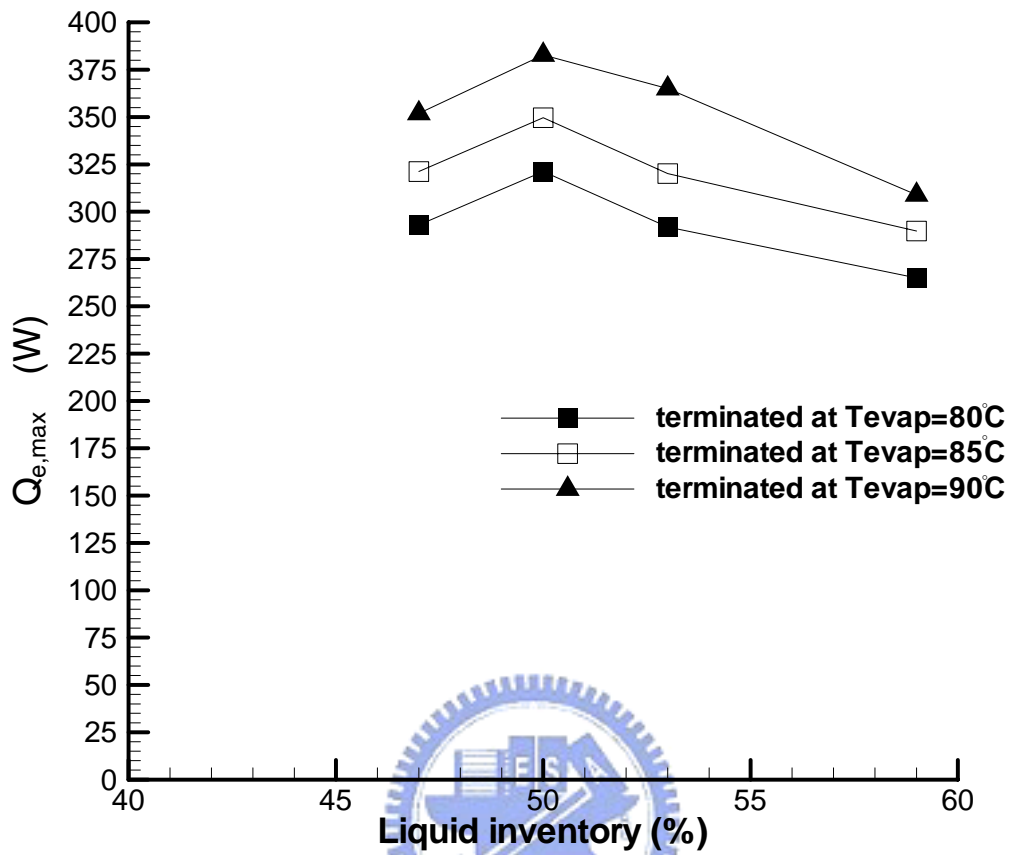
Fig 4.54 Variations of the maximum allowable power input with the liquid inventory

for terminating at various T_{evap} for CPL with the surface roughing on the vertical and

bottom surface of the grooved channels in the evaporator.

CHAPTER 5

CONCLUDING REMARKS
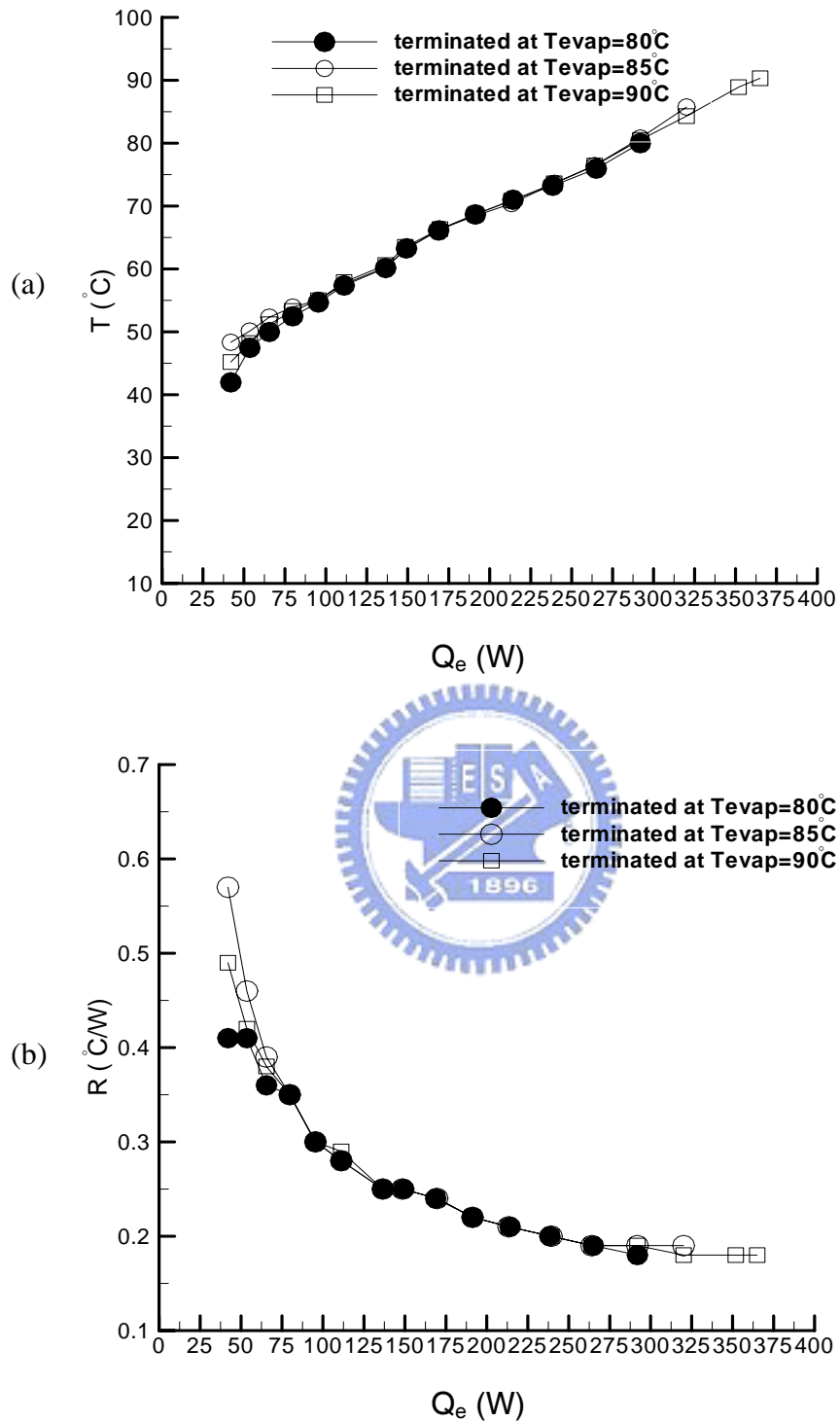
In this study experimental tests are conducted to investigate an improved CPL design for high power density CPU cooling. The evaporator of the CPL is improved by using pin fins to form the grooved channels, heat spreader, and roughing the vertical and bottom surfaces of the grooved channels. The effects of the liquid inventory and the relative height between the condenser and evaporator on the performance of the CPL with the improved designs for its evaporator have been examined in detail. The major results obtained here can be briefly summarized as follows:

(1) An optimal liquid inventory exists at which $Q_{e,max}$ is the highest and R_{th} is the lowest for a given relative condenser-evaporator height for the CPL with a given evaporator design. Moreover, increasing or decreasing the liquid inventory from this optimal value causes a reduction in $Q_{e,max}$ and a raise in R_{th}.

(2) An increase in the relative height between the condenser and evaporator results in a significant improvement in the CPL performance with a much higher $Q_{e,max}$ and a much lower R_{th}.

(3) There is no noticeable enhancement in the heat transfer performance of CPL by using a pin fin block to form the grooved channels.

(4) The use of a large heat spreader in the evaporator can greatly enhance the heat transfer performance of the CPL. The maximum enhancement is nearly 100% in the tested conditions.

(5) Roughing the vertical and bottom surfaces of the grooved channels can also noticeably enhance the heat transfer performance of the CPL.

Reference

1. F. J. Stenger, Experimental feasibility study of water-filled capillary-pumped heat-transfer loops, NASA TM-X-1310, NASA Lewis Research Center, Cleveland, Ohio, 1966.

2. J. Ku, Overview of capillary pumped loop technology, ASME HTD-Vol. 236, 1993, pp. 1-17.

3. Yu. Maidanik, Yu. Fershtater, V. G. pastukhov, M. Chernysheva, Experimental and theoretical investigation of startup regimes of two-phase capillary pumped loops, Society of Automotive Engineers, Paper 932305, 1993.

4. R. Meyer, R. Muller, K. Beckmann, K. Goncharov, E. Kotlyarov, Yu. Maidanik, Investigation of the heat transfer performance of a capillary pumped ammonia loop under gravity, Society of Automotive Engineers, Paper 932304, 1993.

5. T. Hoang, J. Ku, Hydrodynamic aspects of capillary pumped loops, Society of Automotive Engineers, Paper 961435, 1996.

6. T. LaClair, I. Mudawar, Thermal transients in a capillary evaporator prior to the initiation of boiling, International Journal of Heat and Mass Transfer 43 (2000) 3937-3952.

7. T. Hoang, J. Ku, Theory of hydrodynamic stability for capillary pumped loops, ASME HTD-Vol. 307, 1995.

8. J. Ku, T. Hoang, An experimental study of pressure oscillation and hydrodynamic stability in a capillary pumped loop, ASME HTD-Vol. 307, 1995.

9. K. R. Kolos, K. E. Herold, Low frequency temperature and fluid oscillations in capillary pumped loops, AIAA Paper No. 97-3872, 1997.

10. T. O'Connell, T. Hoang, Effects of wick properties on pressure oscillations in a capillary pumped loop, Society of Automotive Engineers, Paper 961434, 1996.

11. T. O'Connell, T. Hoang, J. Ku, Effects of transport line diameters on pressure

oscillations in a capillary pumped loop, AIAA paper No. 96-1833, 1996.

12. J. Ku, Thermodynamic aspects of capillary pumped loop operation, AIAA Paper No.94-2059, 1994.

13. E. Pouzet, J. Joly, V. Platel, J. Grandpeix, C. Butto, Dynamic response of a capillary pumped loop subjected to various heat load transients, International Journal of Heat and Mass Transfer 47 (2004) 2293-2316.

14. E. Bazzo, R. R. Riehl, Operation characteristics of a small-scale capillary pumped loop, Applied Thermal Engineering 23 (2003) 687-705.

15. J. Dickey, G. Peterson, Experimental and analytical investigation of a capillary pumped loop, Journal of Thermophysics and Heat Transfer 8 (3) (1994) 602-607.

16. Q. Liao, T. Zhao, Evaporative heat transfer in a capillary structure heated by a grooved block, Journal of Thermophysics and Heat Transfer 13 (1) (1999) 126-133.

17. P. C. Chen, W. K. Lin, The application of capillary pumped loop for cooling of electronic components, Applied Thermal Engineering 23 (2003) 687-705.

18. T. Zhao, Q. Liao, On capillary-driven flow and phase-change heat transfer in a porous structure heated by a finned surface: measurement and modeling, International Journal of Heat and Mass Transfer 43 (2000) 1141-1155.

19. Q. Liao, T. Zhao, A visual study of phase-change heat transfer in a two-dimensional porous structure with a partial heating boundary, International Journal of Heat and Mass Transfer 43 (2000) 1089-1102.

20. Y. Cao, A. Faghri, Analytical solutions of flow and heat transfer in a porous structure with partial heating and evaporation on the upper surface, International Journal of Heat and Mass Transfer 37 (1994) 1525-1533.

21. Y. Cao, A. Faghri, Conjugate analysis of a flat-plate type evaporator for capillary pumped loops with three-dimensional vapor flow in groove, International Journal of Heat and Mass Transfer 37 (1994) 401-409.

22. X. Huang, W. Liu, A. Nakayama, S. Peng, Modeling for heat and mass transfer with phase change in porous wick of CPL evaporator, Heat and Mass Transfer 41 (2005) 667-673.

23. M. Hanlon and H. Ma, Evaporation heat transfer in sintered porous media, ASME Journal of Heat Transfer 125 (2003) 644-652.

24. C. Figus, Y. Le Bray, S. Bories, M. Prat, Heat and mass transfer with phase change in a porous structure partially heated: continuum model and pore network simulations, International Journal of Heat and Mass Transfer 42 (1999) 2557-2569.

25. B. Mo, M. M. Ohadi, S. V. Dessiatoun, K. H. Cheung, Startup time reduction in an electrohydrodynamically enhanced capillary pumped loop, Journal of Thermophysics and Heat Transfer 13 (1) (1999) 134-139.

26. B. Mo, M. M. Ohadi, S. V. Dessiatoun, K. R. Wrenn, Capillary pumped-loop Thermal performance improvement with electrohydrodynamic technique, Journal of Thermophysics and Heat Transfer 14 (1) (2000) 103-108.

27. I. Muraoka, F. Ramos, V. Vlassov, Experimental and theoretical investigation of a capillary pumped loop with a porous element in the condenser, Int. Comm. Heat Mass Transfer 25 (8) (1998) 1085-1094.

28. T. Hoang, Development of an advanced capillary pumped loop, SAE Paper No. 97ES-16, 1997

29. T. Hoang, Design and test of a proof-of-concept advanced capillary pumped loop , SAE Paper No. 97ES-17, 1997

30. A. Delil, M. Dubois, W. Supper, The European two-phase experiments TPX Ⅰ & Ⅱ, 10th International Heat Pipe Conference, Sttutgart, Germany, 1997.

31. C. Figus, L. Ounougha, P. Bonzom, W. Supper, C. Puillet, Capillary fluid loop developments in Astrium, Applied Thermal Engineering 23 (2003) 1085-1098

32. T. Q. Feng, J. L. Xu, An analytical solution of thermal resistance of cubic heat

spreaders for electronic cooling, Applied Thermal Engineering 24 (2004) 323-337

33. G. Maranzana, I. Perry, D. Maillet, S. Rael, Design optimization of a spreader heat sink for power electronics, International Journal of Thermal Sciences 43 (2004) 21-29

34. Y. H. Hung, Experimental Study of an Improved Capillary Pumped Looped System for Electronics Cooling, M. S. thesis, National Chiao Tung University, Hsunchu, Taiwan, R. O. C., 2006

35. J. P. Holman, "Heat Transfer," 7d ed., McGraw-Hill Book Company, New York, c1990, 355-357.

36. V. Gnielinski, New equations for heat and mass transfer in turbulent pipe and channel flow, International Chemical Engineering 16 (2) (1976) 359-368

37. R. W. Fox and A. T. McDonald, "Introduction to Fluid Mechanics," New York, Wiley, c1978, 357-361.

38. S. J. Kline and F. A. McClintock, "Describing Uncertainties in Single-sample Experiments," Mech. Engng, Vol. 75, (1953), 3-8